Title
Understanding the Mechanobiological Regulation of Brown and Beige Adipocytes

Author
Dempsey, Garrett

Publication Date
2022

Peer reviewed|Thesis/dissertation

Understanding the Mechanobiological Regulation of Brown and Beige Adipocytes

By

Garrett Dempsey

A dissertation submitted in partial satisfaction of the

requirements for the degree of

Doctor of Philosophy

in

Metabolic Biology

in the

Graduate Division

of the

University of California, Berkeley

Committee in Charge:

Professor Andreas Stahl, Chair
Assistant Professor Sona Kang
Professor Sanjay Kumar

Fall 2022

Abstract

Understanding the Mechanobiological Regulation of Brown and Beige Adipocytes

By

Garrett Dempsey

Doctor of Philosophy in Metabolic Biology

University of California, Berkeley

Professor Andreas Stahl, Chair

Obesity, defined as abnormal or excessive fat accumulation, has become a global epidemic. Although some obese individuals are metabolically healthy a majority develop several co-morbidities such as type II diabetes, hypercholesterolemia, and cardiovascular disease. Diet and exercise can be effective strategies to lose weight, but many individuals have difficulty making lifestyle changes. Thus, new therapeutic strategies are needed to combat the growing prevalence of obesity. Our lab has focused on understanding the biological function of brown adipose tissue (BAT) and beige adipose tissue (BeAT), which are promising therapeutic tissues to combat obesity and obesity related diseases. Unlike white adipose tissue which serves a purpose of storing energy for later use, BAT and BeAT catabolize fat and glucose, uncoupling the electron transport chain from ATP production, instead generating heat. BAT and BeAT depots are primarily activated by cold exposure via β-adrenergic receptor signaling. Targeting β-adrenergic signaling to activate BAT and BeAT was a promising therapeutic approach, however β-adrenergic receptors are also found in the heart preventing widespread therapeutic use. A deeper biological understanding of BAT and BeAT may lead to new therapeutic targets. Our lab previously uncovered a novel role for actomyosin mediated-tension facilitating thermogenesis in BAT. This novel mechanism became the basis for three projects described within this dissertation. First, we probed the importance of type II myosin activity in BeAT development and thermogenic function; type II myosin 9 (Myh9) was found to regulate UCP1 mRNA expression, mitochondrial function, and lipid metabolism. Second, in collaboration with the company Atomwise we screened novel type II myosin activators in BAT to determine whether pharmacologically activating type II myosins could increase thermogenesis. Third, we sought to understand the function of the mechanosensitive transcriptional paralogs YAP and TAZ in regulating BeAT differentiation.

Table of Contents

Acknowledgments

Thank you to all who helped me along this journey. Thank you to my mentor Andreas Stahl who supported my work and always gave fresh ideas and perspectives. To my entire dissertation committee Sona Kang and Sanjay Kumar for their support in completing this dissertation. Further thanks to Sanjay Kumar who was also a collaborator; thank you for dedicating your time to frequent project meetings in which you provided valuable insight and expertise. Additional thanks to all our other collaborators including but not limited to Atomwise and Lydia Sohn. I would also like to thank all the campus core facilities I have worked with over the years; Denise Schichnes and Steve Ruzin from the UC Berkeley Biological Imaging Facility for their always gracious technical support on all things biological imaging, Danielle Jorgens and Reena Zalpuri from the University of California Berkeley Electron Microscope Laboratory for advice and assistance in experiment planning, electron microscopy sample preparation, and data collection, lastly Alma Valeros and Hector Nolla from the CRL Flow Cytometry Facility.

Thank you to the entire Stahl lab both past and present for all your support. Special thanks to Ching-Fang Chang, Diyala Shihadih, and Pete Zushin, prior lab members who I spent almost the entirety of my PhD with. Thank you for helping me along this journey from experiment recommendations, to technical assistance, and encouragement. The rest of the Stahl lab, Amanda, Kaitlyn, Irene, Xue, and Lin thank you for the support. I also would like to thank Lu Ling, honorary Stahl lab member and collaborator. I had the privilege to work directly with Lu soon after she joined the Kumar lab about 1.5 years ago. Lu provided technical and intellectual support that pushed our project to the next level.

Thank you to all the undergraduate researchers I had the privilege of mentoring and working with over the years. Your enthusiasm, dedication, and drive was energizing. You all taught me how to become a better teacher and communicator.

Thank you to my family for your constant encouragement and support. Without you I would not be where I am today

Lastly, thank you my girlfriend, partner, best friend, and at times my at home therapist, Lauren. You provided endless encouragement, support, motivation, and love. Without you I don’t think I could have completed this journey.

Chapter 1:
Uncovering the role of type II myosin proteins in beige adipocyte metabolic function

Summary

White adipose tissue (WAT) is the major energy storage organ in the body characterized as having unilocular lipid droplets. Brown adipose tissue (BAT) and beige adipose tissue (BeAT) are characterized as having multilocular lipid droplets and a high mitochondrial density, which oxidize fuel to generate heat through a process termed non-shivering thermogenesis. A deeper understanding of the biology regulating thermogenesis could offer new therapeutic approaches to combat metabolic diseases such as obesity and type 2 diabetes. While it is widely accepted that the actin cytoskeleton is a key regulator of adipocyte differentiation, our lab previously uncovered that the actomyosin network is critical for orchestrating uncoupled respiration in BAT. To date there has been limited investigation into the role of type II myosin-mediated, mechanobiological regulation in beige adipocytes. Here we show that the actomyosin network has a critical role in beige adipocyte thermogenic function. The non-muscle myosin II heavy chain (Myh9) was found to be the most abundant isoform present in BeAT and knockdown of Myh9 caused mitochondrial dysfunction and lipid impairments. Our results showed that mechanical proteins, namely type II Myh9, regulates UCP1 mRNA expression, mitochondrial function, and lipid metabolism. New therapeutic strategies are needed to combat the rising prevalence of obesity and its associated disorders. Targeting the mechanobiological regulation of thermogenesis in BAT and BeAT may offer an exciting new therapeutic approach.

Introduction

Adipocytes can broadly be categorized as either white, brown, or beige. White adipose tissue (WAT) is an energy storage and endocrine organ while brown adipose tissue (BAT) and beige adipose tissue (BeAT) are primarily characterized by their ability to generate heat through a process called non-shivering thermogenesis. Unlike WAT which contains unilocular lipid droplets and few mitochondria, BAT and BeAT contain multilocular lipid droplets and a high density of mitochondria which gives the tissues their characteristic 'brown' appearance. BAT and BeAT contain the protein UCP1 which resides within the inner mitochondrial membrane; UCP1 uncouples the electron transport chain from ATP production instead generating heat[1]. Unlike BAT which is innate, BeAT is thought to arise de novo from mesenchymal stem cells or from the trans-differentiation of white adipocytes[2,3]. The high rate of catabolism in BAT/BeAT requires a readily available fuel supply, which includes glucose and fatty acids[4]. BAT and BeAT are primarily activated through the canonical β-adrenergic receptor (β-AR)/cAMP/PKA signaling pathway[5]. BAT and BeAT express β1, β2, and β3 AR and treatment of mice or humans with β3-

AR agonists results in the activation of BAT leading to improved glucose homeostasis and insulin sensitivity. However, the use of β3-AR agonists in humans has resulted in many adverse side effects such as aortic valve dysfunction[6]. This is because similar signal transduction pathways downstream of adrenergic receptors also exist in the heart. Thus, new mechanistic insights are needed to improve the therapeutic potential of BAT/BeAT in humans.

Previous work in our lab demonstrated that in BAT, β3-AR signaling leads to an induction of cellular tension via type-II myosins, like the response in muscle. The induction of tension is critical for mediating thermogenesis in brown fat[7]. Specifically, we uncovered that during a cold stimulus there is a calcium spike in BAT, activation of muscle specific calcium-calmodulin dependent myosin light chain kinases and activation of specific type II myosins leading to increased tension in BAT cells and tissues; the enhanced cellular tension was found to be coupled to regulation of UCP1 and uncoupled mitochondrial respiration via the activation of transcriptional co-activators Yap and Taz. Although BAT and BeAT have similar physiological functions, beige cells are anatomically different and have been proposed to derive from WAT-vasculature associated pericytes while brown adipose tissue has been proposed to derive from a Myf5+/Pax7+ skeletal muscle lineages[8,9]. Further, in adult humans BAT has been proposed to share many similarities with rodent beige rather than brown fat[10]. Whether tension generation and sensing is also critical for BeAT activation and/or determination of cellular differentiation fates between white and beige, is currently unknown. We speculated that beige adipogenesis and thermogenic activity are regulated by a distinct set of biomechanical signals and that pharmacological activation of this tension dependent pathway can be used for the β-AR independent activation of the tissue laying the foundation for a novel anti-obesity approach.

Tension is generated when myosin motor proteins interact with F-actin filaments and convert chemical energy, ATP, into mechanical energy[11]. During beige adipocyte formation, downregulation of RhoA/ROCK signaling pathway results in the disruption of actin stress fibers leading to the nuclear exclusion of MRTFA and the promotion of the adipogenic program, specifically enhancing beige adipogenesis[12,13]. Although actin reorganization has been shown to be critical for adipogenesis[14], minimal research has been undertaken to determine the interplay of the actomyosin network in regulating metabolic processes. The actomyosin network is composed of F-actin filaments and type II myosins which themselves can form filaments that bind to F-actin. Myosins are a superfamily of proteins that contain actin and myosin binding sites and are categorized into 35 different classes or types[15]. The type II myosins utilize ATP to generate mechanical force. In non-muscle cells for example, type II myosins can contract in response to mechanical signals from the extracellular matrix[16], while in muscle cells, type II myosins contract in response to calcium signaling. To date, 15 type II myosin isoforms have been identified in the human genome and the expression pattern of these myosins depends on cell and tissue types. Type II myosin motor proteins consist of six non-covalently associated polypeptides; two myosin II heavy chains (MYH), two essential light chains (ELC), and two

regulatory light chains (RLC), all of which are encoded by different genes. The heavy chain is typically divided into the head, neck, and tail domains. The head domain contains the ATP and actin binding sites, the neck domain contains ELC and RLC binding sites, and the tail domain consists of a coiled-coil tail which enables the myosin protein to assemble into highly ordered parallel and antiparallel thick filaments[17]. The ELC is thought to provide stability to the heavy chains while the RLC is primarily responsible for regulating type II myosin activity via phosphorylation. The RLC undergoes reversible phosphorylation at multiple amino acid residues, mostly noteable phosphorylation on S19 and T18 regulates type II myosin activity by increasing its ATPase activity and extended 6S conformation that allows simultaneous assembly into thick filaments[18,19]. Phosphorylation states of type II myosins are tightly regulated by multiple phosphatases and kinases. The most commonly studied kinases include myosin light chain kinase (MLCK/MYLK), Rho-associated coiled-coil-containing kinase (ROCK), and myotonic dystrophy kinase-related CDC42-binding kinase (MRCK/CDC42BP)[20]. Interestingly, in many cell types these kinases respond to a wide variety of signaling pathways which converge on RLC phosphorylation to activate type myosin II proteins. For example, influx of cytosolic calcium leads to the activation of calmodulin which binds to MYLK, disinhibiting MYLK's kinase domain enabling phosphorylation and activation of RLC phosphorylation[21,22]. Alternatively, ROCK is activated by RhoA, a GTPase, which itself responds to a variety of cytoskeletal cues[23].
The type II myosins have been shown to primarily be involved in muscle contractions, cytokinesis, cell migration, and stem cell differentiation[24], however work over the last decade suggests type II myosins are also involved in metabolic processes.

Three type II myosin isoforms (Myh9 part of NMII-A, Myh10 part of NM-IIB, and Myh14 par of NM-IIC) are considered non-muscle myosins and have been shown to play an important role in stem cell self-renewal and differentiation[25,26]. Mesenchymal stem cells (MSCs) have been shown to specify lineage and commit to phenotypes based on matrix elasticity; the MSCs differentiate to muscle and bone on stiffer substrates and to neurons on softer substrates, however inhibition of the nonmuscle myosins blocks all elasticity-directed differentiation[27]. In adult neural stem cells, lineage commitment was shown to be mediated through extracellular derived mechanical signals that act through Rho GTPases[28]. A rigid matrix inhibited neural stem cell differentiation, but inhibition of type II myosin activity was able to rescue neuronal differentiation. Type II non muscle myosins in part drive stem cell differentiation through mechanosensitive transcriptional coactivators, such as Yes-associated protein (YAP) and PDZ binding motif (TAZ). RhoA–ROCK-mediated myosin activation was shown to cause YAP nuclear localization which favored MSC differentiation to bone rather than to adipose or cartilage[29]. These results suggest that modulating the activity of non muscle myosins in stem cells could direct differentiation to a particular fate.

In white adipocytes, the type II non-muscle myosins (Myh9 part of NMII-A and Myh10 part of NM-IIB) were found to be involved in GLUT4 mediated glucose uptake[30]. Additionally,

two separate papers suggest that in white adipocytes Myh9 or Myh10 can regulate adipogenesis[31,32]. Both, Myh9 and Myh10 have also been implicated in mitochondrial and lipid droplet function albeit in non-adipocytes. In human osteosarcoma U2OS cells, the actin-binding protein formin-like 1 (FMNL1) facilitates the assembly of Myh9 on lipid droplets to regulate lipid droplet dynamics[33]. In HeLa cells, ARP2/3, which regulates polymerization of actin, was shown to mediate lipid droplet contact with actin by promoting the recruitment of Myh9 to lipid droplets[34]. The recruitment of Myh9 regulated lipid droplet dynamics through an unknown mechanism. Actomyosin activity has also been shown to play a role in mitochondrial dynamics. Specifically, in U2OS cells, INF2-mediated actin polymerization leads to type myosin II recruitment and constriction at the mitochondrial fission site, enhancing subsequent Drp1 accumulation and fission[35]. The actomyosin network may further regulate mitochondrial homeostasis through the cyclic assembly onto mitochondria modulating the fission/fusion balance and promoting mitochondrial network remodeling[36]. High resolution platinum replica electron microscopy suggests that type II myosins may not directly interact with mitochondria but instead lie adjacent to mitochondria promoting mitochondrial constriction by inducing stochastic deformations of the interstitial actin network[37]. Besides their physical interactions with mitochondria, type II myosins have even been shown to modulate endoplasmic-reticulum-to-mitochondrial calcium transfer, mitochondrial Drp1 recruitment, and mitochondrial division[38]. Disruption of type II non-muscle myosin (Myh14 part of NMII-C) results in deafness and was also recently shown to disrupt mitochondrial fission[39,40]. While these papers convincingly show that type II myosins can modulate lipid droplet and mitochondrial dynamics there has been minimal investigation into the functional and physiological consequences of type II myosins within the context of BeAT.

In BAT and BeAT, mitochondrial dynamics and lipid homeostasis are critical functions in maintaining the tissues' thermogenic activity[41,42]. For example, disruption of mitochondrial dynamics through the inhibition or knockout of fission/fusion proteins such as MFN2 or DRP1 can blunt BAT and BeAT activity[43–45]. To date, nobody has investigated the possible role of type II myosins in BeAT thermogenic function. We discovered that BeAT expresses a variety of type II myosin isoforms namely, non-muscle Myh9 (NMIIA), non-muscle Myh10 (NMIIB), non-muscle Myh 14 (NMIIBC), and smooth-muscle myosin 11 (Myh11), with Myh9 being the most abundant. Perturbation of the actomyosin network via type II myosin inhibition resulted in reduction in BeAT thermogenic activity. Probing individual type II myosin function uncovered that Myh9 knockdown (Myh9 KD) was predominantly responsible for reductions in UCP1 mRNA expresion and cellular respiration in BeAT. Further, Myh9 KD during beige adipocyte differentiation decreased lipid accumulation and caused mitochondrial dysfunction. Electron microscopy indicated the mitochondria in Myh9 KD beige adipocytes were more fragmented and had fewer lipid droplet contact sites. These findings provide insight into the role of type II Myh9 in regulating beige adipocyte differentiation and metabolic activity. Activating type II

Myh9 may prove to be a viable option to increase beige adipocyte activity to combat obesity and its associated metabolic disorders.

Results

Type II myosins induce tension in beige adipocytes

To investigate the significance of type II myosin function in beige adipocytes we first differentiated a murine immortalized adipocyte precursor cell line (sWAT)[46] and human adipose tissue derived mesenchymal stem cells (MSC) to beige adipocytes and performed RNAseq. Ranking of all myosin II heavy chains revealed that the non-muscle myosin heavy chains (Myh9) followed by (Myh10) were the most robustly expressed **(Fig. 1A-B)**. The smooth muscle myosin heavy chain (Myh11) and the non-muscle heavy chain (Myh14) were also detected **(Fig. 1A-B)**. Interestingly, most cell types are not known to express all three non-muscle myosin heavy chains (Myh9 part of NMII-A, Myh10 part of NM-IIB, and Myh14 part of NMII-C). The observed myosin II heavy chains expression pattern was confirmed with qPCR in the sWAT cells and in inguinal white adipose tissue (iWAT) from mice **(Fig. 2A-B).** We also quantified the myosin II heavy chain expression pattern in classical brown adipose tissue (BAT) and found that similar to beige adipocytes Myh9 is the most abundant **(Fig. 2C).** To determine if ß-adrenergic signaling alters myosin II heavy chains expression in beige adipocytes, we housed mice at either 23°C or 4°C and isolated mature adipocytes from iWAT. Following cold exposure, which induces browning of iWAT depots, expression of Myh9 and Myh10 were unchanged while Myh11 and Myh14 were reduced **(Fig. 1C)**. Brown adipocytes isolated from BAT only showed a reduction in Myh11 but not Myh9, Myh10 or Myh14 **(Fig. 2D).** Since type II myosins are known to bind actin filaments and generate contractile force we used atomic force microscopy (AFM) to probe whether type II myosins contribute to cellular tension in beige adipocytes[47]. Blebbistatin, a type II myosin antagonist[48], significantly reduced cell stiffness while stimulation with a ß-adrenergic agonist (isoproterenol) induced tension in the cells **(Fig. 1D)**. Actin imaging of blebbistatin treated beige adipocytes indicated altered F-actin branch length which suggests that the altered actin network is contributing to the loss of cellular tension seen with blebbistatin treatment **(Fig. 1E).** Importantly, following 24 hours of cold exposure, iWAT depots from cold exposed mice also showed an almost 4-fold increase in their elastic modulus **(Fig. 1F)**. Thus, ß-adrenergic stimulation of beige adipose tissue (BeAT) induces increased cellular tension seemingly driven by type II myosin function.

Type II myosins regulate beige adipocyte thermogenic function

We again utilized blebbistatin to test the functional consequences of cellular tension generation in beige adipocytes. We found that blebbistatin greatly suppressed UCP1 gene expression, but not expression of the adipogenic marker FABP4, in beige adipocytes **(Fig. 3A)**.

Comparatively, blebbistatin treatment had no significant effects on 3T3L1 white adipocyte gene expression **(Fig. 3B)**, suggesting that type II myosin inhibition via blebbistatin doesn't alter general adipogenic function. We next tested the effects of blebbistatin treatment on mitochondrial respiration and found that in beige adipocytes blebbistatin significantly reduced basal and maximal respiration while uncoupled respiration trended downwards **(Fig. 3C).** Blebbistatin treatment also significantly reduced basal, uncoupled, and maximal respiration following ß3-AR stimulation **(Fig. 3D).** Reductions in basal and maximal respiration suggest a role for type II myosin mediated tension in mitochondrial homeostasis within beige adipocytes. Interestingly, blebbistatin treatment had no effect on white adipocyte mitochondrial respiration implying that type II myosins are required for UCP1 expression and uncoupled, i.e. thermogenic, respiration in beige but not white adipocytes **(Fig. 3E).** Previous studies have demonstrated that in white adipocytes the actomyosin network is necessary for the translocation of membrane receptors such as Glut4 and adiponectin[49,50,51], however we did not investigate type II myosins role in membrane receptor trafficking in our studies. Conversely, we sought to determine whether induction of type II myosin activity could increase the thermogenic activity in beige adipocytes. EMD57003 is a commercially available type II myosin activator[52] which binds to the myosin motor domain increasing the ATPase activity. Beige adipocytes treated with EMD57003 had no significant change in UCP1 expression compared to control **(Fig. 4B)**. However, when EMD57003 was treated in combination with isoproterenol, UCP1 mRNA expression significantly increased compared to isoproterenol alone. Increasing myosin ATPase activity therefore enhanced ß3-AR induced signaling **(Fig. 4C)**. It is possible that isoproterenol signaling leads to type II myosin conformational changes which enables EMD57003 binding and activation of the ATPase domain.

Type II myosin siRNA screen

After establishing that type II myosins are important for beige adipocyte thermogenic function we wanted to determine which of the myosin II heavy chain isoforms expressed in beige adipocytes was responsible for the thermogenic defects originally observed with blebbistatin. Based on abundance, we initially focused on Myh9 and Myh10. We isolated the stromal vascular fraction (SVF) from inguinal white adipose tissue of mice. The SVF cells were differentiated to either a white or beige fate and transfected with siRNA targeting either Myh9 or Myh10. Both Myh9 and Myh10 siRNA resulted in ~90% reduction in their respective mRNA levels **(Fig. 5A)**. However, Myh10 siRNA also caused a significant reduction in Myh9 mRNA levels suggesting some off-target effects. Nevertheless, knockdown of Myh9 but not Myh10 during 8 days of differentiation resulted in a significant reduction of UCP1 mRNA expression in beige adipocytes compared to control **(Fig. 5B)**. In both beige and white adipocytes, knockdown of either Myh9 or Myh10 increased the expression of general adipogenic genes such as FABP4 and PPARg **(Fig. 5B-C).** Conversely, Myh9 GFP tagged overexpression in beige adipocytes

resulted in a significant increase in UCP1 mRNA expression but did not appear to affect general adipogenic mRNA levels **(Fig. 5D)**. These results suggest that Myh9 but not Myh10 is important for beige adipocyte development and thermogenic function while Myh10 may be important for general adipogenesis.

Type II Myh9 but not Myh10 regulates thermogenesis in beige adipocytes

Using immunofluorescence microscopy (IF) we found that both Myh9 and Myh10 are localized both in cortical actomyosin bundles as well as intracellularly, particularly in the vicinity of lipid droplets (LDs) in beige adipocytes **(Fig. 6A)**. We created stable cell lines that can be differentiated toward beige adipocytes with doxycycline-inducible shRNA-mediated knockdown (pINDUCER11)[53] of either Myh9 or Myh10. Induction of Myh10-specific knockdown (Myh10KD) for 7 days during differentiation generated beige adipocytes with greatly diminished Myh10 protein and mRNA levels (85% and 80% reduction respectively) **(Fig. 6B-C)**. This resulted in a reduction in cellular storage modulus by 75% as determined by AFM **(Fig. 6D)**. Despite this efficient knockdown and reduction in cellular tension, loss of Myh10 did not affect UCP1 mRNA expression nor the expression of other adipogenic hallmark genes **(Fig. 6E).** However, UCP1 protein levels were slightly increased with Myh10KD **(Fig. 6F)**. There was no significant change in cellular respiration with Myh10KD **(Fig. 6G)**. Thus, the blebbistatin induced loss of UCP1 expression and impaired cellular respiration are not a general result of loss of cellular tension but due to a specific subset of type II myosins operating independent of Myh10. Using a similar approach, Myh9-specific knockdown (Myh9KD) for 7 days during differentiation was also able to significantly reduce protein and mRNA levels (50% and 80% reduction respectively) **(Fig. 7A-B)**. As with Myh10, reduction of Myh9 resulted in decreased cellular storage modulus (66% reduction) **(Fig. 7C)**. High resolution microscopy indicated disrupted actin stress fibers in the Myh9KD cells compared to control **(Fig. 7D).** Importantly, Myh9KD during beige adipocyte differentiation significantly reduced UCP1 mRNA expression and protein levels while having no effect on general markers of adipogenesis **(Fig. 7E-F)**. Knockdown of Myh9 also resulted in the impairment of basal and maximal mitochondrial respiration indicating Myh9 plays a critical role in mitochondrial homeostasis in beige adipocytes beyond UCP1 **(Fig. 7G)**. To test whether Myh9KD blunts β-adrenergic induced thermogenic function in beige adipocytes, we induced knockdown of Myh9 during differentiation followed by isoproterenol treatment. Myh9KD had no effect on isoproterenol induced UCP1 mRNA expression **(Fig. 7H).** However, we did find that Myh9KD reduced β-adrenergic induced maximal mitochondrial respiration **(Fig. 7I)**, again indicating that Myh9 may regulate mitochondrial function in beige adipocytes.

Loss of Myh9 impairs BeAT mitochondrial function

Since our data indicated that loss of Myh9 impaired mitochondrial respiration **(Fig. 7G)**, we decided to further probe mitochondrial function in Myh9KD beige adipocytes. A previous

study in HeLa cells showed that cyclic assembly of the actin network onto mitochondria modulates the fission/fusion dynamics[36]. Using IF microscopy we found Myh9 to be localized in the vicinity of mitochondria **(Fig. 8A)**. To better visualize mitochondrial morphology upon Myh9KD we utilized transmission electron microscopy (TEM) and found that Myh9KD caused mitochondria to become smaller and more fragmented **(Fig. 8B-C).** Moreover, fewer mitochondria were forming lipid droplet contact sites resulting in an increased cytoplasmic population **(Fig. 8D-E)**. These sites are thought to be critical for efficient ß-oxidation[54] but, in brown adipocytes, may also be involved in triacylglycerol synthesis and lipid droplet growth[55]. In addition to mitochondrial morphology changes we also found that mitochondrial superoxide production was increased and mitochondrial membrane potential was decreased **(Fig. 8F-G)**, further indicating Myh9KD caused mitochondrial dysfunction. Superoxide produced in the mitochondria is derived from electrons leaking from the electron transport chain[56], thus an increase in superoxide can indicate mitochondrial stress. A depolarization and loss of mitochondrial membrane potential is typically a sign of mitochondrial dysfunction[57]. We used live-cell mitochondrial imaging to track alterations of fission/fusion dynamics over time. Interestingly, Myh9KD caused a visible disruption of mitochondrial motility **(Fig. 8H).**

To further determine the extent to which mitochondria were dysfunctional, we isolated mitochondria from Myh9KD cells and found they had impaired basal respiration compared to control cells further **(Fig. 9A)**. Since previous study found that non-muscle myosin II facilitates mitochondrial fission through tension induced mitochondrial deformations[37], we measured the protein abundance of the fission protein DRP1 and fusion proteins OPA1 and MFN2. We observed no changes in the levels of fusion proteins OPA1 and MFN2 **(Fig. 9B-C).** We also observed no significant difference in the ratio of phosphorylated DRP1 to total DRP1 levels, although total DRP1 was slightly decreased **(Fig. 9D)**. Although the abundance of fission and fusion proteins were generally unchanged, it is possible that localization of either of these proteins may be altered with Myh9KD. Myh9KD also did not affect mitophagy suggesting that mitochondrial dysfunction is likely occurring upstream of mitochondria degradation. Our data clearly indicates that Myh9KD causes mitochondrial dysfunction, however we have not yet uncovered the precise mechanism.

Loss of Myh9 impairs BeAT lipid metabolism:

Concomitant with the alterations in mitochondrial function and lipid droplet association we also observed changes in the lipid droplets themselves. IF microscopy showed that Myh9 is enriched at mitochondrial-lipid droplet interfaces and forms cage-like structures around the lipid droplets (**Fig. 10A**). Analysis of TEM images indicated that knockdown of Myh9 resulted in smaller lipid droplet sizes (**Fig. 10B-C**) which translated into quantitative differences in neutral lipid staining (**Fig. 10D**). Reduced lipid droplet size was not a result of enhanced lipolysis, which at basal level was reduced, and was unchanged following ß3-AR stimulation (**Fig. 10E**) following

Myh9KD. Fatty acid uptake was significantly reduced in the Myh9 KD cells compared to control which may explain the reduction in total lipid accumulation (**Fig. 10F**). In addition, we found that the gene expression of genes related to lipolysis and fatty acid uptake were downregulated (**Fig. 10G**). Thus, Myh9KD significantly affects lipid metabolism in beige adipocytes.

RNAseq of Myh9 knockdown in beige adipocytes

To get an unbiased assessment of the transcriptional changes in Myh9KD beige adipocytes we performed RNAseq. Comparison of control and Myh9KD beige adipocytes highlighted decreased expression in various adipogenic pathways such as "brown fat differentiation" and "response to cold" as well as tension related pathways including "signaling by Rho GTPases" **(Fig. 11A).** Kegg pathway analysis revealed multiple biological pathways, such as regulation of actin, regulation of lipolysis, and insulin signaling, as significantly enriched with Myh9KD **(Fig. 11B)**. Interestingly, HOMER motif analysis of transcription factors involved in the observed gene expression changes identified members of the Krüppel-like factors (KLF) family including KLF9, -4, -5, and -10 as the top hits **(Fig. 11C).** We previously observed that the YAP/TAZ mediated the mechanical signals in classical brown fat[7], however YAP/TAZ did not appear to be implicated in Myh9KD induced thermogenic alterations in beige adipocytes. These findings point to an exciting potential role for the KLF family of transcription factors in Myh9-dependent tension signaling in BeAT. Importantly, a recent paper showed that KLF9, the main KLF member implicated by our data, is induced by ß-adrenergic agonists and is required for browning of WAT following cold exposure[58]. In addition, KLF2 and KLF4 have been identified as mechanosensitive transcription factors in vascular endothelium[59], laying precedent for other KLF family members to be mechanosensitive. We first tested whether Myh9KD reduces KLF9 mRNA expression levels and found that there was no change **(Fig. 11D).** Next, we measured KLF9 expression levels after isoproterenol-induced ß-AR activation and found that KLF9 levels were increased **(Fig. 11E).** This data supports the results found by Fan et al, which showed that KLF9 is cold-inducible and stimulates thermogenesis. To determine if we could rescue the reduction of UCP1 expression observed with Myh9KD knocked down both KLF9 and Myh9 for 7 days during beige adipocyte differentiation. We found that KLF9 knockdown reduced UCP1 expression while double knockdown of KLF9 and Myh9KD further decreased UCP1 expression **(Fig. 11F)**. These data suggest that KLF9 plays an important role in regulating UCP1 expression, however we can not conclude whether Myh9 regulates KLF9 transcriptional activity. Although Myh9KD did not change KLF9 expression levels **(Fig. 11D)** post-translational modifications are known to alter the subcellular localization of the KLF family of proteins[60]. IF microscopy could be utilized to determine whether Myh9KD alters the nuclear localization of KLF9. In addition, we could test whether KLF9 overexpression in Myh9KD beige adipocytes would rescue UCP1 expression in Myh9KD cells. Whether Myh9 could regulate KLF9 transcriptional activity is currently unknown but provides an attractive testable hypothesis.

Discussion

Here we have identified a unique type II myosin expression pattern in BeAT. Type II non-muscle myosin 9 (Myh9) was the most abundantly expressed isoform followed by the expression of non-muscle myosin (Myh10), smooth muscle myosin (Myh11), and non-muscle myosin (Myh14). Our findings suggest that in BeAT type II myosins generate contractile force upon β--adrenergic induced signaling and conversely, pharmacological disruption of type II myosin activity with blebbistatin decreases cellular tension and thermogenesis. To discern whether blebbistatin effects were due to the inhibition of a specific type II myosin isoform we probed the individual functions of Myh9 and Myh10, the two most abundantly expressed isoforms. Interestingly, we found that Myh9 but not Myh10 reduced UCP1 expression and cellular respiration. Moreover, we uncovered that Myh9KD in beige adipocytes caused mitochondrial dysfunction which may or may not be secondary to UCP1 transcriptional changes. Our data is the first to indicate that a type II myosin, Myh9, is important for maintaining UCP1 expression and mitochondrial function in beige adipocytes.

Type II myosins make up the major contractile proteins in the body, most notably in cardiac, skeletal, and smooth muscle[61]. While the non-muscle myosins (Myh9, Myh10, and Myh14) have predominantly been studied in the context of cell migration, few studies have implicated these proteins in metabolic processes, particularly in adipocytes. Both Myh9 and Myh10 have been linked to mitochondrial fission/fusion dynamics[35,37], which is an important process in thermogenic adipose tissue, however these results have not been linked to any meaningful biological outcomes. In white adipocytes, both Myh9 and Myh10 have been shown to be involved in adipogenesis and insulin-stimulated glucose uptake. Interestingly, Myh9 overexpression inhibited adipogenesis in primary adipocytes[31] while in Myh10 knockdown inhibited adipogenesis in the immortalized 3T3L1 preadipocyte cell line[32]. These seemingly opposing results may be explained by the different lineage stages of the cells or different mechanisms of Myh9 and Myh10. Additionally, in mature white adipocytes, both Myh9 and Myh10 have been shown to be involved in insulin-stimulated GLUT4 docking at the plasma membrane to facilitate glucose uptake[30,62]. Whether type II myosins are also important for beige adipocyte differentiation and function has not been fully investigated. Recently, myosin phosphatase target subunit 1- protein phosphatase 1β (MYPT1-PP1β) was shown to inhibit UCP1 activation in beige adipocytes. Knockdown of MYPT1-PP1β increased actomyosin tension-mediated activation of YAP/TAZ which directly stimulated Ucp1 gene expression, increasing cold tolerance in mice[63]. This study supports our hypothesis that type II myosins are important for thermogenesis in beige adipocytes.

Type II myosin activity is regulated by phosphorylation at the regulatory light chain subunits (RLC). Takahashi and others found that a type II myosin phosphatase, MYPT1-PP1β, inhibits UCP1 expression. Similarly, using the type II myosin inhibitor blebbistatin we also found

that myosin inhibition reduces UCP1 expression and mitochondrial respiration. As identified from our data, beige adipocytes express multiple myosin isoforms, however Takahashi and others did not investigate which type II myosin isoform may be responsible for regulating UCP1 expression. Our results suggest that Myh9 is a critical isoform that regulates UCP1 expression in beige adipocytes. Aside from the transcriptional regulation of UCP1 mediated through Myh9, we also found that Myh9 affects mitochondrial function.

Loss of Myh9 resulted in stark morphological changes, with more fragmented mitochondria and less mitochondria-lipid droplet contact sites as observed with TEM. After further analysis of mitochondrial health we found that the mitochondria in Myh9KD beige adipocytes were producing more ROS and had a reduced mitochondrial membrane potential suggesting increased mitochondrial stress and dysfunction. To our surprise, live cell mitochondrial imaging identified strikingly reduced mitochondrial motility with Myh9KD. Mitochondrial motility has been known to have important functions in neurons[64], but there has not been any functional characterization of mitochondrial movement in adipocytes. In brown adipose tissue, mitochondria bound to lipid droplets (peri-droplet mitochondria) were found to have unique bioenergetics and composition to support lipid droplet expansion compared to cytoplasmic mitochondria[55]. In our model, it is possible that the actomyosin network may be involved in facilitating peri-droplet mitochondria and cytoplasmic mitochondrial motility within beige adipocytes. Further investigation is required to determine whether Myh9 is directly involved in mitochondrial motility and if the observed loss of mitochondrial motility is a cause of mitochondrial dysfunction seen with Myh9KD.

We are the first to show that type II non-muscle Myh9 is the most abundantly expressed type II myosin in adipocytes. In beige adipocytes, loss of Myh9 resulted in a reduced cellular tension, a loss of UCP1 expression and mitochondrial dysfunction. Questions still remain regarding how the loss of Myh9 alters the transcriptional regulation of UCP1 and mitochondrial bioenergetics. There are likely two scenarios which may act in parallel; 1) Myh9KD leads to a loss of cellular tension and thus alterations in a mechanosensitive transcriptional cascade and 2) the actomyosin network, specifically, Myh9 directly interacts with mitochondria and/or lipid droplets to coordinate bioenergetics in beige adipocytes. Understanding the mechanisms around Myh9 regulation of thermogenesis may spawn novel therapeutic approaches to combat obesity and other metabolic disorders.

Figures

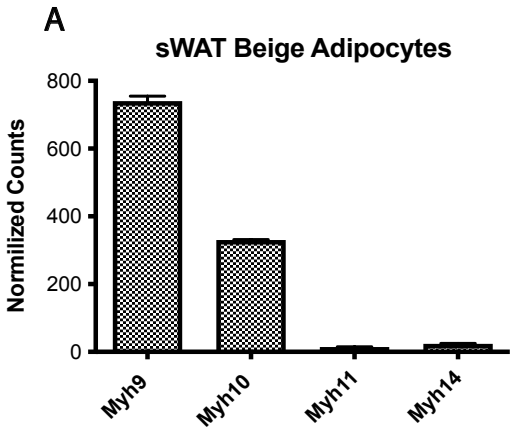
A
sWAT Beige Adipocytes
Normilized Counts
800
600
400
200
0
Myh9
Myh10
Myh11
Myh14

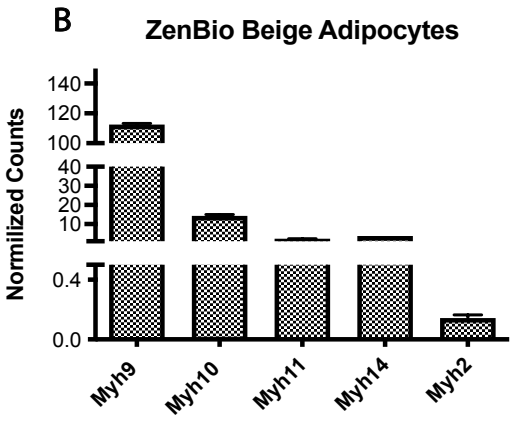
B
ZenBio Beige Adipocytes
Normilized Counts
140
120
100
40
30
20
10
0.4
0.0
Myh9
Myh10
Myh11
Myh14
Myh2

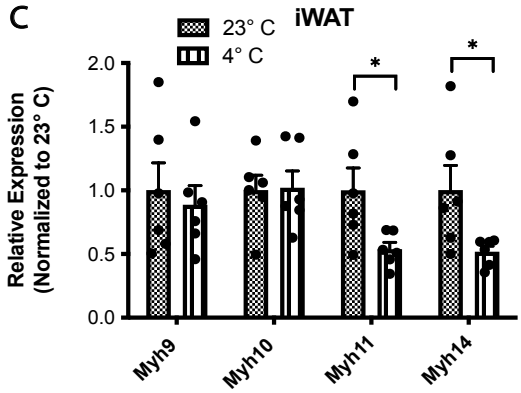
C
iWAT
23° C
4° C
Relative Expression
(Normalized to 23° C)
2.0
1.5
1.0
0.5
0.0
*
*
Myh9
Myh10
Myh11
Myh14

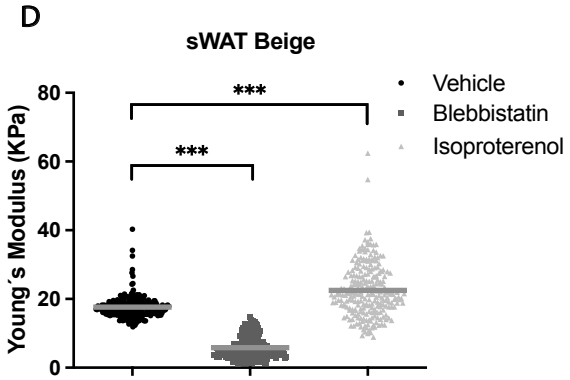
D
sWAT Beige
Young´s Modulus (KPa)
80
60
40
20
0
***
***
Vehicle
Blebbistatin
Isoproterenol

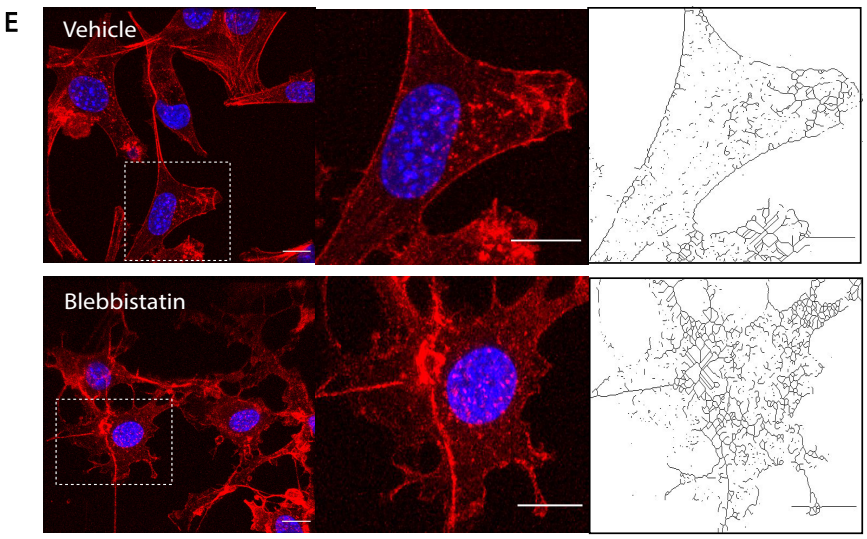
E
Vehicle
Blebbistatin

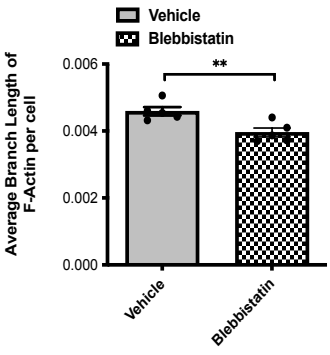
F
Vehicle
Blebbistatin
Average Branch Length of
F-Actin per cell
0.006
0.004
0.002
0.000
**
Vehicle
Blebbistatin

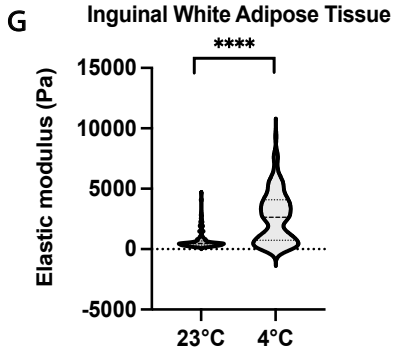

Figure 1. Type II myosins induce tension in beige adipocytes. A. Normalized transcript counts from RNAseq of mouse beige adipocytes, n=3 biologically independent samples. B. Normalized transcript counts from RNAseq of human beige adipocytes, n=3 biologically independent samples. C. Relative mRNA expression of inguinal white adipose tissue from mice housed at either 23°C or 4°C for 24 hours, n=6 mice/group. D. Atomic force microscopy of mouse beige adipocytes treated overnight with 100uM of blebbistatin or for 30 minutes with 1uM isoproterenol n=5 cells/group. E. Immunofluorescence microscopy of mouse beige adipocytes treated overnight with 100uM of blebbistatin, stained for actin (red). F. Average F-actin branch length of control or blebbistatin treated cells as seen in Fig. E, n=5 cells/group. G. Atomic force microscopy of inguinal white adipose tissue from mice housed at either 23°C or 4°C for 24 hours n=2 tissue pads/group.

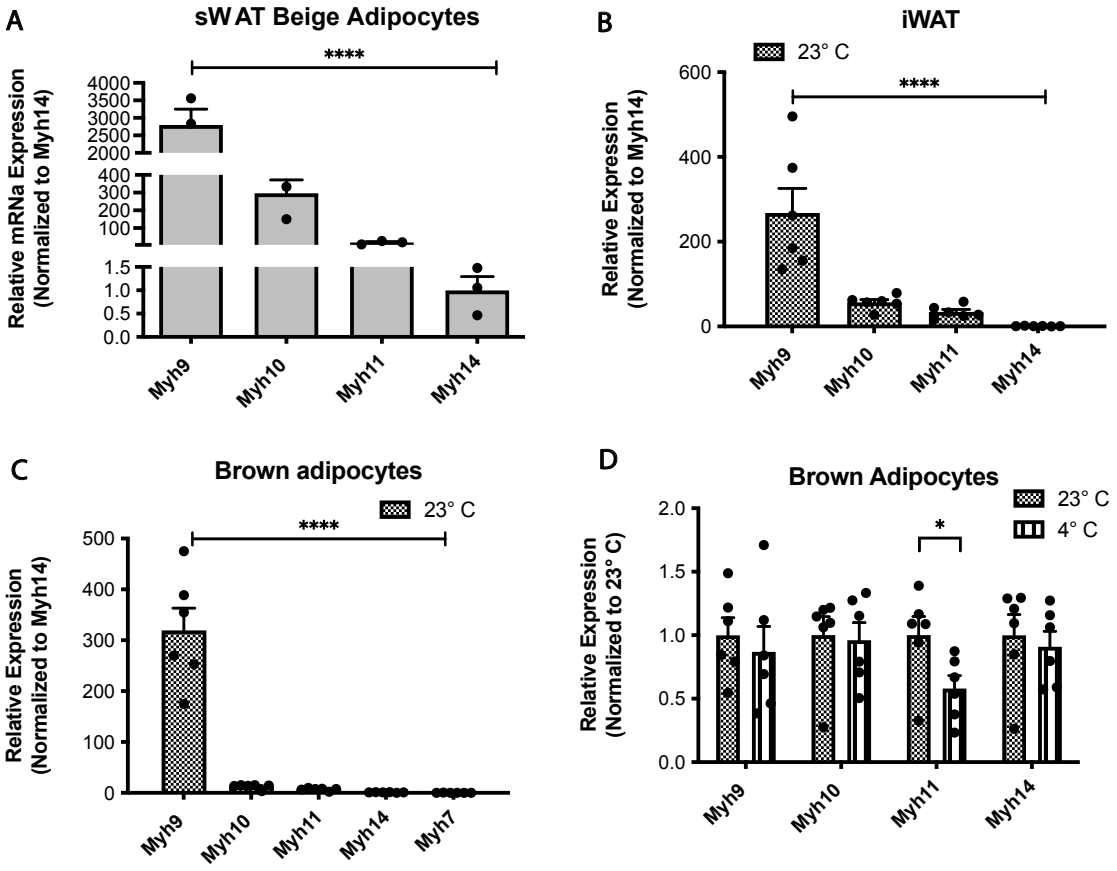

Figure 2. Type II myosin expression in iWAT and BAT. A. Relative mRNA expression from mouse beige adipocytes, n=3 independent biological replicates. B. Relative mRNA expression from inguinal white tissue of mice housed at 23°C, n=6 independent biological replicates. C. Relative mRNA expression from brown adipose tissue of mice housed at 23°C, n=6 independent biological replicates. D. Relative mRNA expression from brown adipose tissue of mice housed at either 23°C or 4°C for 24 hours, n=6 independent biological replicates.

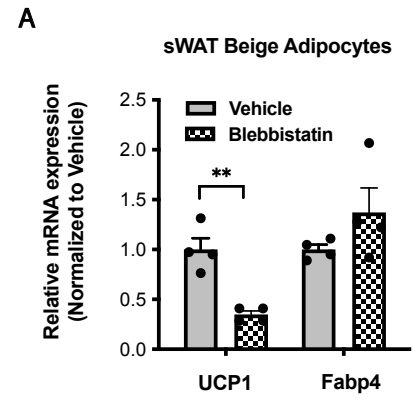
A
sWAT Beige Adipocytes
Relative mRNA expression (Normalized to Vehicle)
Vehicle
Blebbistatin
**
UCP1
Fabp4

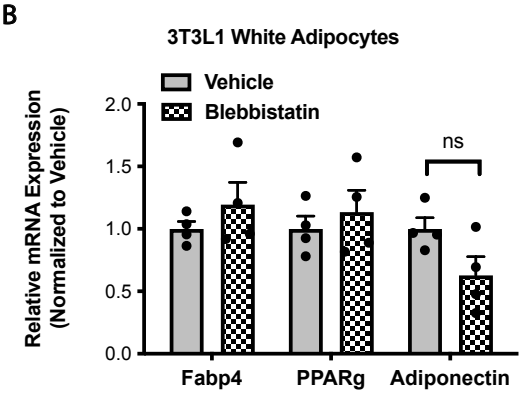
B
3T3L1 White Adipocytes
Relative mRNA Expression (Normalized to Vehicle)
Vehicle
Blebbistatin
ns
Fabp4
PPARg
Adiponectin

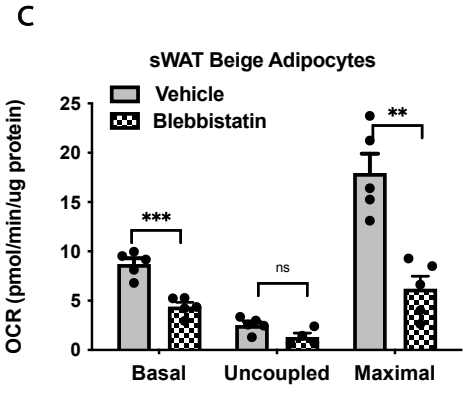
C
sWAT Beige Adipocytes
OCR (pmol/min/ug protein)
Vehicle
Blebbistatin
***
ns
**
Basal
Uncoupled
Maximal

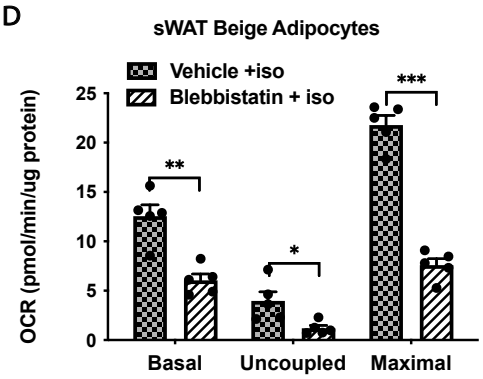
D
sWAT Beige Adipocytes
OCR (pmol/min/ug protein)
Vehicle +iso
Blebbistatin + iso
**
*
***
Basal
Uncoupled
Maximal

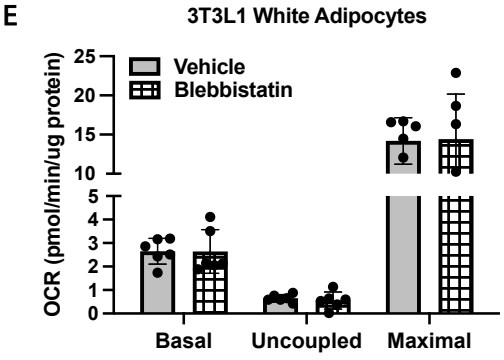
E
3T3L1 White Adipocytes
OCR (pmol/min/ug protein)
Vehicle
Blebbistatin
Basal
Uncoupled
Maximal

F

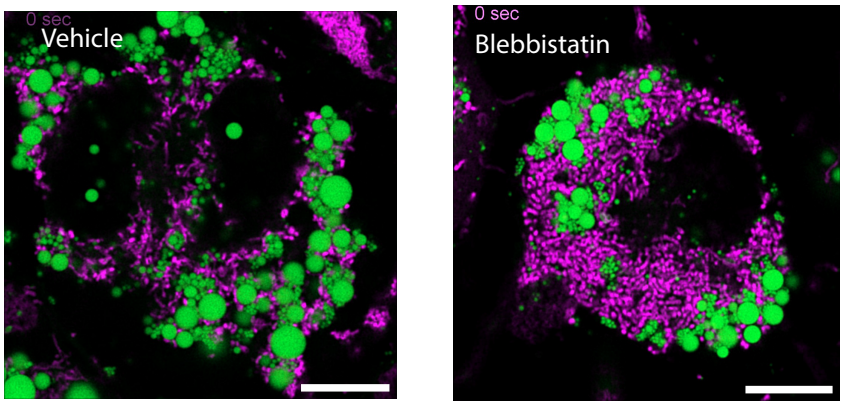

Figure 3. Type II myosins regulate beige adipocyte thermogenic function. A. Relative mRNA expression from mouse beige adipocytes treated overnight with 100uM blebbistatin or control, n=4 biologically independent samples. B. Relative mRNA expression from 3T3L1 white adipocytes treated overnight with 100uM blebbistatin or control, n=4 biologically independent samples. C-D. Oxygen consumption rates from mouse beige adipocytes. C. Cells treated overnight with 100uM blebbistatin or control, n=5 biologically independent samples. D. Cells treated overnight with 100uM blebbistatin and for 45 minutes with 1uM isoproterenol, n=5 biologically independent samples. E. Oxygen consumption rates from white adipocytes treated overnight with 100uM blebbistatin or control, n=6 biologically independent samples. F. Immunofluorescent microcopy of mouse beige adipocytes treated overnight with 100uM blebbistatin or control and stained for lipid (green) and mitochondria (purple).

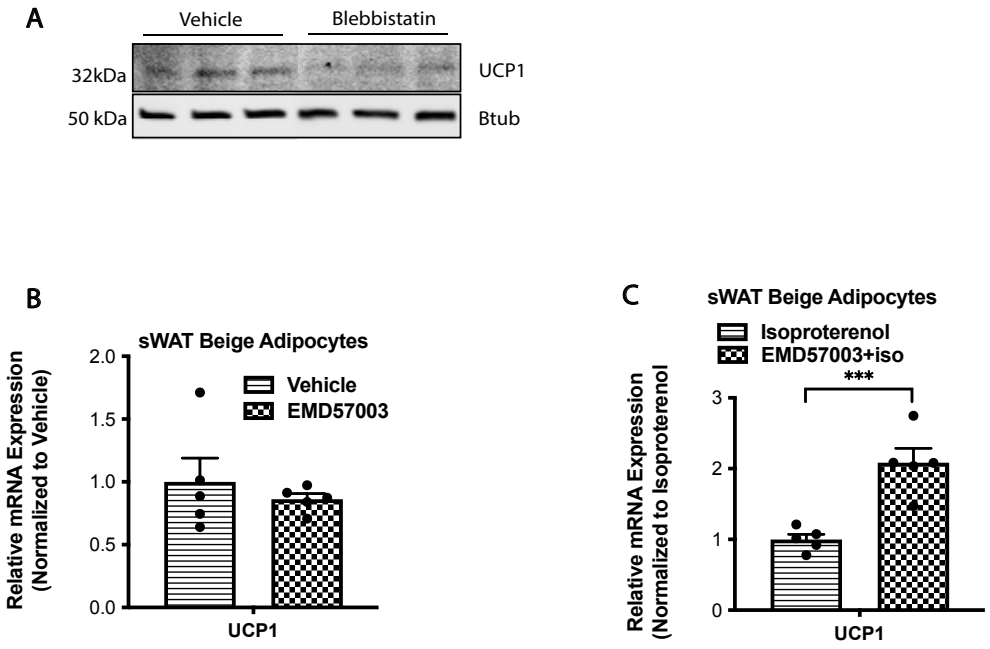

Figure 4. Targeting type II myosin activity with blebbistatin and EMD57003. A. Western blot of UCP1 from mouse beige adipocytes treated overnight with 100uM of blebbistatin, n=3 independent biological replicates. B. Relative mRNA expression of mouse beige adipocytes treated overnight with 10uM of EMD57003 or control, n=5 independent biological replicates. C. Relative mRNA expression of mouse beige adipocytes treated overnight with 10uM of EMD57003 and 1 hour with 1uM of isoproterenol or 1uM of isoproterenol, n=5 independent biological replicates.

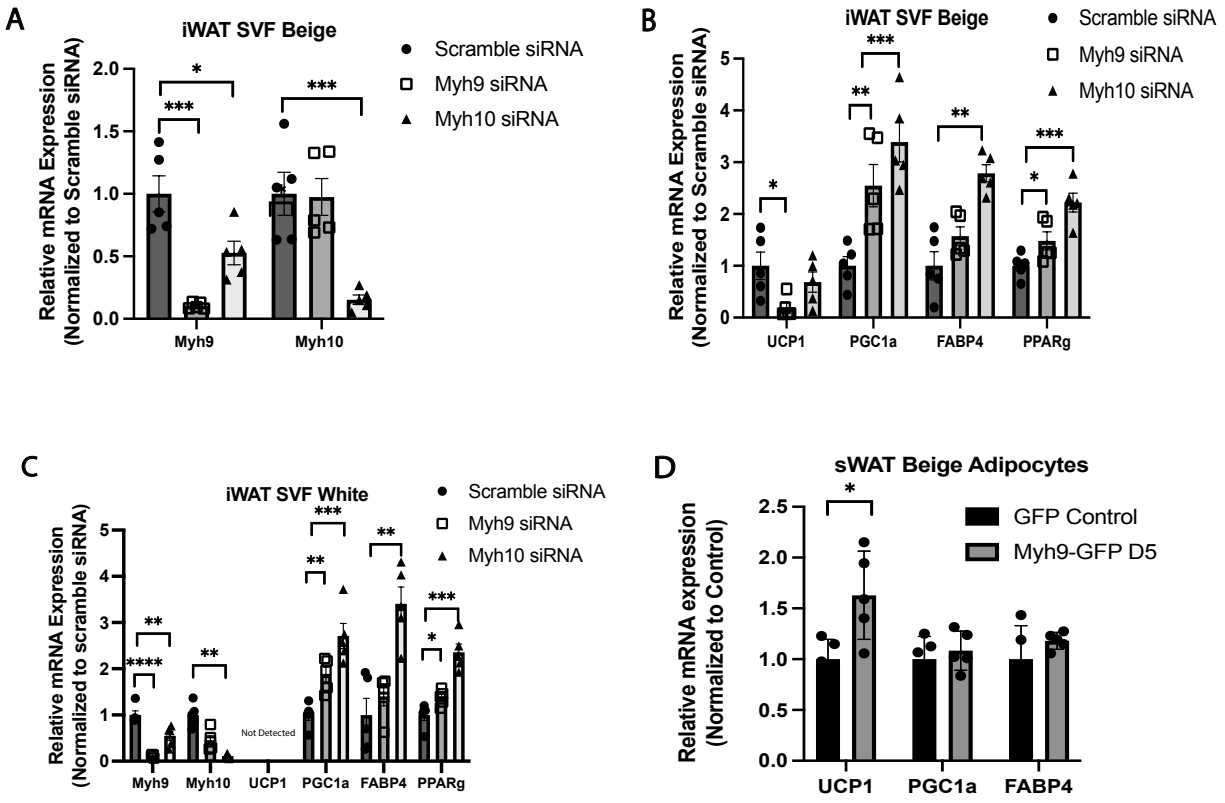

Figure 5. SVF iWAT siRNA screen. A-C. Relative mRNA expression from stromal vascular fraction (SVF) of inguinal white adipose tissue transfected with either scramble, Myh9, or Myh10 targeting siRNA. A-B. Relative mRNA expression of SVF differentiated toward beige adipocytes, n=5 biologically independent samples. C. Relative mRNA expression of SVF differentiated toward white adipocytes, n=5 biologically independent samples. D. Relative mRNA expression from mouse beige adipocytes transfected with either GFP control plasmid or Myh9-GFP tagged plasmid on day 5 of differentiation, n=5 biologically independent samples.

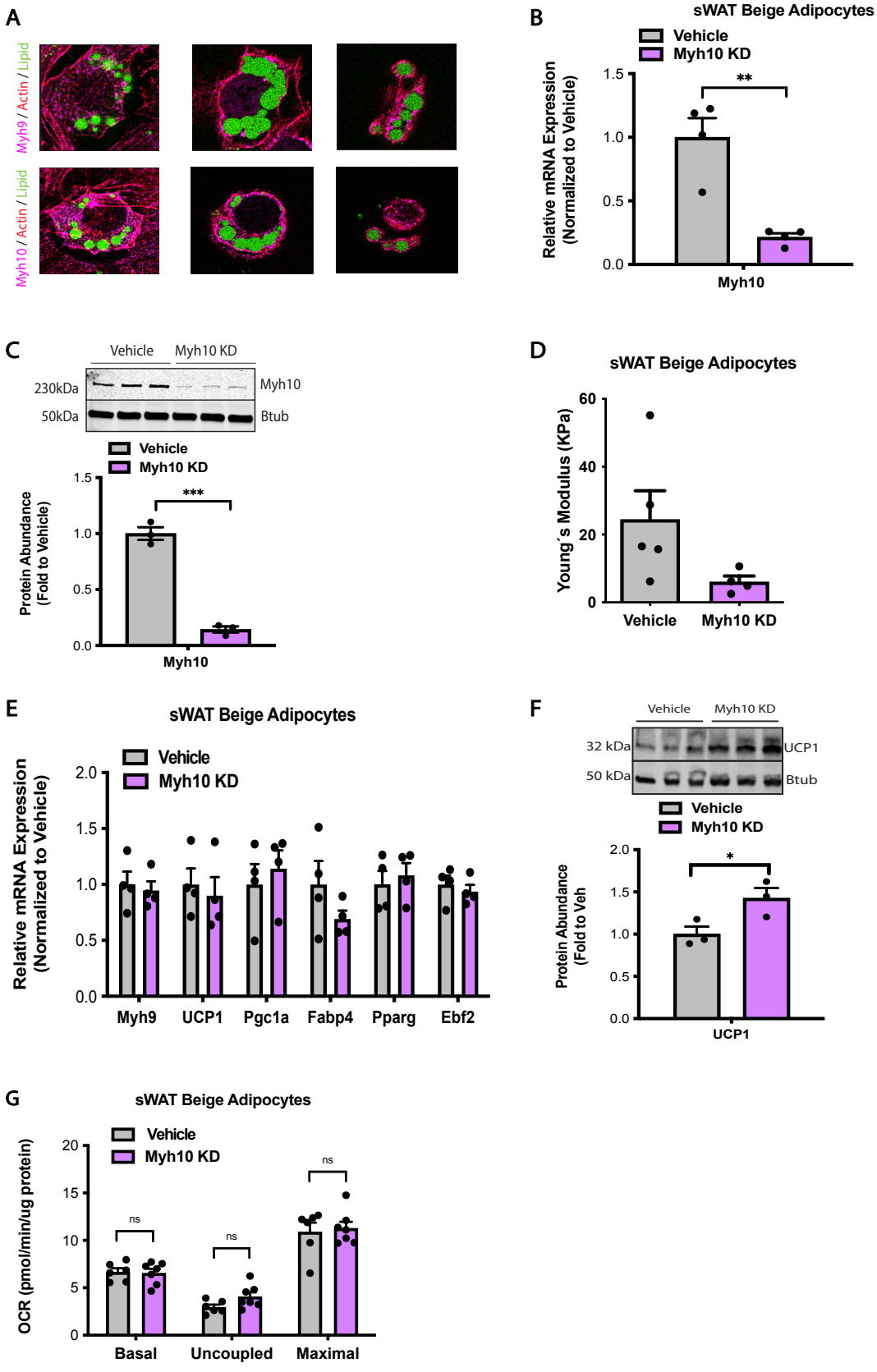
A
Myh9 / Actin / Lipid
Myh10 / Actin / Lipid
B
sWAT Beige Adipocytes
Vehicle
Myh10 KD
Relative mRNA Expression (Normalized to Vehicle)
**
Myh10
C
Vehicle
Myh10 KD
230kDa
50kDa
Myh10
Btub
Protein Abundance (Fold to Vehicle)
***
Myh10
D
sWAT Beige Adipocytes
Young´s Modulus (KPa)
Vehicle
Myh10 KD
E
sWAT Beige Adipocytes
Relative mRNA Expression (Normalized to Vehicle)
Myh9
UCP1
Pgc1a
Fabp4
Pparg
Ebf2
F
Vehicle
Myh10 KD
32 kDa
50 kDa
UCP1
Btub
Protein Abundance (Fold to Veh
*
UCP1
G
sWAT Beige Adipocytes
OCR (pmol/min/ug protein)
ns
Basal
Uncoupled
Maximal

Figure 6. Type II Myh10 does not regulate thermogenesis in beige adipocytes. Knockdown (KD) of Myh10 is during 7 days of differentiation unless otherwise stated. A. Immunofluorescence microscopy of fixed mouse beige adipocytes stained for either Myh9 or Myh10 (purple), lipid (green), and actin (red). B. Relative Myh10 mRNA expression from mouse beige adipocytes, vehicle vs Myh10 KD, n=4 biological independent samples. C. Western blot of Myh10 from mouse beige adipocytes, vehicle vs Myh10KD, n=3 biological independent samples. D. Atomic force microscopy from mouse beige adipocytes, vehicle vs Myh10KD, n=5-6 cells per group. E. Relative mRNA expression of adipogenic genes from mouse beige adipocytes, vehicle vs Myh10KD, n=4 biological independent samples. F. Western blot of UCP1 from mouse beige adipocytes, vehicle vs Myh10KD, n=3 biological independent samples. G. Oxygen consumption rates from mouse beige adipocytes, vehicle vs Myh10KD, n=6-7 biological independent samples.

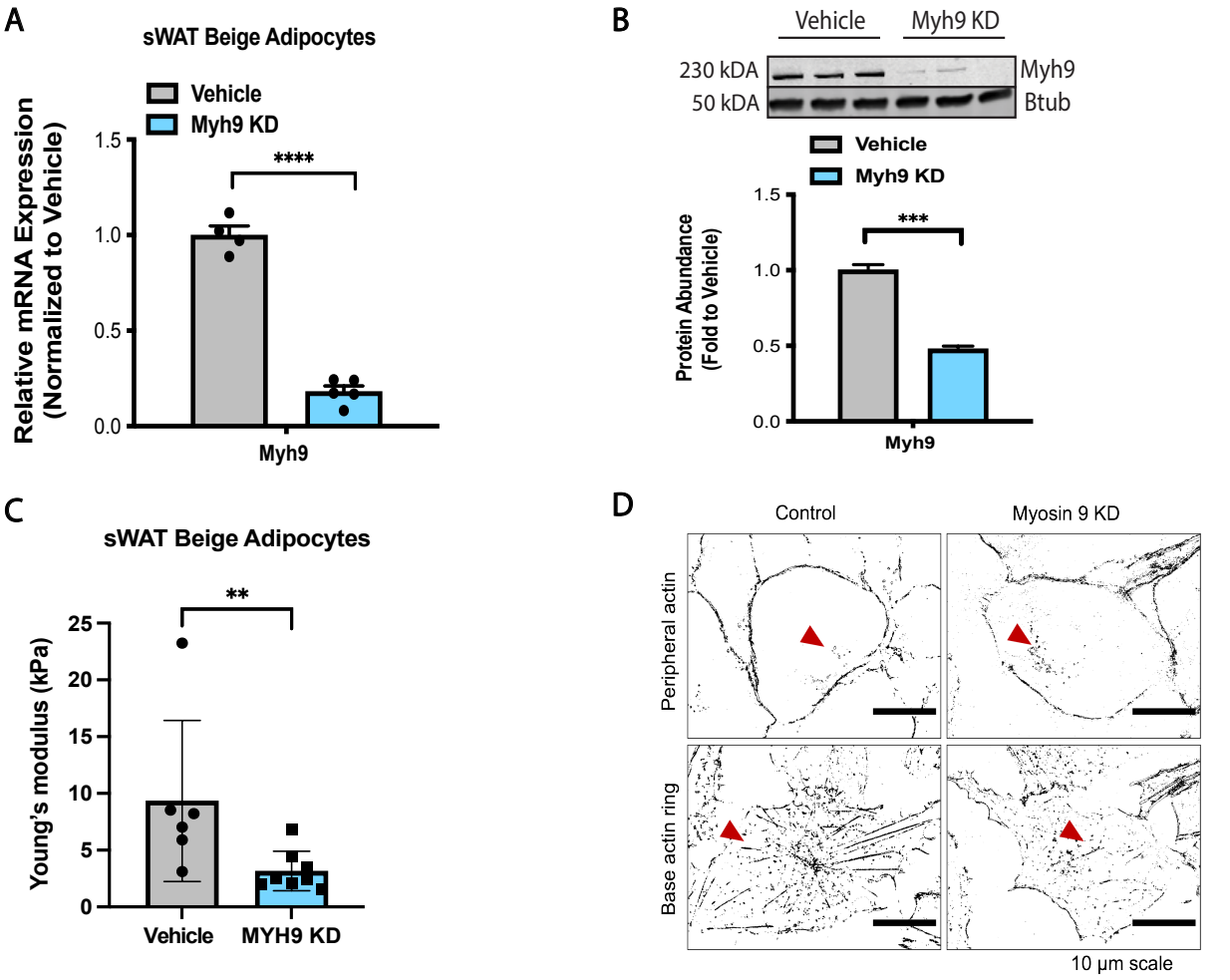
A
sWAT Beige Adipocytes
Vehicle
Myh9 KD
Relative mRNA Expression (Normalized to Vehicle)
****
Myh9
B
Vehicle
Myh9 KD
230 kDA
50 kDA
Myh9
Btub
Protein Abundance (Fold to Vehicle)
***
Myh9
C
sWAT Beige Adipocytes
Young's modulus (kPa)
**
Vehicle
MYH9 KD
D
Control
Myosin 9 KD
Peripheral actin
Base actin ring
10 µm scale
E
sWAT Beige Adipocytes
Relative mRNA Expression (Normalized to Vehicle)
*
Myh10
UCP1
Pgc1a
Fabp4
Pparg
Ebf2
F
32 kDA
50 kDA
UCP1
Protein Abundance (Fold to Vehicle)
**

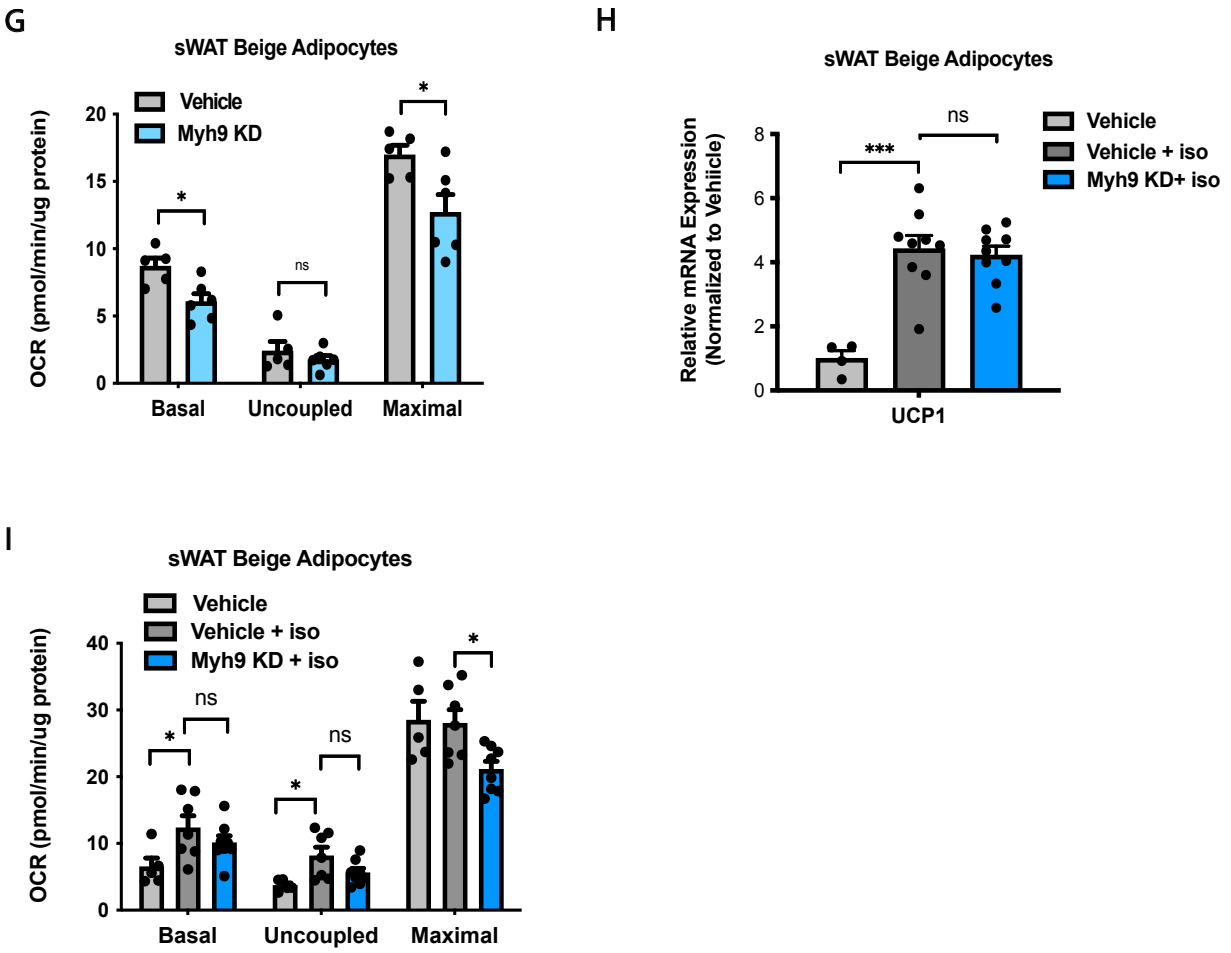

Figure 7. Type II Myh9 but not Myh10 regulates thermogenesis in beige adipocytes. Knockdown (KD) of Myh9 is during 7 days of differentiation unless otherwise stated. A. Relative Myh9 mRNA expression from mouse beige adipocytes, vehicle vs Myh9KD, n=4 biological independent samples. B. Western blot of Myh9 from mouse beige adipocytes, vehicle vs Myh9KD, n=3 biological independent samples. C. Atomic force microscopy from mouse beige adipocytes, vehicle vs Myh9KD, n=5-6 cells per group. D. Structured illumination microscopy from mouse beige adipocytes, vehicle vs Myh9KD, image skeletonized to portray peripheral and base actin network. E. Relative mRNA expression of adipogenic genes from mouse beige adipocytes, vehicle vs Myh9KD, n=4 biological independent samples. F. Western blot UCP1 from mouse beige adipocytes, vehicle vs Myh9KD, n=3 independent biological replicates. G. Oxygen consumption rates from mouse beige adipocytes, vehicle vs Myh9KD, n=5-6 biological independent samples. H. Relative mRNA expression from mouse beige adipocytes, vehicle vs Myh9KD, treated for 1 hour with or without 1uM of isoproterenol, n=4-8 independent biological replicates. I. Oxygen consumption rates from mouse beige adipocytes, vehicle vs Myh9KD, treated for 1 hour with or without 1uM of isoproterenol, n=5-7 independent biological replicates.

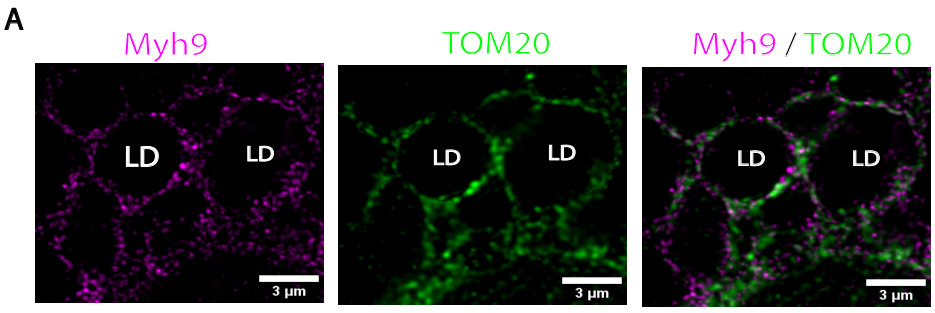
A
Myh9
TOM20
Myh9 / TOM20
LD
LD
3 μm

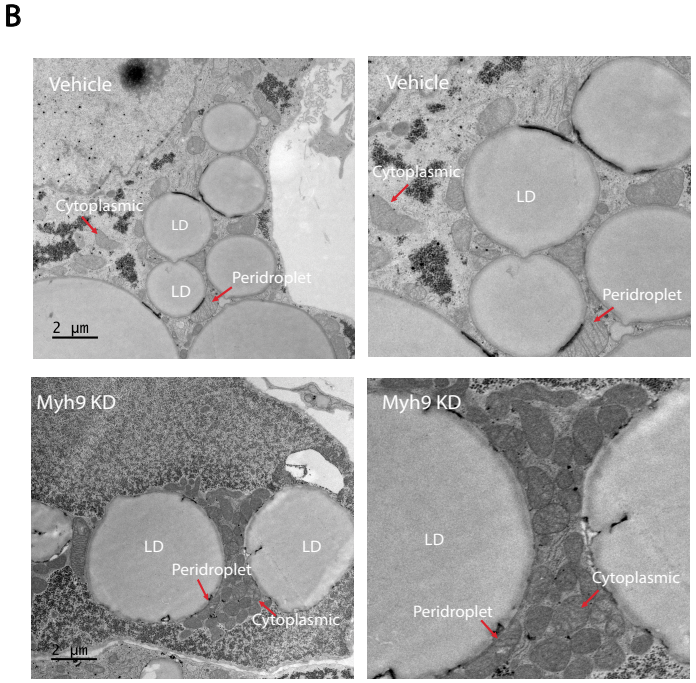
B
Vehicle
Cytoplasmic
LD
Peridroplet
2 μm
Myh9 KD

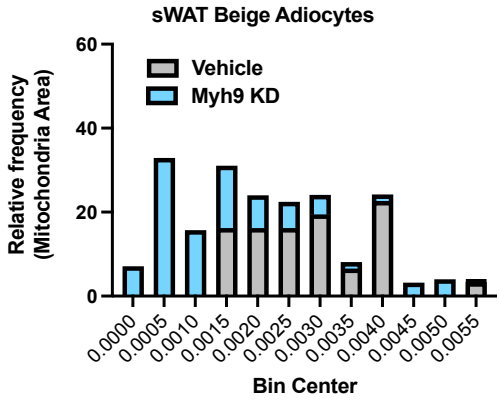
C
sWAT Beige Adiocytes
Vehicle
Myh9 KD
Relative frequency (Mitochondria Area)
Bin Center

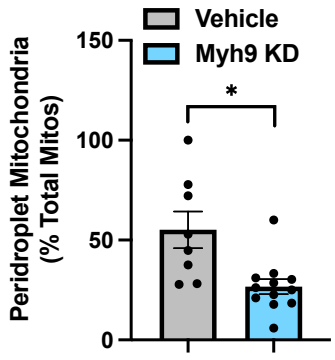
D
Vehicle
Myh9 KD
Peridroplet Mitochondria (% Total Mitos)
*

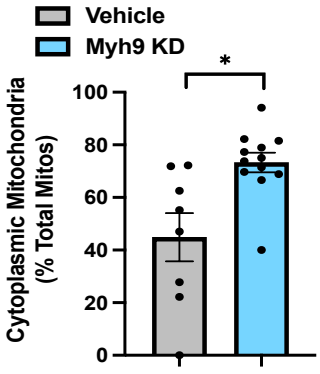
E
Vehicle
Myh9 KD
Cytoplasmic Mitochondria (% Total Mitos)
*

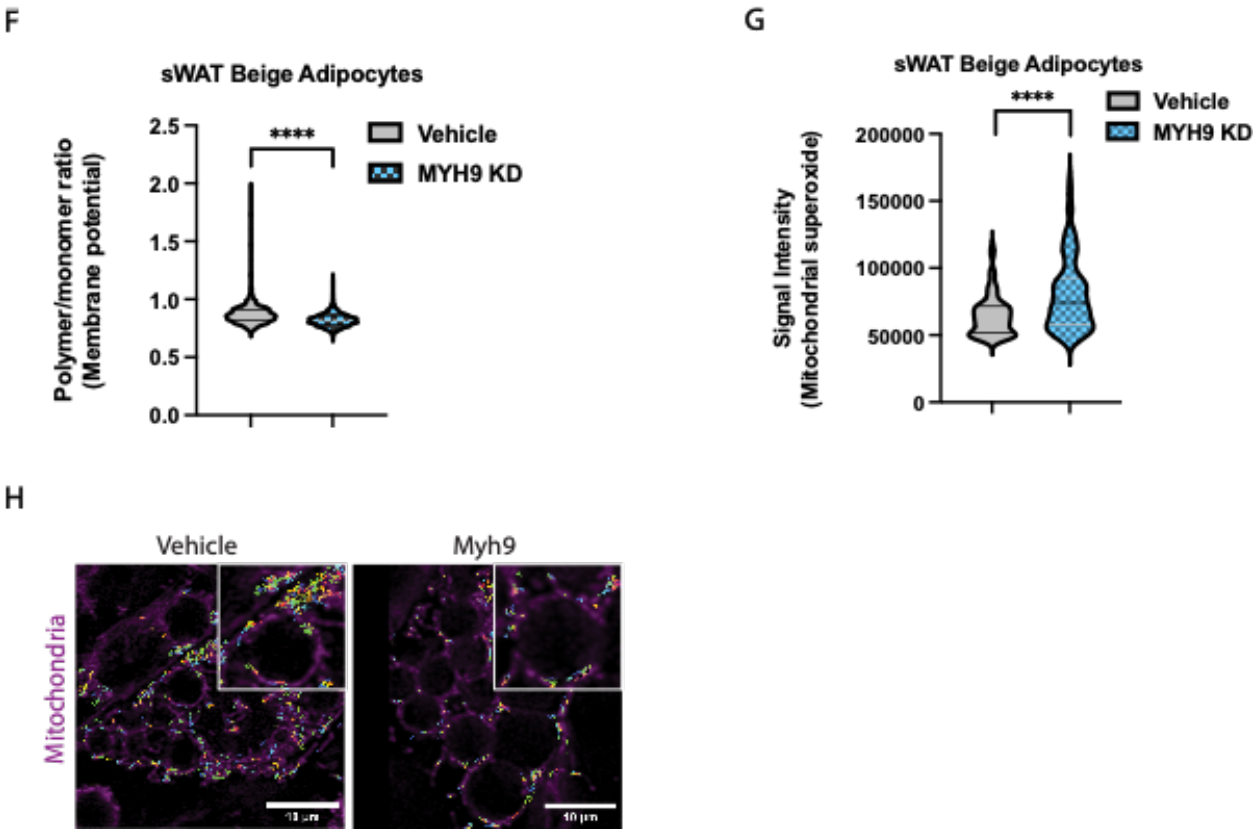

Figure 8. Loss of Myh9 impairs BeAT mitochondrial function. Knockdown (KD) of Myh9 is during 7 days of differentiation unless otherwise stated. A. Immunofluorescent microscopy of mouse beige adipocytes stained for Myh9 (purple) or mitochondria (green), lipid droplets labeled (LD). B-E. Transmission electron microscopy from mouse beige adipocytes, vehicle vs Myh9KD. B. Mitochondria in contact with lipid droplets (LD) are labeled as peridroplet mitochondria and mitochondria without any LD contact are labeled cytoplasmic. C. Frequency distribution of mitochondria area from TEM images, n=8-12 images per group. D-E. Number peridroplet and cytoplasmic mitochondria as a percent of total mitochondria, n=8-12 images per group. F. Mitochondrial membrane potential from mouse beige adipocytes, vehicle vs Myh9KD, n=6-7 cells/group. G. Mitochondrial superoxide production from mouse beige adipocytes, vehicle vs Myh9KD, n=6-7 cells/group. H. Heatmap of mitochondrial motility from live cell mitochondria imaging, vehicle vs Myh9KD.

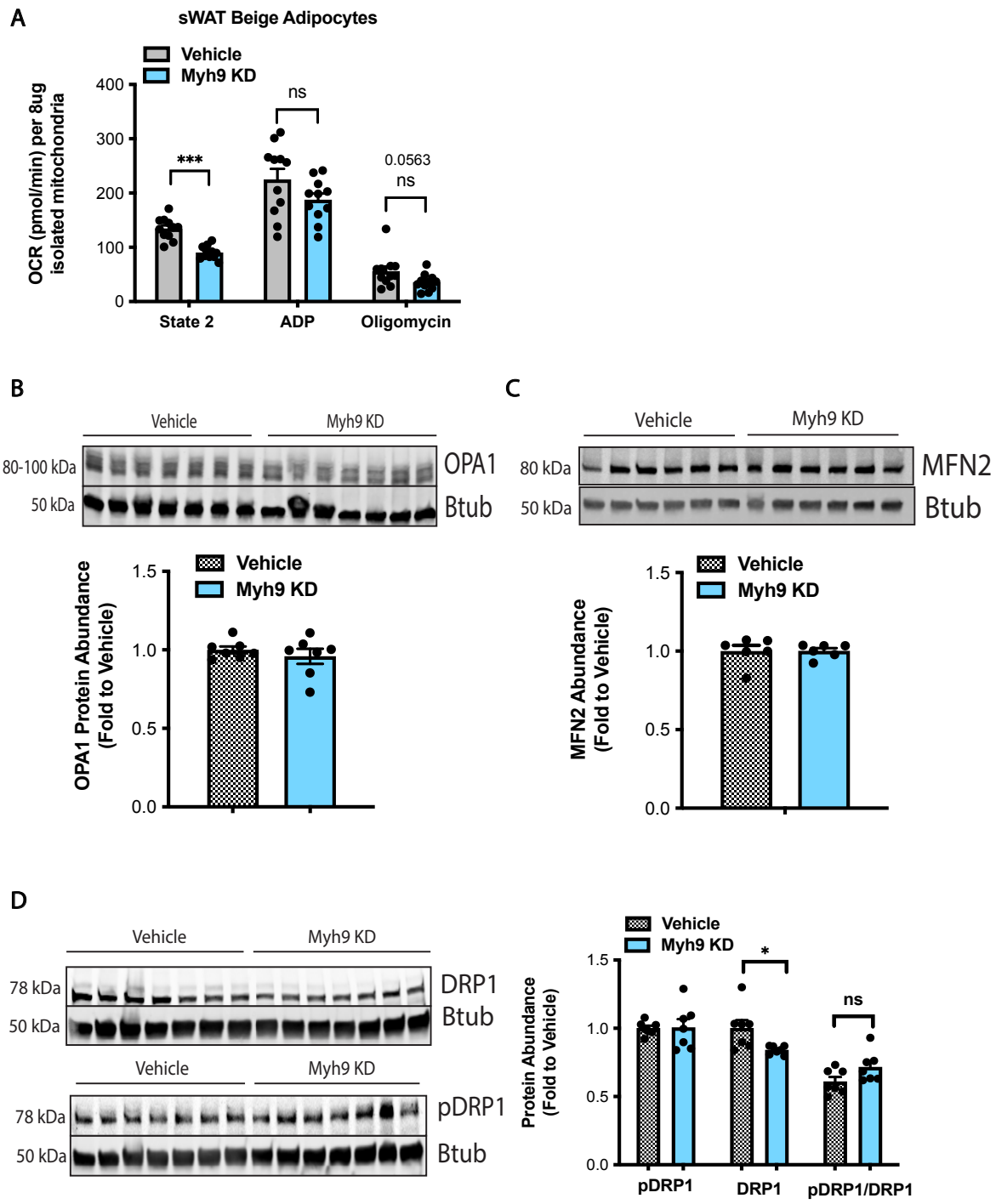

Figure 9. Mitochondrial fission/fusion protein abundance. Knockdown (KD) of Myh9 is during 7 days of differentiation unless otherwise stated. A. Oxygen consumption rates from mitochondria isolated from mouse beige adipocytes, vehicle vs Myh9KD, n=10 independent biological replicates. B-D. Western blot of mitochondria fission/fusion proteins from mouse beige adipocytes, vehicle vs Myh9KD, n=6-7 independent biological replicates.

A

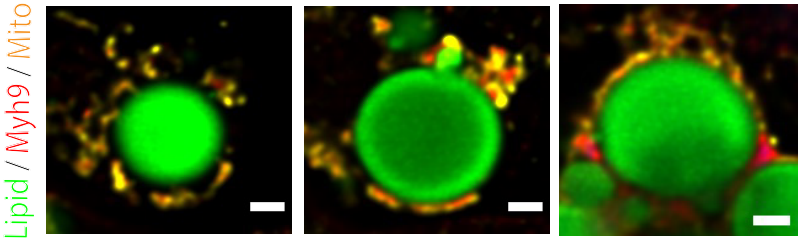
Lipid / Myh9 / Mito

B

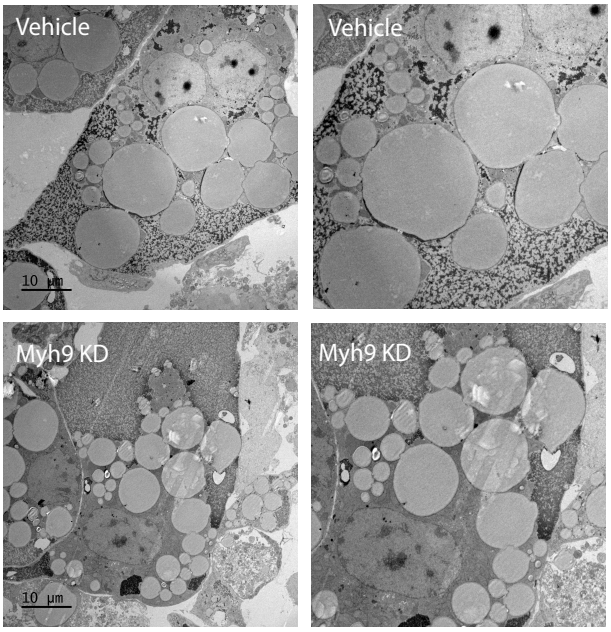
Vehicle
Vehicle
10 μm
Myh9 KD
Myh9 KD
10 μm

C

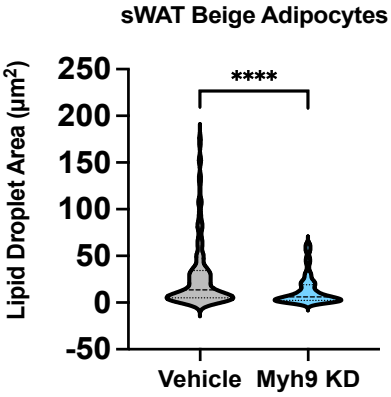
sWAT Beige Adipocytes
Lipid Droplet Area (μm²)
250
200
150
100
50
0
-50
****
Vehicle
Myh9 KD

D

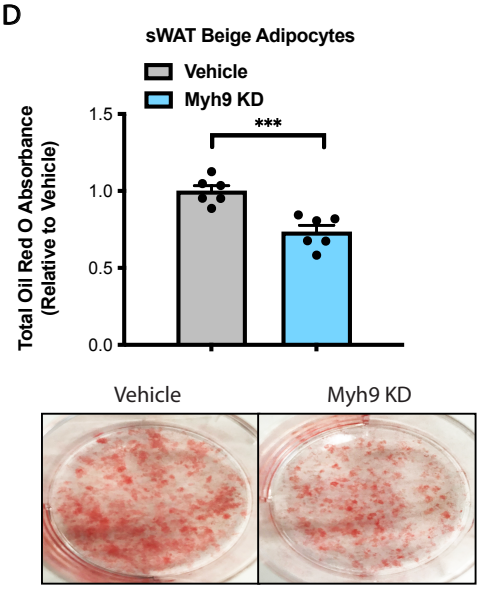
sWAT Beige Adipocytes
Vehicle
Myh9 KD
Total Oil Red O Absorbance (Relative to Vehicle)
1.5
1.0
0.5
0.0
***
Vehicle
Myh9 KD

E

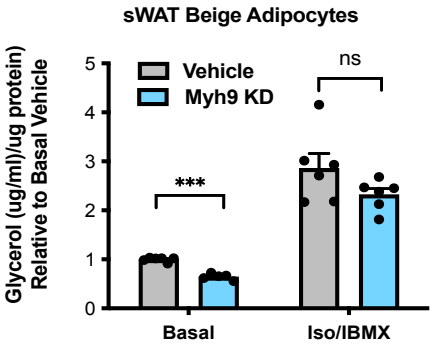
sWAT Beige Adipocytes
Vehicle
Myh9 KD
Glycerol (ug/ml)/ug protein) Relative to Basal Vehicle
5
4
3
2
1
0
***
ns
Basal
Iso/IBMX

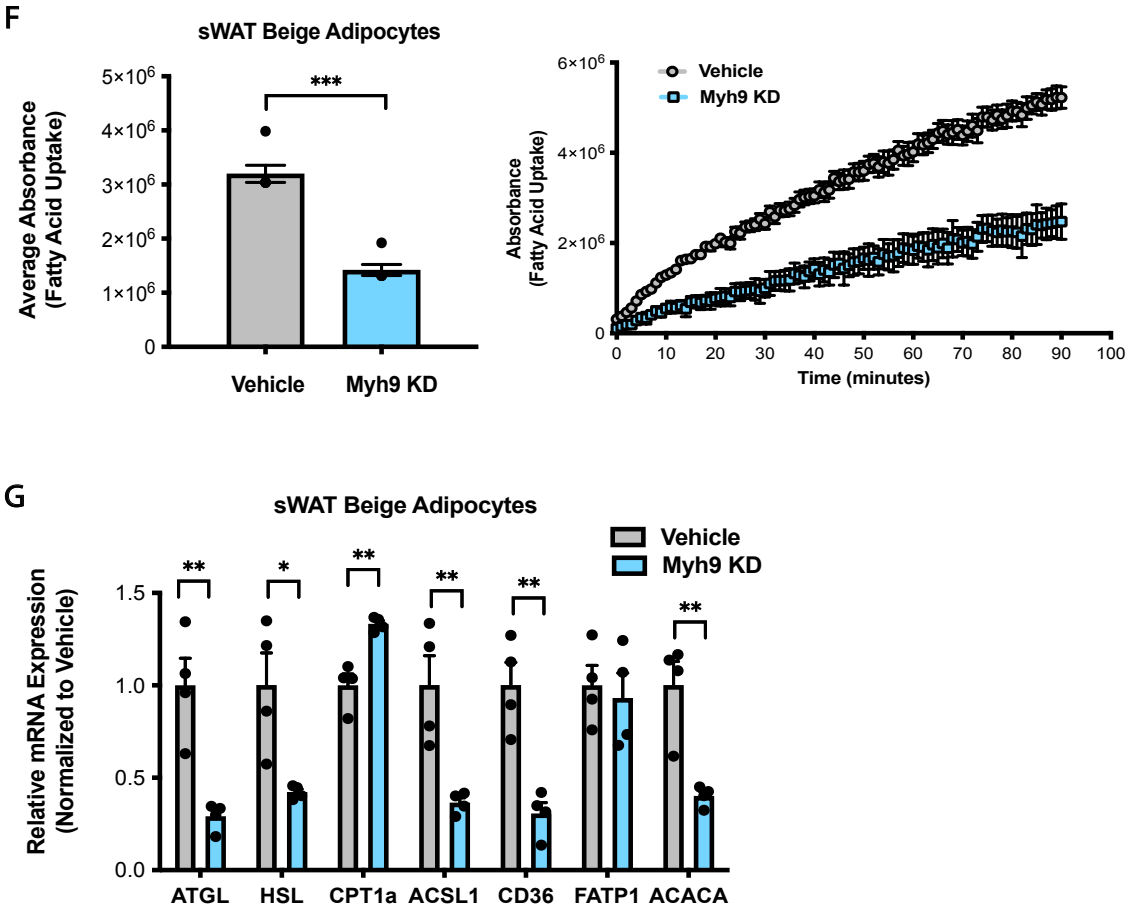

Figure 10. Loss of Myh9 impairs BeAT lipid metabolism. Knockdown (KD) of Myh9 is during 7 days of differentiation unless otherwise stated. A. Immunofluorescent microscopy of mouse beige adipocytes stained with Myh9 (red) or mitochondria (yellow), lipid droplets (green). B-C. Transmission electron microscopy from mouse beige adipocytes, vehicle vs Myh9KD. C. Lipid droplet area from TEM images n=10-12 cells/group. D. Oil red O staining from mouse beige adipocytes, vehicle vs Myh9KD, n=6 biological independent samples. E. Glycerol levels from mouse beige adipocytes, vehicle vs Myh9KD, n=5 biological independent samples. F. Fatty acid uptake assay from mouse beige adipocytes, vehicle vs Myh9KD, n=4 biological independent samples. G. Relative mRNA expression of lipid metabolism genes from mouse beige adipocytes, vehicle vs Myh9KD, n=4 biological independent samples.

A

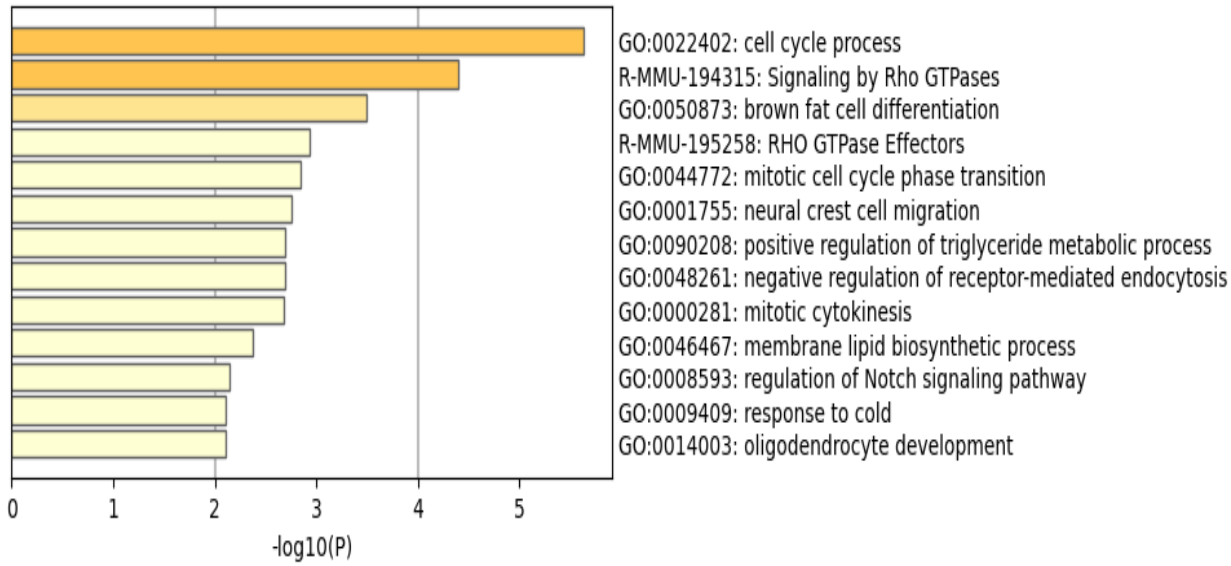
GO:0022402: cell cycle process
R-MMU-194315: Signaling by Rho GTPases
GO:0050873: brown fat cell differentiation
R-MMU-195258: RHO GTPase Effectors
GO:0044772: mitotic cell cycle phase transition
GO:0001755: neural crest cell migration
GO:0090208: positive regulation of triglyceride metabolic process
GO:0048261: negative regulation of receptor-mediated endocytosis
GO:0000281: mitotic cytokinesis
GO:0046467: membrane lipid biosynthetic process
GO:0008593: regulation of Notch signaling pathway
GO:0009409: response to cold
GO:0014003: oligodendrocyte development
0
1
2
3
4
5
-log10(P)

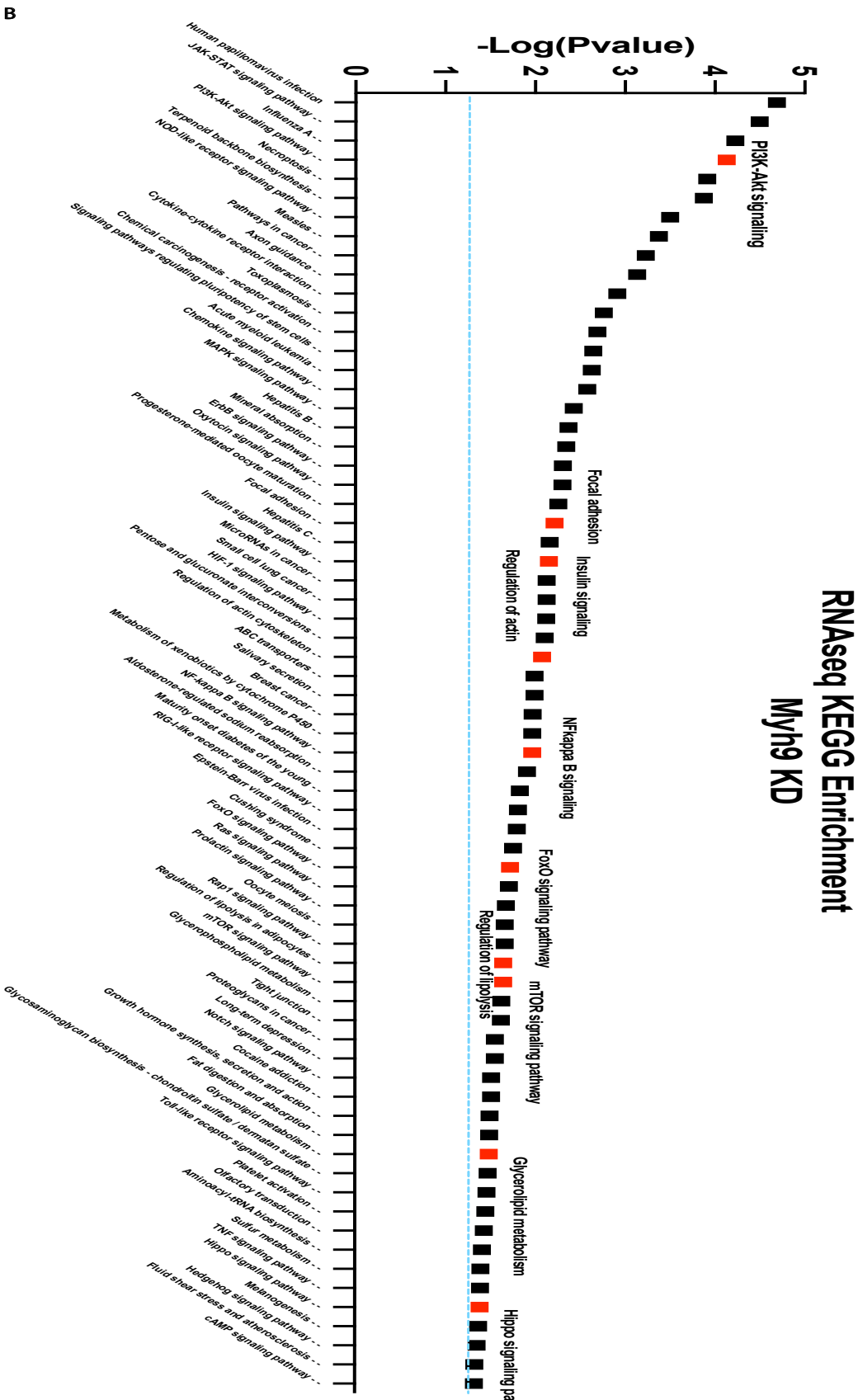
B
RNAseq KEGG Enrichment
Myh9 KD
-Log(Pvalue)
0
1
2
3
4
5
PI3K-Akt signaling
Focal adhesion
Insulin signaling
Regulation of actin
NFkappa B signaling
FoxO signaling pathway
mTOR signaling pathway
Regulation of lipolysis
Glycerolipid metabolism
Hippo signaling pathway
Human papillomavirus infection
JAK-STAT signaling pathway
Influenza A
PI3K-Akt signaling pathway
Necroptosis
Terpenoid backbone biosynthesis
NOD-like receptor signaling pathway
Measles
Pathways in cancer
Axon guidance
Cytokine-cytokine receptor interaction
Toxoplasmosis
Chemical carcinogenesis - receptor activation
Signaling pathways regulating pluripotency of stem cells
Acute myeloid leukemia
Chemokine signaling pathway
MAPK signaling pathway
Hepatitis B
Mineral absorption
ErbB signaling pathway
Oxytocin signaling pathway
Progesterone-mediated oocyte maturation
Focal adhesion
Hepatitis C
Insulin signaling pathway
MicroRNAs in cancer
Small cell lung cancer
HIF-1 signaling pathway
Pentose and glucuronate interconversions
Regulation of actin cytoskeleton
ABC transporters
Salivary secretion
Breast cancer
Metabolism of xenobiotics by cytochrome P450
NF-kappa B signaling pathway
Aldosterone-regulated sodium reabsorption
Maturity onset diabetes of the young
RIG-I-like receptor signaling pathway
Epstein-Barr virus infection
Cushing syndrome
FoxO signaling pathway
Ras signaling pathway
Prolactin signaling pathway
Oocyte meiosis
Rap1 signaling pathway
Regulation of lipolysis in adipocytes
mTOR signaling pathway
Glycerophospholipid metabolism
Tight junction
Proteoglycans in cancer
Long-term depression
Notch signaling pathway
Cocaine addiction
Growth hormone synthesis, secretion and action
Fat digestion and absorption
Glycerolipid metabolism
Glycosaminoglycan biosynthesis - chondroitin sulfate / dermatan sulfate
Toll-like receptor signaling pathway
Platelet activation
Olfactory transduction
Aminoacyl-tRNA biosynthesis
Sulfur metabolism
TNF signaling pathway
Hippo signaling pathway
Melanogenesis
Hedgehog signaling pathway
Fluid shear stress and atherosclerosis
cAMP signaling pathway

C

Rank	Motif	Name	P-value	log P-pvalue	q-value (Benjamini)
1		Klf9(Zf)/GBM-Klf9-ChIP-Seq(GSE62211)/Homer	1e-2	-6.207e+00	0.7334
2		Klf4(Zf)/mES-Klf4-ChIP-Seq(GSE11431)/Homer	1e-2	-6.129e+00	0.7334
3		KLF5(Zf)/LoVo-KLF5-ChIP-Seq(GSE49402)/Homer	1e-2	-5.728e+00	0.7334
4		Sp1(Zf)/Promoter/Homer	1e-2	-5.194e+00	0.7334
5		KLF10(Zf)/HEK293-KLF10.GFP-ChIP-Seq(GSE58341)/Homer	1e-2	-5.028e+00	0.7334

D

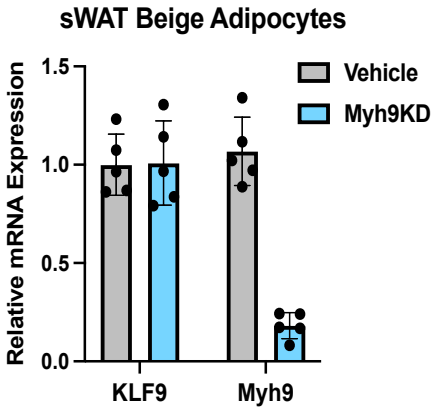

E

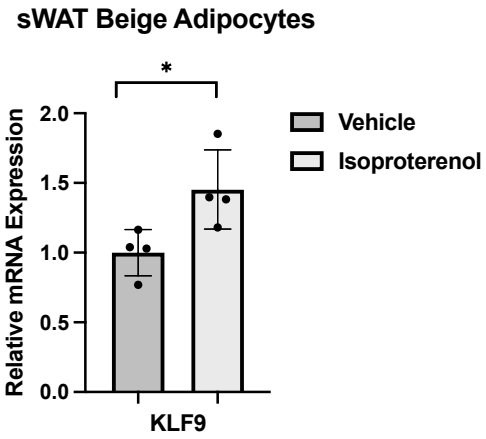

F

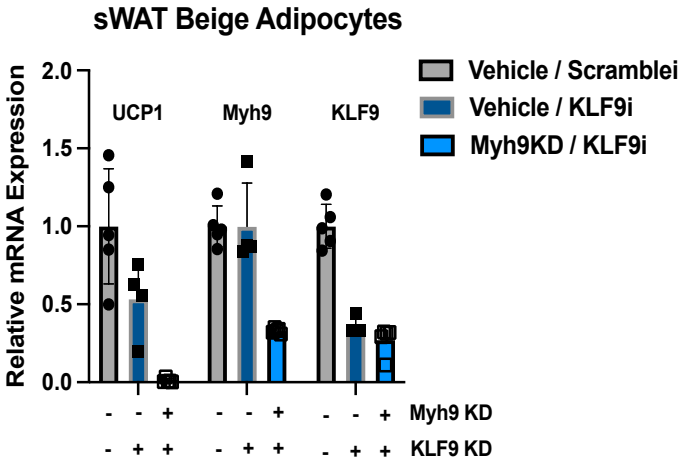

Figure 11. RNAseq of Myh9 knockdown in beige adipocytes. Knockdown (KD) of Myh9 is during 7 days of differentiation. A. Gene Ontology (GO) pathway analysis of downregulated pathways from Myh9KDmouse beige adipocytes. B. KEGG pathway analysis of downregulated pathways from Myh9Kd mouse beige adipocytes with
C. Homer motif analysis of the most downregulated genes from Myh9KD mouse beige adipocytes. D. Relative mRNA expression from mouse beige adipocytes, vehicle vs Myh9KD, n=5 independent biological replicates. E. Relative mRNA expression from mouse beige adipocytes, vehicle vs Myh9KD, treated with or without 1uM of isoproterenol for 1 hour, n=4 independent biological replicates. E. Relative mRNA expression from mouse beige adipocytes, control, Myh9KD, or KLF9KD, (+) indicates knockdown and (–) indicates no knockdown of indicated gene, n=5 independent biological replicates.

Chapter 2:
Pharmacological activation of type II myosins to increase thermogenesis in brown and beige adipose tissue

Summary

Brown adipose tissue (BAT) and beige adipose tissue (BeAT) hold the promise of combating a variety of metabolic disorders such as obesity, diabetes, and cardiovascular disease. While originally thought to be present only in newborns to protect against heat loss, BAT and BeAT are now appreciated to be present in adults and the tissues can be activated following cold exposure. Mechanistic studies in animal models uncovered that cold exposure activates thermogenesis in BAT primarily through B3-adrenergic receptors. B3-adrenergic receptor activation was thought to be a viable therapeutic target to increase BAT activity in humans, however due to its systemic expression pharmacological targeting of B3-adrenergic receptors to increase thermogenesis can result in serious side effects. A more in-depth biological understanding of BAT and BeAT has thus been required to uncover novel pharmacological targets to increase thermogenesis in humans. Previous work in our lab uncovered that BAT possesses a muscle-like gene expression profile like that of muscle cells. Specifically, BAT was found to express type II myosins, which generate intracellular tension and are required for thermogenesis. Perturbation of the actomyosin network blunts cell stiffness and consequently thermogenesis. Given that the actomyosin mediated tension in BAT is necessary for BAT's thermogenic function we sought to exploit this mechanism for potential therapeutic purposes. In collaboration with Atomwise, a biotech company which uses artificial intelligence for drug discovery, we tested libraries of type II myosin agonists to determine if pharmacological activation of tension in BAT would increase BAT thermogenesis. Through our screen we identified top compound 'hits' which were able to increase thermogenesis independent of B3-AR activation.

Introduction

The unabated growth of obesity and its associated disease such as cardiovascular disease and type 2 diabetes reflects an unmet need to develop safe and effective therapeutic strategies. A promising approach to combat obesity and its associated metabolic diseases involves increasing energy expenditure[65]. An exciting anti-obesity target is brown adipose tissue (BAT) and beige adipose tissue (BeAT), both of which are major consumers of glucose and fatty acids. Compared to white adipose tissue which is a major energy storage tissue, BAT/BeAT are primarily involved in thermoregulation. BAT/BeAT generate heat through the protein UCP1 which uncouples the electron transport chain from ATP production. In BAT/BeAT

thermogenesis requires an increase in fuel utilization and oxidative metabolism, which can protect against obesity, glucose intolerance, impaired insulin secretion, and dyslipidemia[66]. Historically, BAT/BeAT were thought to only be present in newborns and hibernating animals to maintain optimal body temperature. However, improved imaging techniques such as computed tomography (PET/CT) and magnetic resonance PET/MR provided the first clinical evidence of BAT/BeAT activity in adults[66,67].

Since the identification of BAT/BeAT in adults, expansion and/or activation of BAT/BeAT has gained significant traction as a therapeutic strategy for various metabolic disorders[68,69]. Additonal studies in humans have indicated that BAT can become activated as well as expanded upon cold exposure[70,71,72]. For example, in young healthy men, two hours of cold exposure everyday for 20 days resulted in a 45% increase in BAT volume with BAT oxidative metabolism increased more than twofold[73]. In other studies the increase in BAT activity is associated with weight loss, an increase in fat oxidation, and improvements in glucose and insulin sensitivity[70,74,71,75]. A retrospective study of 52,000 individuals who previously had been diagnosed with cancer found that those with detectable BAT had a lower prevalence of various cardiometabolic diseases such as type 2 diabetes, coronary artery disease, congestive heart failure, and hypertension compared to individuals without detectable BAT[76]. Taken together these clinical studies suggest that BAT may be an effective therapy for a variety of metabolic related diseases. Cold exposure is the most potent environmental stimuli to induce BAT/BeAT activity[77], however cold exposure as a therapeutic strategy is difficult to implement due to its variable therapeutic window as well as the uncomfortable nature of being cold. Thus, an FDA approved therapy that could activate BAT/BeAT would be highly beneficial.

Therapeutic targeting of BAT can broadly be grouped into either pharmacological or cell therapy approaches. Pharmacological approaches to increase thermogenesis date as far back as the 1930s when the compound 2,4-dinitrophenol (DNP) was widely used for inducing weight loss[78]. DNP is a protonophore which shuttles protons across the mitochondrial inner membrane, dissipating the mitochondrial proton gradient resulting in the production of heat[79]. The use of DNP was prohibited by the FDA in 1938 due to adverse side effects such as hepatotoxicity and vision problems[80]. Within the last decade interest in protonophores have re-emerged with advanced formulations of DNP improving hypertriglyceridemia, fatty liver, and insulin resistance in rodent models[81–83]. However, their use in clinical models remains limited due to side effects caused by increasing H+ conductance across all biological membranes. Another pharmacological approach to activate BAT/BeAT involves targeting β3-adrenergic receptors (β3-ARs). β3-ARs are predominantly found on adipocytes and β3-AR activation via epinephrine or norepinephrine is the primary pathway involved in activation of UCP1-dependent thermogenesis[84,85,86,87]. The administration of the β3-AR agonist CL 316,243 has shown to increase insulin sensitivity and fat oxidation in healthy males[88]. Mirabegron, an oral β3-AR agonist, is approved to treat overactive bladder and has also been shown to acutely

stimulate BAT activity[89,90,91]. However, the use of β3-AR agonists in humans have been limited due to increases in blood pressure and heart rate caused by the stimulation of adrenergic receptors present in cardiomyocytes[92]. Instead of targeting upstream receptors of thermogenesis, others have focused on the pharmacological activation of downstream transcriptional regulators. Peroxisome proliferator-activated receptor γ (PPARγ) is a member of the nuclear receptor superfamily of ligand-activated transcription factors and is found predominantly in adipose tissue[93]. PPARγ is a master regulator of adipose tissue formation and is involved in regulating the thermogenic program in BAT/BeAT[94–98]. Thiazolidinediones (TZDs), which are potent PPARγ activators, have shown to successfully manage insulin and glucose sensitivity in patients with type 2 diabetes[99]. Beyond type 2 diabetes, TZDs have promising therapeutic effects in other metabolic diseases such as cardiovascular disease and dyslipidemia[100]. However, the clinical use of PPARγ agonists have revealed a number of adverse side effects such as edema, weight gain, macular edema and heart failure[101–103].

Others have looked to bypass pharmacological activation of BAT/BeAT altogether and instead increase BAT/BeAT mass and activity by transplantation. Multiple animal studies have shown that BAT transplantation can improve glucose metabolism, insulin sensitivity, and reduce both adiposity and body mass [104,105,106,107]. The potential translational relevance to these BAT/BeAT transplantation studies would be the utilization of an ex vivo cellular approach, to develop BAT/BeAT from human precursor cells and re-implant them into the donor. A variety of groups showed that BAT progenitor cells could be isolated from tissue, differentiated ex vivo and implanted into mice. The transplanted cells were able to reduce obesity-associated metabolic syndromes and enhance systemic glucose tolerance[108,109]. In the Stahl lab, ongoing research has focused on developing a cell scaffold technology to support the differentiation of white adipose tissue–derived multipotent stem cells into UCP1-expressing beige adipose tissue. This novel cell scaffold technology was optimized to establish functional brown fat–like depots in mice which was able to elevate core body temperature during cold challenges, enhance respiration rates, improve glucose homeostasis, and reduce weight gain[110]. Parallel work in the lab led to the discovery of a novel actomyosin regulatory component in brown and beige adipose tissue[7]. Specifically, we found that BAT/BeAT tissue expresses a unique type II myosin expression pattern. Activation of thermogenesis through β3-AR signaling increases cellular tension mediated through type II myosin activity while inhibition of type II myosins results in a reduction of contractility and thermogenesis.

Type II myosins exist as a hexamer, containing two heavy chains, two essential light chains, and two regulatory light chains. The heavy chains contain an actin binding domain and ATPase activity while the light chains are involved in structure and regulatory activity[7,15]. The motor function of type II myosins involves an ATPase cycle that alters the biochemical and conformational states of the myosin head domain. The myosin head domain binds actin after the hydrolysis of ATP and generates mechanical force upon the release of phosphate[111].

Release of ADP allows the dissociation of the myosin head domain from actin and rebinding of ATP[112,113]. Numerous small molecule myosin modulators are currently being developed to treat patients with cardiomyopathies[112]. These pharmaceutical agents are typically grouped into two categories based on their ability to activate or inhibit myosin contractility. Current pharmacological agents of type II myosins typically target the head domain and thus alter the ATPase cycle. The compound MYK-461 (mavacamten) is now FDA approved for the treatment of hypertrophic cardiomyopathy, an inherited disease that causes hyperdynamic contraction and impaired relaxation. MYK-461 decreases the ATPase activity on β–cardiac myosin heavy chain (MYH7) thus reducing contractility and suppressing hypertrophy[114,115]. Omecamtiv mecarbil (OM) is a common cardiac type II myosin activator and currently is waiting FDA approval after positive phase 3 clinical results which showed the drug significantly reduced the risk of cardiovascular death or heart failure events compared to placebo[116]. Mechanistics studies showed that OM increases the rate of phosphate release from the myosin head domain ultimately increasing the fraction of cycle time in which myosins are bound to actin, resulting in higher force production[117,118].

Interestingly, data published from our lab, showed that omecamtiv mecarbil increased UCP1 expression and respiration in mice[7]. Our novel findings that type II myosins are involved in BAT/BeAT thermogenesis along with extensive literature on mechanical activation of these proteins allowed us to hypothesize that type II myosin activation may be a novel therapeutic target to pharmacologically increase BAT/BeAT thermogenesis. This strategy could be the foundation for a novel approach to treat obesity-associated disorders such as type-2 diabetes and cardiovascular disease. To develop small molecule agonists specific for type II myosins we took part in the Atomwise AIMS Awards Program which provides non-profit researchers with virtual screening and compounds for physical testing at no cost. Atomwise, a biotech company based in San Francisco, initiated a virtual screen of millions of commercially available chemical compounds using their proprietary artificial intelligence discovery engine (AtomNet). The virtual screen predicts chemical compounds that most likely would bind to the chosen site or sites on the target protein. Through our collaboration with Atomwise we were able to screen over 100 type II myosin agonists and identified top compound hits that increased BAT and BeAT thermogenesis. Further compound optimization and confirmation of the mechanism of action of the type II myosin activators will lay the groundwork for a novel approach to activate thermogenesis in humans.

Results

AtomNet virtual screen

Previously our lab identified actomyosin mediated tension as a key mediator BAT thermogenic activity. The actomyosin network is composed of type II myosin filaments which

convert chemical energy in mechanical force. Our lab showed that omecamtiv mecarbil (OM), a small-molecule activator of cardiac myosin[119] can induce thermogenesis in BAT[7]. In collaboration with Atomwise we sought to identify novel type II myosin activators of BAT focusing on type II myosin heavy chains (Myh1, Myh4, Myh9, and Myh11) due to previous tissue expression data generated in the lab. Activation of these myosin isoforms provide a means to pharmacologically enhance the metabolic activity of BAT/BeAT via mechanoregulation. Atomwise used the crystal structure of Myh7 in complex with OM as a template to build homology models of MyH1, MyH4, MyH9 and MyH11. Subsequently the models were aligned with the MyH7-OM complex and the region corresponding to an OM binding site was determined for each of the proteins to define the compound target site **(Fig. 1A)**. After *in silico* modeling, Atomwise recommended screening be performed toward the targets Myh4 and Myh11 based on critical differences in binding residues, which were found to be almost identical across the proteins**.** Specifically, MyH11 and MyH4 were the recommended targets of virtual screen based on the F84/Y85, E92/M93 and N717/S715 differences which are not only adjacent to OM in the MyH7-OM complex but also present significant differences in the chemical nature of the side chains **(Fig. 1B-D)**.

Type II myosin activators increase UCP1 expression in brown and beige adipocytes

After completion of the virtual screen Atomwise identified 90 Myh4 targeting compounds and 73 Myh11 targeting compounds. The list of the compounds can be found in **Table 1** and **Table 2**. As a primary screen for thermogenic activity, we tested for changes in UCP1 mRNA expression. Using an immortalized brown pre-adipocyte cell line (sBAT)[46], we differentiated the cells to mature brown adipocytes after which were treated overnight with Myh11 or Myh4 targeting compounds in combination with isoproterenol. We previously found that β3-AR stimulation induced tension through the actomyosin network which facilitated thermogenesis[7]. Thus, we decided to treat brown adipocytes with the myosin targeting compounds in combination with isoproterenol to determine if myosin activation could further increase isoproterenol induced UCP1 expression. After overnight treatment the cells were collected and processed for qPCR to measure UCP1 mRNA expression **(Fig. 2A)**. Approximately 65% of the Myh11 compounds decreased UCP1 mRNA expression **(Fig. 2B)**. However, to our delight approximately, 20% of the Myh11 myosin activators increased UCP1 mRNA expression compared to control which we identified as our compound hits **(Fig. 2C).** Like the Myh11 compounds, the Myh4 compounds resulted in an increase, decrease or no change in UCP1 mRNA expression **(Fig. 3A)**. Approximately 37% of the compounds decreased UCP1 mRNA expression **(Fig. 3B)** while ~16% increased UCP1 mRNA expression in combination with isoproterenol **(Fig. 3C)**. Isoproterenol increases UCP1 mRNA expression through the canonical β3-AR signaling pathway, thus our data suggested that the compound hits were working

synergistically with isoproterenol. We hypothesized that the compounds that decreased UCP1 mRNA expression may be disrupting myosin activity and thus blunting thermogenesis.

To determine if the compound hits were limited to a biological function in just brown adipocytes we tested the hits in additional cell lines. Similar to the sBAT cells we used an immortalized pre-adipocyte cell line (sWAT)[46] that we differentiated to mature beige adipocytes which were then treated overnight with Myh11 or Myh4 hits in combination with isoproterenol. We tested 9 of the Myh11 hits and found that 4 significantly increased UCP1 mRNA expression in combination with isoproterenol while of the 14 Myh4 hits tested, 4 significantly increased UCP1 mRNA expression in combination with isoproterenol **(Fig. 4A-B)**. Additionally, we tested 12 Myh4 hits and 6 Myh11 hits in human preadipocytes (ZenBio) differentiated toward a brown-like fate. Four Myh4 hits and 3 Myh11 hits significantly increased UCP1 mRNA expression in combination with isoproterenol **(Fig. 4C-D)**. These results suggest that type II myosin induction can increase UCP1 mRNA expression across a variety of thermogenic cell lines. Interestingly, not all of the hits identified in the original brown adipocyte screen were able to increase UCP1 mRNA expression in beige adipocytes. This may be due to different expression patterns or activity of myosin isoforms across cell lines.

Type II myosin activators induce UCP1 expression independent of β3-AR stimulation

Once we identified the initial hits in brown adipocytes we tested their ability to increase UCP1 expression without isoproterenol induced β3-AR signaling. Again, using the sBAT cell line we treated mature cells overnight with or without the myosin activators. Of the Myh11 hits, only one compound 0247682153 significantly increased UCP1 mRNA expression without isoproterenol while 7 of the Myh4 hits increased UCP1 mRNA expression without isoproterenol **(Fig. 5A-B)**. To determine the optimal dose we selected the most potent myosin activator, compound 0246504505, and completed a titration experiment. Mature sBAT cells were treated with either 0µm, 0.5µm, 1µm, 2.5µm, 5µm, 7µm, 10µm, or 20µm of compound 0246504505. The compound displayed an inverted U-shaped dose response with an almost 10x increase in UCP1 mRNA expression with 5µm compared to control **(Fig. 5C)**. We also performed a time course experiment to determine the transcriptional timeframe by which UCP1 mRNA expression is increased following treatment with compound 0246504505. The sBAT cells were treated for 30 minutes, 1 hour, 3 hours, 5 hours and 7 hours. After just 30 minutes of treatment UCP1 mRNA expression increased ~2.5x and reached maximum expression at 5 hours compared to non-treated control **(Fig. 5D)**. Here we identified the most potent concentration and treatment duration for compound 0246504505 to increase UCP1 mRNA expression in brown adipocytes.

Type II myosin activators increase mitochondrial respiration

To determine whether our observed increase in UCP1 mRNA expression would translate to functional improvements in thermogenesis we utilized the Seahorse XF assay to measure mitochondrial respiration. The seahorse mitochondrial stress test allows us to measure key parameters of mitochondrial respiration through the direct injection of electron transport chain complex inhibitors[120]. We measured basal, uncoupled, and maximal respiration with 9 of our top Myh4 targeting hits and 6 of our top Myh11 targeting hits in combination with isoproterenol that we identified from our initial UCP1 mRNA expression screen **(Fig. 6A-C)**. Only 3 of the compounds, 0246504460, 0246504505, and 0246513623, significantly increased uncoupled respiration in brown adipocytes **(Fig. 6D)**. We then tested the 3 compounds' ability to increase uncoupled respiration independent of isoproterenol. Interestingly, compound 0246504460 dramatically increased basal and uncoupled respiration to levels that are typically seen with the synthetic mitochondrial membrane uncoupler FCCP **(Fig. 6E)**. Thus, we hypothesized that the compound 0246504460 may be acting as a mitochondrial uncoupler rather than a type II myosin activator.

To test our hypothesis we first isolated mitochondria from mouse brown adipose tissue and measured mitochondrial respiration upon injection with the myosin activators. Given that isolated mitochondria would be free of the actomyosin network as well as cellular signaling pathways we hypothesized that any increase in respiration would be a direct result of mitochondrial membrane uncoupling. Direct injection of compound 0246504460 immediately increased mitochondrial respiration to an equivalent level as seen with FCCP, a known mitochondrial membrane uncoupler, confirming our hypothesis **(Fig. 7A)**. To our satisfaction compound 0246504505 had no effect on mitochondrial respiration **(Fig. 7A)**, suggesting that compound 0246504505 was indeed increasing UCP1 mRNA expression and mitochondrial respiration through type II myosin activation. We next decided to measure mitochondrial respiration in 3T3L1 white adipocytes treated with myosin activators. 3T3L1 white adipocytes do not express UCP1 and are not expected to be activated through actomyosin mediated tension mechanisms; therefore, any increase in cellular respiration could indicate the compounds may be acting through an actomyosin independent mechanism. Two of the compounds tested, 0246504460 and 0246513623 increased cellular respiration while again compound 0246504505 had no effect on respiration in 3T3L1 white adipocytes **(Fig. 7B)**. Although compound 0246504460 appeared to be acting as a mitochondrial uncoupler, its structure appeared more similar to 0246504505 than to FCCP **(Fig. 7C-E).** Given compound 0246504505 was our most potent activator of UCP1 mRNA expression, we were encouraged that the compound did not increase respiration in isolated mitochondria or in white adipocytes. These data strengthened our belief that 0246504505 was in fact increasing thermogenesis through type II myosin activation.

Investigation into the mechanism of the myosin activators

Type II myosin proteins utilize ATP to generate mechanical force via a process called the 'powerstroke' cycle[111]. To better understand the mechanism by which the compounds may be activating type II myosins we used a kinetic ATPase assay, developed by Cytoskeleton Inc, to measure the utilization of ATP from purified myosin proteins[121]. We utilized purified SI fragments of type II myosins which contain both the actin binding domain and ATPase domain, allowing us to probe whether the myosin activators could increase myosin activity by increasing the ATPase cycle. We reconstituted the actomyosin network using purified cardiac actin and purified S1 fragments from smooth muscle myosin. After the addition of ATP we confirmed that we could measure the kinetic ATPase activity of the myosin fragment while the myosin fragment reconstituted without actin served as a negative control **(Fig. 8A)**. We next treated the reconstituted actomyosin with two commercially available myosin activators, omecamtiv mecarbil (OM) and EMD57003, and two of our compound hits 0247682153 and 0246504505 **(Fig. 8B-C)**. EMD57003 is an established ATPase activator[122] and as expected increased the ATPase activity of the purified smooth muscle myosin. Compounds 0247682153 and 0246504505 did not increase the ATPase activity along with OM, which is specific for cardiac muscle myosin. We repeated the experiment but included compound 0247678842 as a negative control which had decreased UCP1 mRNA expression from our initial screen. As expected, EMD57003 increased the ATPase activity, however compound 0247678842 decreased the ATPase activity of smooth muscle myosin **(Fig. 8D-E)**. Presumably, compound 0247678842 is inhibiting myosin activity which may explain why the compound decreased UCP1 expression in brown adipocytes. Since compounds 0247682153 and 0246504505 did not increase the ATPase activity of smooth muscle myosin, we utilized the purified S1 fragment of cardiac muscle myosin. OM increased the ATPase activity of purified cardiac muscle myosin, but compounds 0247682153 and 0246504505 had no effect **(Fig. 8F)**.

Although our compounds 0247682153 and 0246504505 failed to increase the ATPase activity in these assays, we only utilized purified smooth muscle myosin and cardiac muscle myosin. Therefore, we can not rule out the possibility of our compounds are increasing the ATPase activity of other type II myosins such as a skeletal muscle myosin or a non-muscle myosin which are both present in BAT and BeAT. Additionally, we cannot exclude the possibility that our compounds may increase myosin activity through mechanisms separate from ATPase activity. OM for example has been shown to increase cardiac myosin activity by stabilizing the lever arm allowing more myosins to bind to actin[119]. Further studies are needed to determine the mechanism of myosin activation as well as the specificity to myosin isoforms.

Assays to access cell stiffness at a single cell level

Type II myosins generate contractile force within cells, thus we decided to directly measure cellular tension to further probe the mechanism of the myosin activators. To measure cell tension changes we utilized atom force microscopy (AFM) which enables the measurement

of mechanical properties of cells. Previously, our lab showed that in brown adipocytes, the β3-AR agonist isoproterenol increases tension while blebbistatin, a type II myosin inhibitor decreases tension[7]. Beige adipocytes were pre-treated with either blebbistatin, isoproterenol, or compound 0246504471 for 30 minutes prior to AFM measurements. Blebbistatin decreased cell tension, while isoproterenol and compound 0246504471 increased cell tension **(Fig. 9A)**. This assay gave us confidence that the myosin activators were in fact acting through myosin activity to increase UCP1 expression and thermogenesis. Although AFM is a powerful tool to measure single cell stiffness changes at high resolution, the assay is not high-throughput. To screen dozens of myosin activators for tension changes we looked to establish a high-throughput method. Mechano-node-pore sensing (mechano-NPS) is a single-cell microfluidic analysis method that enables the quantification of cell diameter, resistance to compressive deformation, transverse deformation under constant strain, and recovery time after deformation from hundreds of cells in under 30 minutes[123]. Cells are flowed through a microfluidic device containing a sizing pore to isolate single cells followed by a contraction channel to measure the cells response to mechanical stress **(Fig. 9B-C).** The mechanical measurement of cells is defined by a dimensionless parameter, referred to as the whole cell deformability index (wCDI). The wCDI is calculated based on the functional relationship among the biophysical parameters of a cell and fluid flow and is inversely proportional to traditional parameters such as elastic modulus. Preliminary testing suggested that the mechano-NPS detected increased tension after acute isoproterenol treatment and decreased tension after overnight blebbistatin treatment in brown adipocytes **(Fig. 9D)**. We also tested stiffness changes in the Myh9KD sWAT cells (as described in chapter 1) and found that Myh9KD significantly increased the wCDI indicating reduced tension compared to control cells **(Fig. 9E)**. These preliminary results suggest that we can screen myosin activators for tension induction in brown and beige adipocytes. AFM can analyze only just a few cells per hour while in the equivalent amount of time we were able to get measurements of upwards of a hundred cells. In the future we can measure tension effects from multiple myosin activators in a single day.

Discussion

Brown and beige adipose tissue are promising therapeutic targets for the treatment of various metabolic diseases such as obesity, type II diabetes, and cardiovascular disease. In this chapter we attempted to identify novel type II myosin activators that could increase BAT thermogenesis. Our lab was the first to describe the role of actomyosin mediated cellular tension in regulating UCP1 expression[7] and we hypothesized that tension induction in BAT offered a unique therapeutic approach to combat a variety of metabolic disorders. A joint collaboration was established between our lab and Atomwise to develop type II myosin activators that would increase thermogenesis in BAT. Atomwise identified over 100 new small

molecule entities that had the potential to increase type II myosin activity, using their proprietary machine learning platform named AtomNet. As an initial screen we tested all compounds *in vitro* using the sBAT brown adipocyte cell line[46] to measure UCP1 mRNA expression. Of the 163 compounds screened, ~18% increased UCP1 mRNA expression. Although our goal was to increase UCP1 mRNA expression we were encouraged to identify inhibitors of UCP1 mRNA expression as this suggested that disruption of myosin activity negatively affects thermogenesis. After our UCP1 mRNA expression screen we measured mitochondrial respiration with 14 of the top hits to show functional consequences of myosin activation. Of the 14 compounds tested, 4 increased mitochondrial respiration without co-stimulation with isoproterenol. Increased mitochondrial respiration indicates increased fuel utilization which would translate to an increase in calories burned *in vivo*. Further investigation into the increased respiration effects clearly demonstrated that compound 0246504460 was acting as a mitochondrial uncoupler rather than a type II myosin activator. On the other hand, compound 0246504505 was identified as a potent activator of UCP1 mRNA expression and uncoupled respiration potentially acting through the actomyosin network.

To prove that the myosin activators were indeed increasing myosin function we sought to determine whether the compounds would increase the ATPase activity of purified myosins. Type II myosins generate mechanical force through a 'powerstroke' cycle. When bound to ATP, type II myosin is released from actin filaments. The hydrolysis of ATP to ADP and phosphate enables type II myosin to rebind to actin filaments. The release of phosphate causes a conformational change triggering the force generating step or 'powerstroke.' The release of ADP and binding of a new ATP molecule causes a conformational change in the type II myosin and release from actin. Thus, an increase in ATP consumption would indicate an increase in myosin activity. Although our positive controls, EMD57003 and OM increased the ATPase activity of purified smooth muscle myosin and cardiac myosin respectively, we found that our compound hits had no effect. We did not however test other type II myosin isoforms so our compound hits could be selective for either skeletal muscle myosin or non-muscle myosin. Additionally, we cannot rule out the possibility that the compounds may increase myosin function through a mechanism separate from the ATPase function.

In collaboration with Atomwise we were able to identify potent activators of thermogenesis in BAT. These compounds could become the basis for a new therapeutic approach to combat a variety of metabolic diseases. Additionally, studies are needed to fully understand the mechanism of action and therapeutic potential of the myosin activators. Such studies may include tension measurements as well as repeating the ATPase assay with multiple isoforms of purified myosin. Identifying the crystal structure of the myosin-compound interaction would also help elucidate the mechanism of action. Eventually, the myosin activators should be tested *in vivo* to determine the extent to which they could increase BAT/BeAT thermogenesis. The studies throughout this chapter have set the groundwork for

continued exploration into the potential of therapeutically increasing BAT/BeAT activity via type II myosin activators.

Figures

A

(1) MyH7: F84, A91, M92, T94, L96, S118, G119, L120, F121, F489, M493, E497, V698, G701, I702, C705, P710, N711, R712, I713, L770
(2) MyH1: Y85, A92, M93, T95, L97, S119, G120, L121, F122, F492, M496, E500, V702, G705, I706, C709, P714, S715, R716, I717, L774
(3) MyH4: Y85, A92, M93, T95, L97, S119, G120, L121, F122, F492, M496, E500, V702, G705, I706, C709, P714, S715, R716, I717, L774
(4) MyH9: F80, A87, E88, T90, L92, S114, G115, L116, F117, F480, M484, E488, V697, G700, I701, C704, P709, N710, R711, V712, L768
(5) MyH11: F84, A91, E92, T94, L96, S118, G119, L120, F121, F487, M491, E495, V704, G707, I708, C711, P716, N717, R718, I719, L775
(6) MyH10: F84, A91, E92, T94, L96, S118, G119, L120, F121, F487, M491, E495, V704, G707, I708, C711, P716, N717, R718, I719, L775

B Myh7-OM

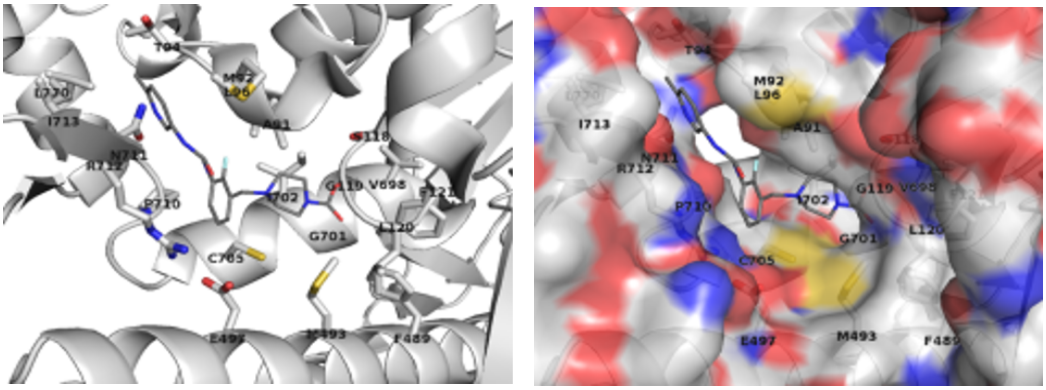

C Myh11-OM

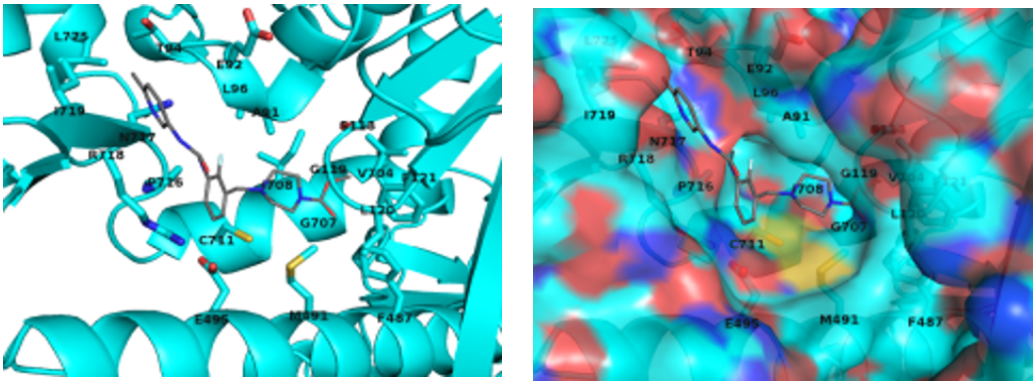

D Myh4-OM

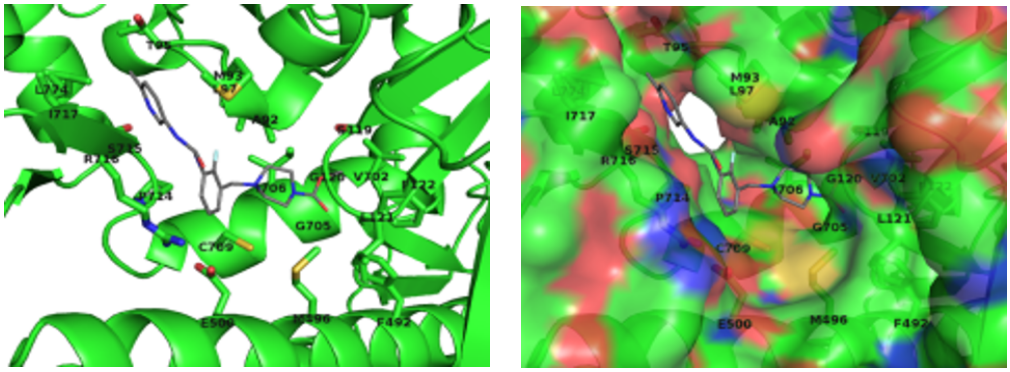

Figure 1. AtomNet Virtual Screen. A. Residues of the target site in myosin proteins that were aligned with the Myh7-OM complex and the region corresponding to an OM binding site was determined for each of the myosin proteins to define the target site. B. Myh7-OM binding site from crystal structure (PDBID:4pa0). C. Model of Myh11-OM binding site. D. Model of Myh4-OM binding site.

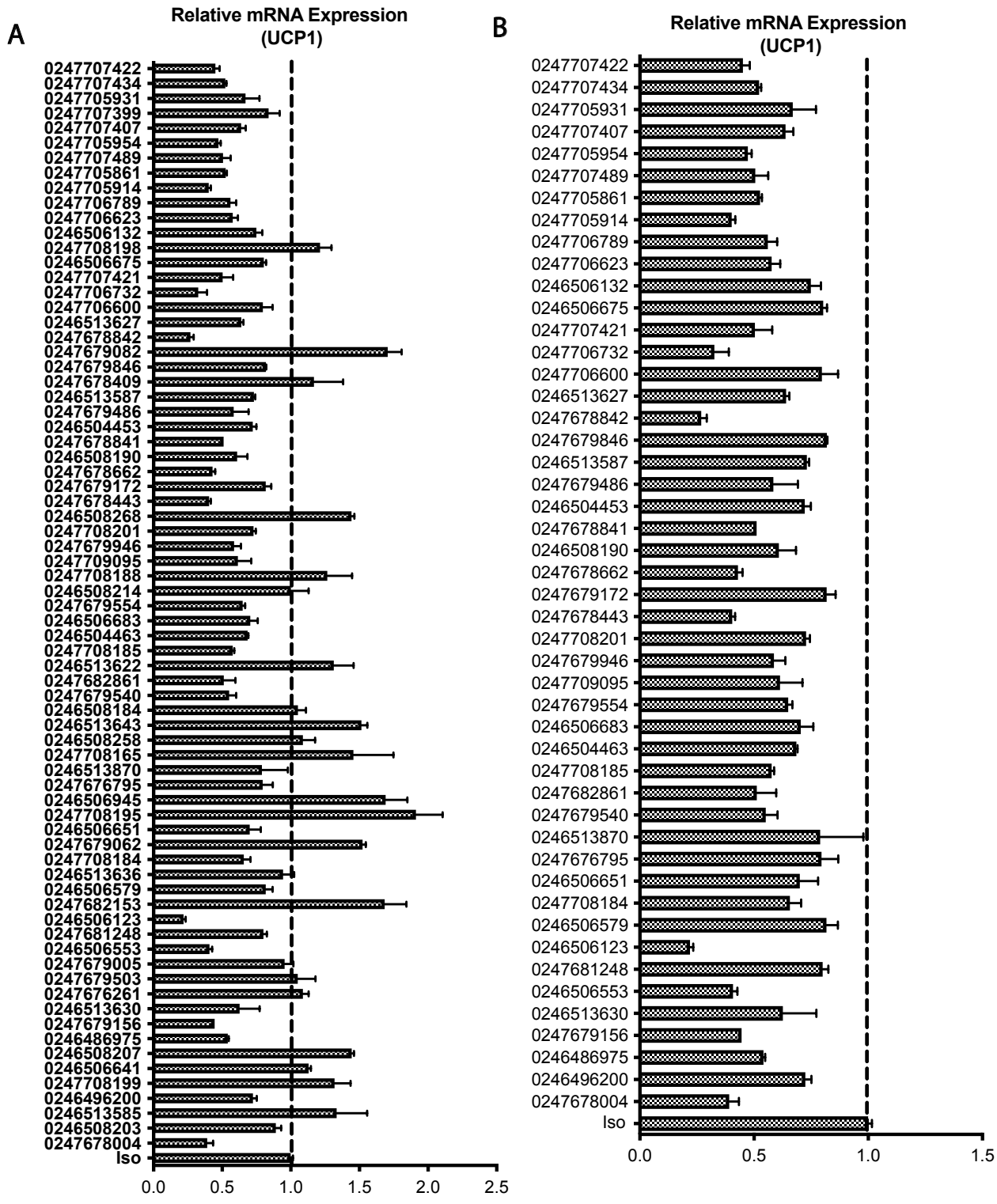
A
Relative mRNA Expression
(UCP1)
0247707422
0247707434
0247705931
0247707399
0247707407
0247705954
0247707489
0247705861
0247705914
0247706789
0247706623
0246506132
0247708198
0246506675
0247707421
0247706732
0247706600
0246513627
0247678842
0247679082
0247679846
0247678409
0246513587
0247679486
0246504453
0247678841
0246508190
0247678662
0247679172
0247678443
0246508268
0247708201
0247679946
0247709095
0247708188
0246508214
0247679554
0246506683
0246504463
0247708185
0246513622
0247682861
0247679540
0246508184
0246513643
0246508258
0247708165
0246513870
0247676795
0246506945
0247708195
0246506651
0247679062
0247708184
0246513636
0246506579
0247682153
0246506123
0247681248
0246506553
0247679005
0247679503
0247676261
0246513630
0247679156
0246486975
0246508207
0246506641
0247708199
0246496200
0246513585
0246508203
0247678004
Iso
0.0
0.5
1.0
1.5
2.0
2.5
B
Relative mRNA Expression
(UCP1)
0247707422
0247707434
0247705931
0247707407
0247705954
0247707489
0247705861
0247705914
0247706789
0247706623
0246506132
0246506675
0247707421
0247706732
0247706600
0246513627
0247678842
0247679846
0246513587
0247679486
0246504453
0247678841
0246508190
0247678662
0247679172
0247678443
0247708201
0247679946
0247709095
0247679554
0246506683
0246504463
0247708185
0247682861
0247679540
0246513870
0247676795
0246506651
0247708184
0246506579
0246506123
0247681248
0246506553
0246513630
0247679156
0246486975
0246496200
0247678004
Iso
0.0
0.5
1.0
1.5

C

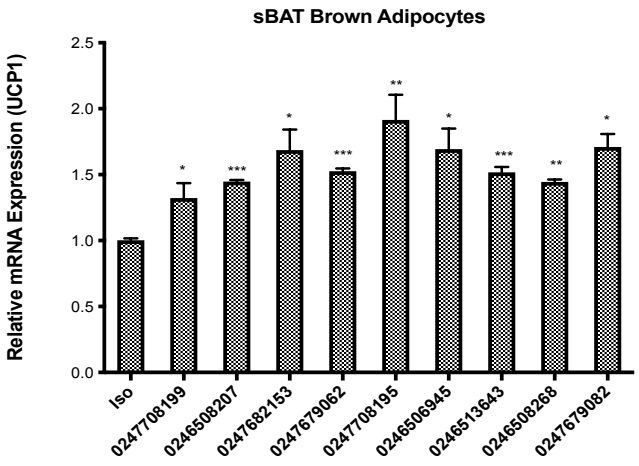

Figure 2. Myh11 activators UCP1 expression screen. A-C . Relative UCP1 mRNA expression of brown adipocytes treated overnight with 10uM of Atomwise myosin targeting compounds and 1uM of isoproterenol. A. UCP1 mRNA expression from the complete Myh11 targeting compound screen, n=3 independent biological replicates. B. UCP1 mRNA expression from the compounds in (A) that caused a decrease in UCP1 expression compared to control, n=3 independent biological replicates. C. UCP1 mRNA expression from the compounds in (A) compounds that significantly increased UCP1 expression, n=3 independent biological replicates.

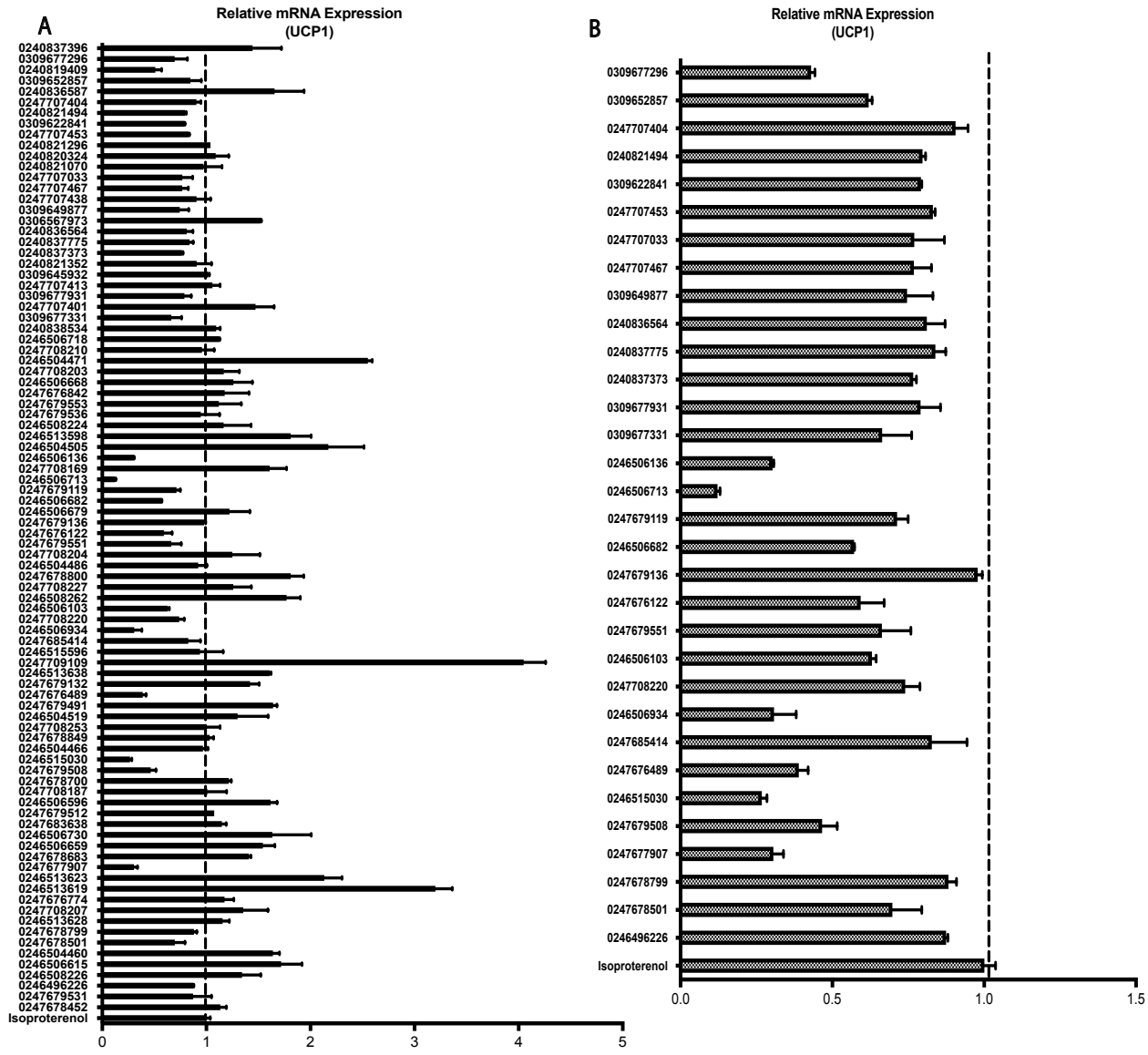
A
Relative mRNA Expression
(UCP1)
0240837396
0309677296
0240819409
0309652857
0240836587
0247707404
0240821494
0309622841
0247707453
0240821296
0240820324
0240821070
0247707033
0247707467
0247707438
0309649877
0306567973
0240836564
0240837775
0240837373
0240821352
0309645932
0247707413
0309677931
0247707401
0309677331
0240838534
0246506718
0247708210
0246504471
0247708203
0246506668
0247676842
0247679553
0247679536
0246508224
0246513598
0246504505
0246506136
0247708169
0246506713
0247679119
0246506682
0246506679
0247679136
0247676122
0247679551
0247708204
0246504486
0247678800
0247708227
0246508262
0246506103
0247708220
0246506934
0247685414
0246515596
0247709109
0246513638
0247679132
0247676489
0247679491
0246504519
0247708253
0247678849
0246504466
0246515030
0247679508
0247678700
0247708187
0246506596
0247679512
0247683638
0246506730
0246506659
0247678683
0247677907
0246513623
0246513619
0247676774
0247708207
0246513628
0247678799
0247678501
0246504460
0246506615
0246508226
0246496226
0247679531
0247678452
Isoproterenol
0
1
2
3
4
5
B
Relative mRNA Expression
(UCP1)
0309677296
0309652857
0247707404
0240821494
0309622841
0247707453
0247707033
0247707467
0309649877
0240836564
0240837775
0240837373
0309677931
0309677331
0246506136
0246506713
0247679119
0246506682
0247679136
0247676122
0247679551
0246506103
0247708220
0246506934
0247685414
0247676489
0246515030
0247679508
0247677907
0247678799
0247678501
0246496226
Isoproterenol
0.0
0.5
1.0
1.5

C

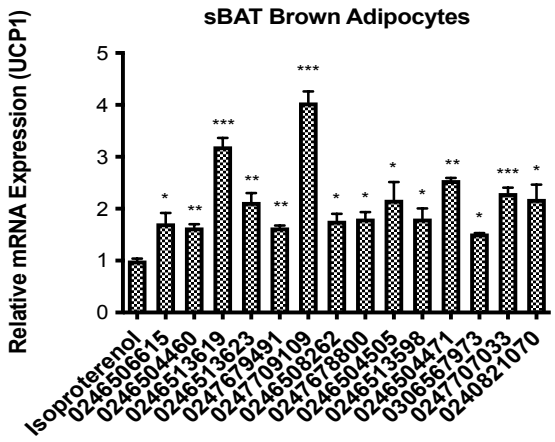

Figure 3. Myh4 Activators UCP1 expression screen. A-C . Relative UCP1 mRNA expression of brown adipocytes treated overnight with 10uM of Atomwise myosin targeting compounds and 1uM of isoproterenol. A. UCP1 mRNA expression from the complete Myh4 targeting compound screen, n=3 independent biological replicates. B. UCP1 mRNA expression from the compounds in (A) that caused a decrease in UCP1 expression compared to control, n=3 independent biological replicates. C. UCP1 mRNA expression from the compounds in (A) compounds that significantly increased UCP1 expression, n=3 independent biological replicates.

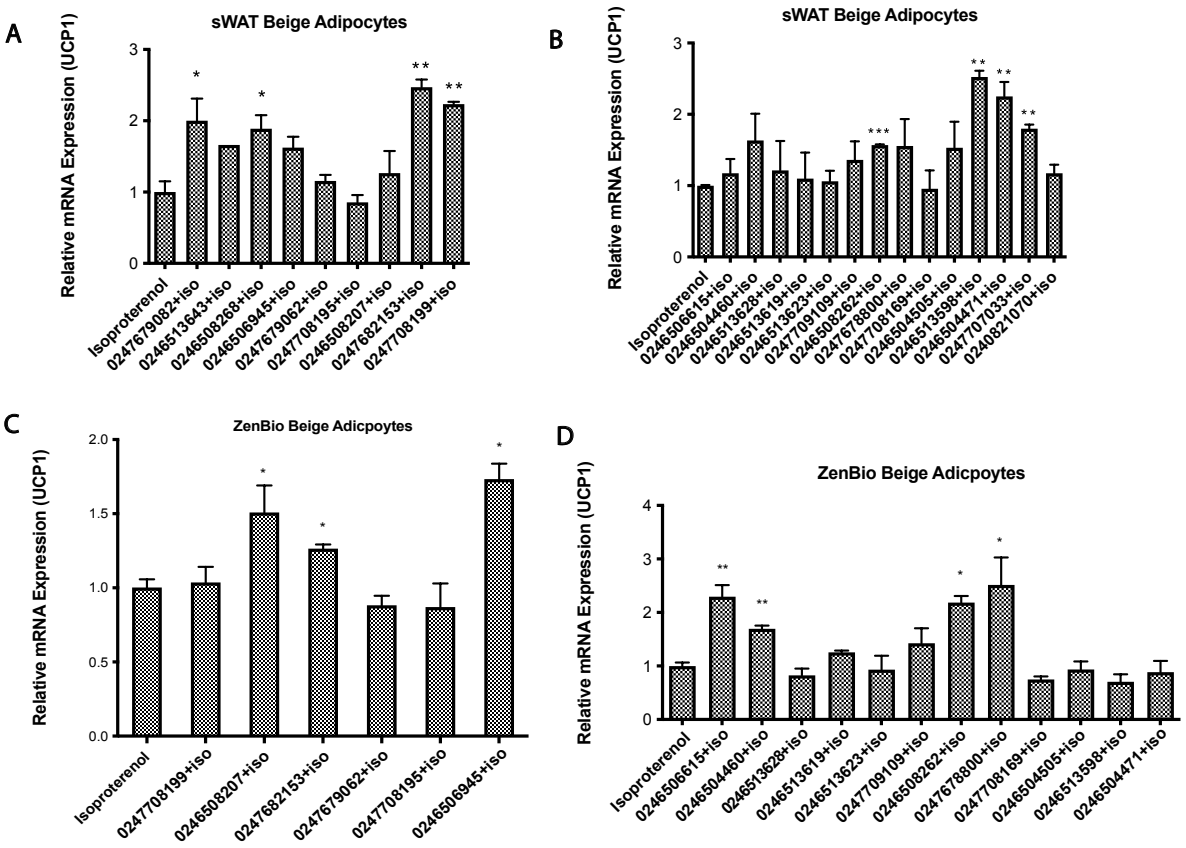

Figure 4. Beige adipocyte activator screen. A-D. Relative UCP1 mRNA expression of beige adipocytes treated overnight with 10uM of Atomwise myosin targeting compounds and 1uM of isoproterenol. A. UCP1 mRNA expression of Myh11 compounds tested in mouse beige adipocytes, n=3 independent biological replicates. B. UCP1 mRNA expression of Myh4 compounds tested in mouse beige adipocytes, n=3 independent biological replicates. C. UCP1 mRNA expression of Myh11 compounds tested in human beige adipocytes, n=3 independent biological replicates. D. UCP1 mRNA expression of Myh4 compounds tested in human beige adipocytes, n=3 independent biological replicates.

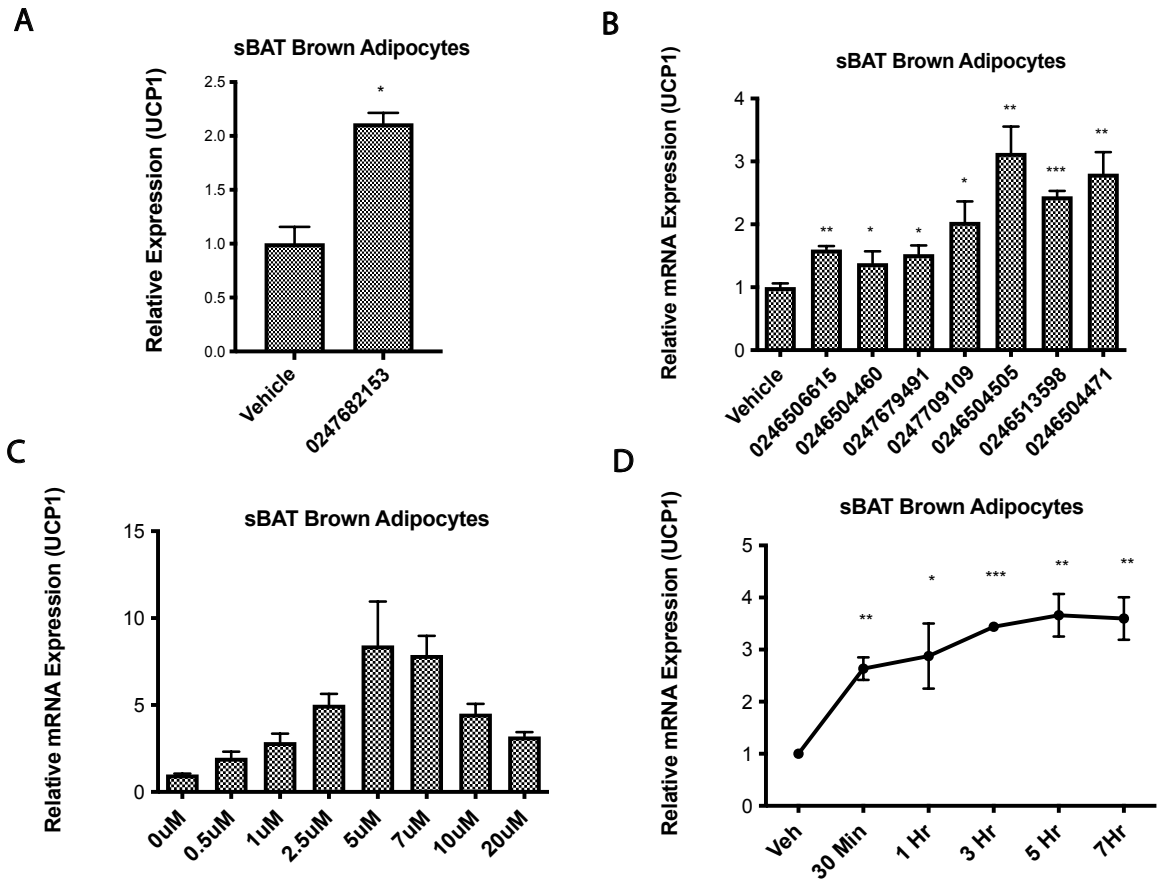

Figure 5. Myosin Activators without Isoproterenol. A-B. Relative UCP1 mRNA expression of brown adipocytes treated with Atomwise myosin targeting compounds. A. UCP1 mRNA expression of Myh11 compound #024762153 treated overnight at 10uM, n=3 independent biological replicates.. A. UCP1 mRNA expression of Myh4 targeting compounds treated overnight at 10uM, n=3 independent biological replicates. C. UCP1 mRNA expression of Myh4 compound #0246504505 treated overnight at 0, 0.5, 1, 2.5, 5, 7, 10, or 20uM, n=3 independent biological replicates. D. UCP1 mRNA expression of Myh4 compound #0246504505 treated at 10uM for 30 minutes, 1 hour, 3 hours, 5 hours, or 7 hours, n=3 independent biological replicates.

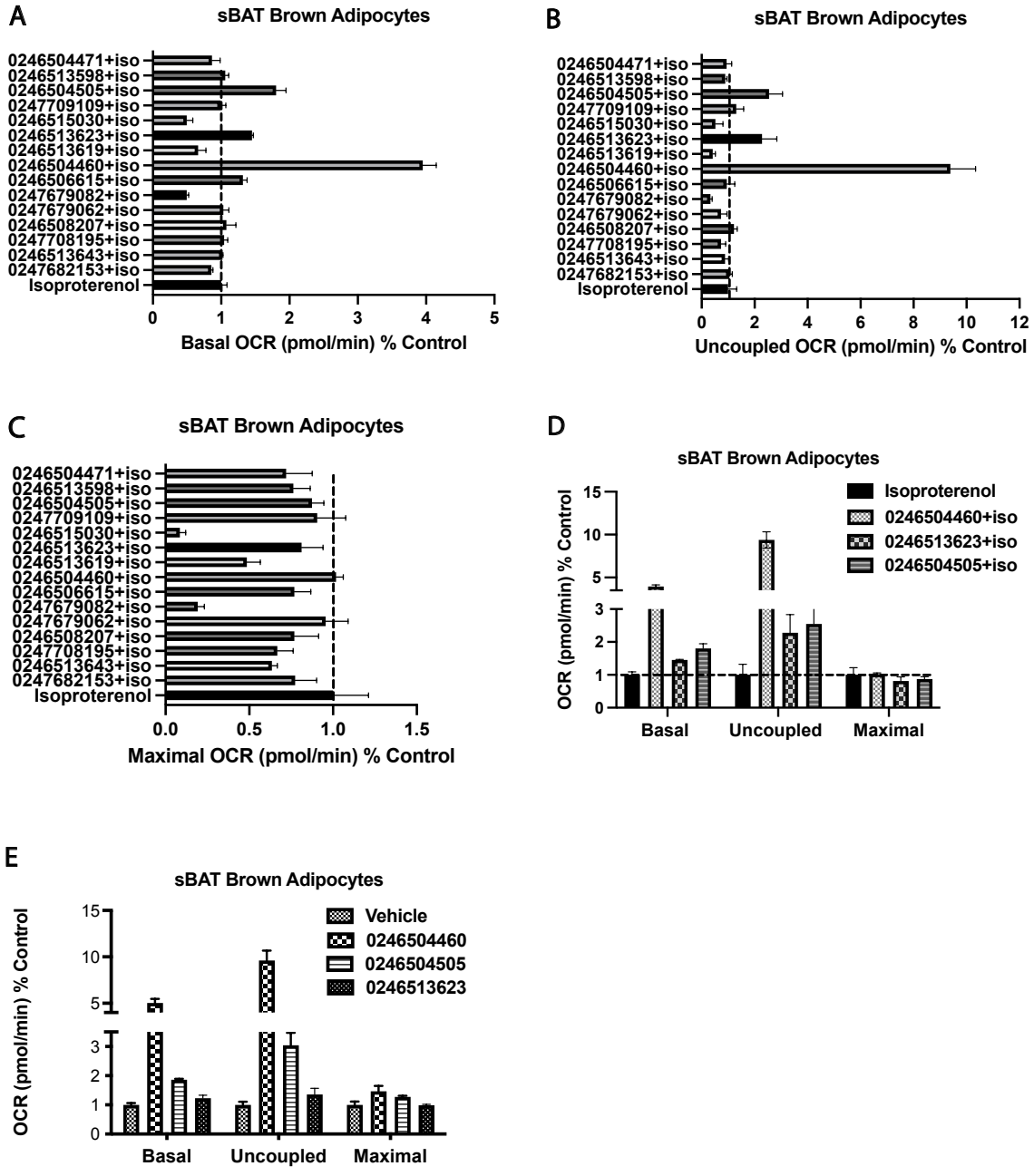

Figure 6. Respiration Screen. A-D. Oxygen consumption rates of brown adipocytes treated overnight with 1uM of isoproterenol and 10uM of Atomwise myosin targeting compounds or 1uM of isoproterenol. A. Basal oxygen consumption rate of brown adipocytes, n=5 independent biological replicates. B. Uncoupled oxygen consumption rate of brown adipocytes, n=5 independent biological replicates. C. Maximal oxygen consumption rate of brown adipocytes, n=5 independent biological replicates. D. Basal, uncoupled and maximal respiration from 3 of the myosin targeting compounds that increased respiration from (A-C). E. Oxygen consumption rates of brown adipocytes treated overnight with 10uM of Atomwise myosin targeting compounds or control, n=5 independent biological replicates.

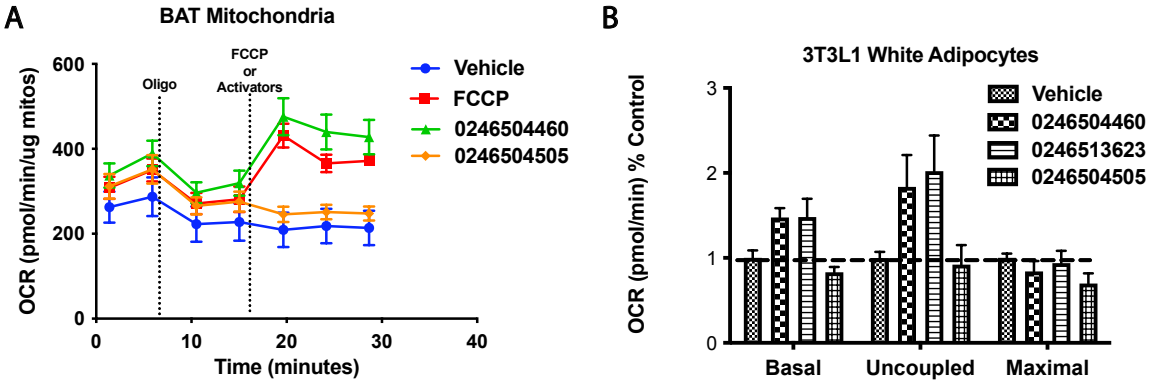

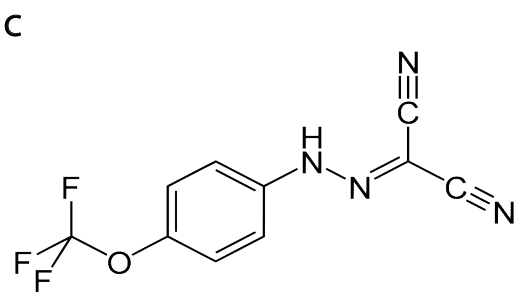

FCCP

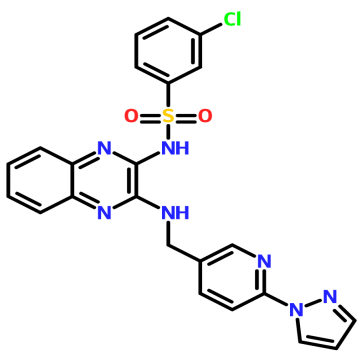

0246504460 (MCULE-4332030827)

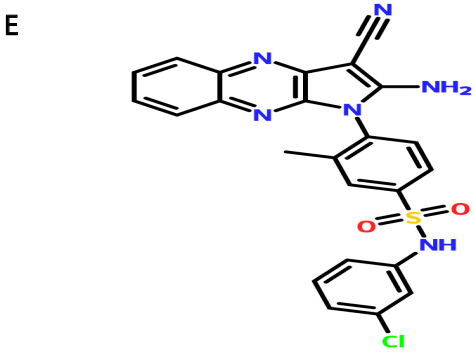

0246504505 (MCULE-7219070444)

Figure 7. A. Oxygen consumption rates of isolated mitochondria from brown adipose tissue injected with oligomycin, followed by either 4uM of FCCP, 10uM of compound 0246504460, 10uM of compound 0246504505, or control, n=5 independent biological replicates. B. Basal, uncoupled and maximal respiration rates of 3T3L1 white adipocytes treated overnight with 10uM of compound 0246504460, 0246513623, 0246504505, or control, n=5 independent biological replicates. C-E . Compound structures.

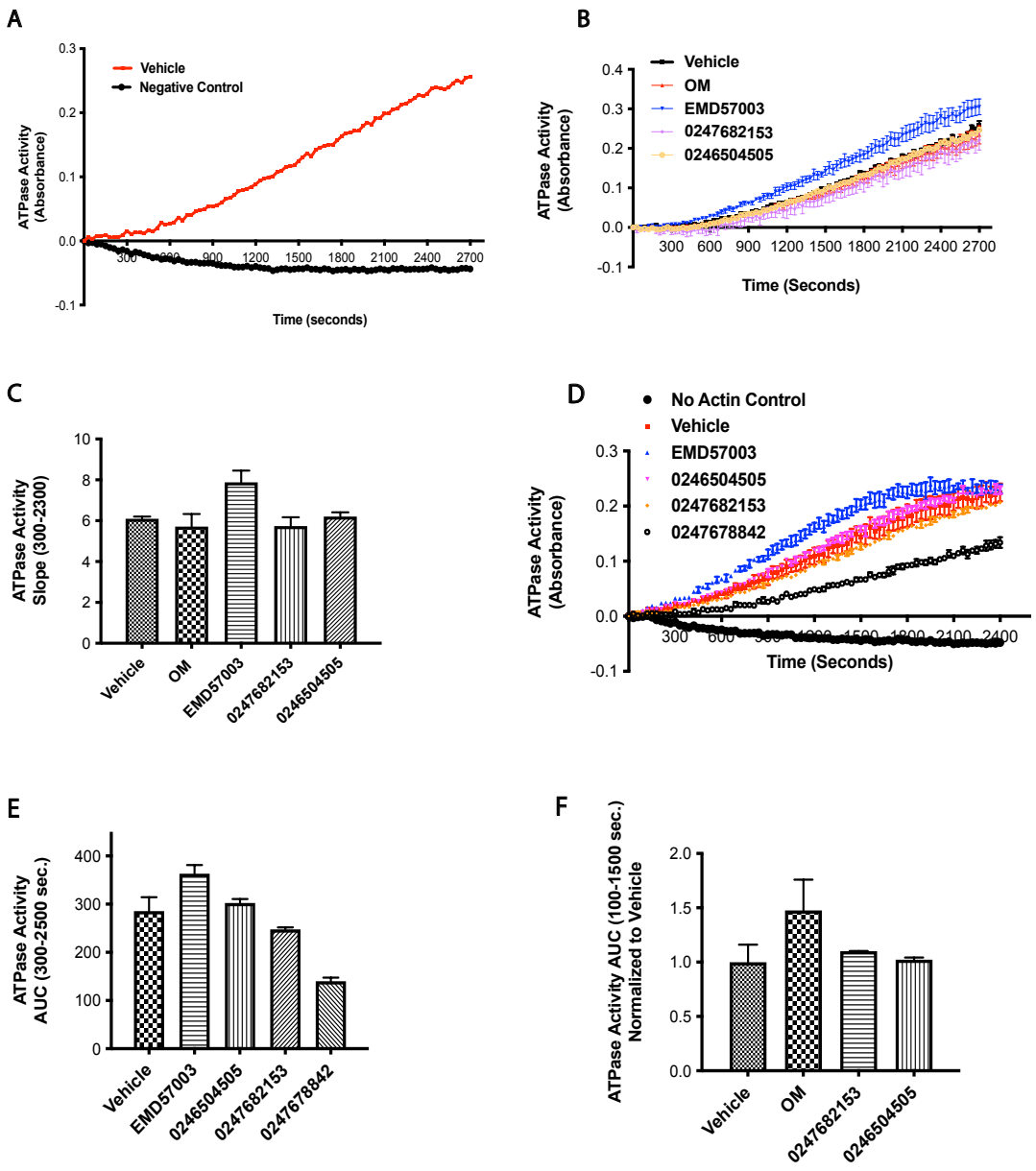

Figure 8. ATPase Assay. A-F. Cytoskeleton Inc. ATPase assay utilizing purified cardiac actin from bovine heart muscle and purified S1 fragment from type II myosin. A. Kinetic absorbance of Pi release from reconstituted cardiac actin and S1 smooth muscle myosin compared to the negative control containing no cardiac actin. B-C. Kinetic absorbance of Pi release from reconstituted cardiac actin and S1 smooth muscle myosin treated with 10uM of OM, EMD57003, 0247682153, 0246504505, or control shown as raw absorbance (B) or AUC (C). D-E. Kinetic absorbance of Pi release from reconstituted cardiac actin and S1 smooth muscle myosin treated with 10uM of EMD57003, 0247682153, 0246504505, 0247678842, or control shown as raw absorbance (D) or AUC (E). F. Kinetic absorbance of Pi release from reconstituted cardiac actin and S1 cardiac muscle myosin treated with 10uM of OM, 0247682153, 0246504505, or control shown as AUC.

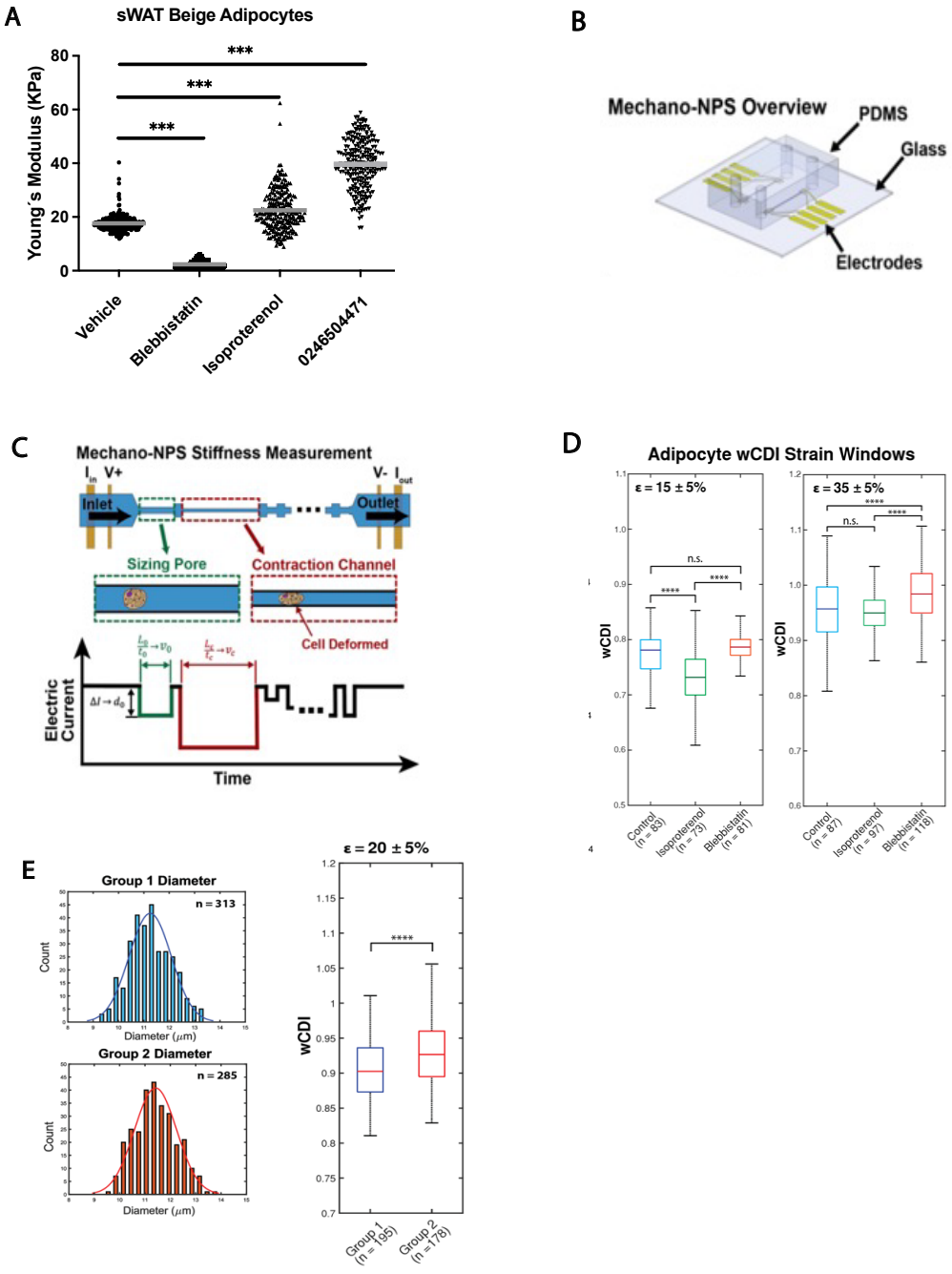

Figure 9. High-Throughput Tension Measurements. A. Atomic force microscopy of mouse beige adipocytes treated overnight with 100uM blebbistatin, 30 minutes with 1uM isoproterenol, 30 minutes with 10uM compound 0246504471, or control. B. Microfluidic chip design. C. Internal chip design from (B), cells are flowed through the inlet, traverse through a sizing pore followed by a contraction channel to measure the cells response to mechanical stimulus. D. Mechano-NPS measurements from brown adipocytes treated overnight with 100uM of blebbistatin, 30 minutes with 1uM of isoproterenol, or control. E. Mechano-NPS measurements from mouse beige adipocytes with Myh9KD for 7 days or control (Group 1=Control, Group 2=Myh9KD).

Chapter 3:
Role of Yap/Taz in brown and beige adipose tissue function

Summary

Cells are constantly exposed to mechanical stimuli that may arise from neighboring cells or the surrounding extracellular matrix (ECM). The signaling by which physical cues are relayed into biological and chemical responses is termed mechanotransduction. A variety of transcription factors have been identified for their ability to relay mechanical information into transcriptional responses. Two such mechanosensitive transcription factors are the paralogs YAP/TAZ. YAP/TAZ are involved in the regulation of multiple biological processes such as organ growth, cell differentiation, wound healing, and cancer metastasis. In the context of cell differentiation YAP/TAZ can mediate lineage decisions of MSCs to either osteoblasts or adipocytes. Recent studies including work from our lab implicated YAP/TAZ transcriptional activity in mediating thermogenesis in brown adipose tissue. YAP/TAZ were shown to respond to actomyosin mediated tension to increase UCP1 expression and thermogenesis. In this chapter we sought to further investigate the role of YAP/TAZ in beige adipose tissue differentiation and metabolic function. We hypothesized that within the first few days of differentiation YAP/TAZ are inactivated but are reactivated in mature beige adipocytes to translate actomyosin signals into the thermogenic transcriptional program. However, we uncovered that YAP and TAZ have non-redundant functions during beige adipocyte respiration. YAP levels during differentiation are also tightly controlled as either YAP inhibition or YAP overexpression decreased UCP1 mRNA expression in beige adipocytes. Future work is required to parse out the specific functions of YAP and TAZ during beige adipocyte development.

Introduction

Cells can respond to both biochemical and mechanical cues. Mechanical cues from the external environment may manifest as stiffness changes from the extracellular matrix, shear stress, or cyclic stretching[124]. These mechanical stimuli are translated into chemical signals that can be transmitted throughout the cell to control various aspects of cell behavior. Stem cell lineage commitment is particularly sensitive to mechanical signals. For example, in the adipogenic cell line 3T3-F442A, cell spreading on fibronectin surfaces inhibited adipogenesis while disruption of the actin cytoskeleton recovered the cells differentiation potential[125,126]. Controlling cell shape in human derived mesenchymal stem cells (hMSC), has also been shown to alter differentiation outcomes between osteogenesis and adipogenesis mediated through RhoA-ROCK signaling[127]. Cells' ability to respond and translate mechanical signals in chemical and biological responses is termed mechanotransduction.

Mechanotransduction is ultimately linked to the activity of nuclear transcription factors which relay the initial physical signals into a biological response. Yes-associated protein (YAP) and Transcriptional coactivator with PDZ-binding motif (TAZ) are homologous transcriptional co-regulators that are widely recognized as nuclear relays of mechanical signals exerted by ECM rigidity and cell shape[128]. YAP/TAZ regulate many diverse biological processes such as mechanosensing, tumorigenesis, and wound healing[129,130]. YAP is a 65KDa protein while TAZ is a 43KDa protein, lacking 3 domains present in YAP but sharing nearly half of its protein sequence identity[131]. In an inactive state, YAP and TAZ are sequestered in the cytosol while in an active state, YAP and TAZ translocate to the nucleus where they interact with TEAD transcription factors to regulate target gene expression[132]. Signaling mechanisms that regulate YAP and TAZ activity are typically divided into two categories; those that act via the canonical Hippo Signaling pathway and those that are independent of it. The Hippo signaling cascade is involved in diverse physiological processes such as organ growth, regeneration, and cancer progression[133]. Recently, the Hippo pathway model of regulating organ growth has been challenged with a provocative new paper that argues Hippo signaling only instructs organ growth and size when cells are mechanically strained[134]. The kinase cascade of the Hippo pathway converges on YAP and TAZ which are regulated via phosphorylation states. Activation of the Hippo pathway through focal adhesions or receptor tyrosine kinases causes the phosphorylation of MST1/2 leading to the phosphorylation and activation of LATS kinase which directly phosphorylates YAP and TAZ inhibiting nuclear translocation. YAP and TAZ phosphorylation creates a binding site for 14–3-3 proteins which sequester YAP and TAZ in the cytoplasm eventually leading to proteasomal degradation[129,130]. Independent of the canonical Hippo signaling pathway, YAP and TAZ are also regulated through G-protein mediated signaling[135], cytoskeletal tension[136], and extracellular matrix stiffness[137].

In MSCs, YAP and TAZ play an important role in determining lineage commitment. In 2005, TAZ transcriptional activity was first reported to dictate MSC differentiation towards osteoblasts[138]. TAZ was found to coactivate the master osteogenic transcription factor Runx2 while inhibiting the master adipogenic transcription factor PPARγ. Numerous follow up studies confirmed that TAZ activation promotes osteogenic differentiation while inhibiting adipogenesis[139–141]. In a mouse model of obesity induced insulin resistance, TAZ inhibition increased adipogenesis which led to increased insulin sensitivity, improved glucose tolerance, and decreased adipose tissue inflammation[142]. El Ouarrat et al., discovered that within adipose tissue TAZ binds to PPARγ acting as a co-repressor and negative regulator of PPARγ transcriptional activity. While the role of TAZ in regulating adipogenesis has been well documented, the role of YAP in adipocyte differentiation has resulted in some conflicting results.

In 3T3L1 preadipocytes YAP overexpression suppressed white adipogenesis[143], while YAP knockout in osteoblast-lineage cells promoted adipogenic differentiation[144]. The different

stages of differentiation along with different cell types may explain the conflicting results. In vivo, YAP overexpression was shown to drive obesity suggesting YAP may promote adipogenesis[145]. Further investigation found that YAP overexpression resulted in a feedback downregulation of both its own transcriptional activity and TAZ. TAZ downregulation led to an increase in PPARγ transcriptional activity, promoting adipocyte differentiation. While YAP and TAZ appear to be important mediators of adipocyte commitment and differentiation, they have also been shown to protect mature adipocytes from cell death during obesity[146]. Using an Adiponectin-Cre YAP/TAZ knockout mouse model, Wang et al., found that when fed a high-fat diet, mice developed lipodystrophy including massive adipocyte death, a compensatory increase in adipogenesis and infiltration by immune cells. The authors concluded that cytoskeletal tension in obese adipocytes drives the transcriptional activation of YAP and TAZ which protects against increased adipocyte cell death. Interestingly, the involvement of YAP and TAZ in adipogenesis has primarily been in the context of white adipose tissue and obesity. Few studies have implicated YAP and TAZ activity in brown or beige adipocyte differentiation and function.

Our lab was the first to identify that actomyosin-mediated tension regulates the thermogenic capacity of brown adipocytes through YAP and TAZ[7]. Recently, in beige adipocytes, β3-AR signaling was shown to inhibit myosin phosphatase target subunit 1- protein phosphatase 1β (MYPT1-PP1β), a regulator of type II myosin activity. Inhibition of MYPT1-PP1β resulted in an increase in actomyosin mediated tension driving YAP and TAZ transcriptional activity thus increasing the thermogenic gene expression profile in beige adipocytes[63]. In this chapter we further investigated the role of YAP and TAZ during beige adipocyte differentiation. In addition, we attempted to investigate the consequences of YAP and TAZ knockout *in vivo*. We found that Adiponectin-Cre YAP knockout mice had reduced respiration rates and reduced UCP1 mRNA expression in white adipose tissue. Interestingly, during beige adipocyte differentiation *in vitro* either YAP knockdown or YAP overexpression decreased UCP1 mRNA expression. These data suggest that YAP levels and timing of YAP activity are tightly regulated in beige adipocytes. To better understand the mechanobiological regulation of adipose tissue, further investigation into the regulation of YAP and TAZ activity are needed.

Results

Induction of YAP/TAZ during cold induced browning and beige adipocyte differentiation

YAP and TAZ transcriptional activity have been shown to blunt adipogenesis, however in mature brown or beige adipocytes YAP and TAZ can drive the thermogenic gene expression profile. Thus, we hypothesized that during early adipocyte differentiation YAP and TAZ are inactivated to facilitate actin reorganization and differentiation but are reactivated in mature brown and beige adipocytes to facilitate thermogenesis. In the sWAT beige adipocyte cell line

we measured YAP and TAZ mRNA levels during differentiation. On day 1 and day 3 of differentiation both YAP and TAZ mRNA levels increased, returned to baseline on day 5 and increased again by day 8 **(Fig. 1A)**. The mRNA expression profile of two YAP/TAZ target genes, CTGF and BMP4, did not mirror that of YAP/TAZ suggesting that YAP/TAZ may primarily be regulated post-translationally **(Fig. 1A)**. Total protein levels of YAP and TAZ during differentiation or after β3-AR induced signaling remained relatively constant **(Fig. 1B).** Phosphorylation of YAP at serine 127 leads to cytoplasmic retention and eventual proteasomal degradation[147]. Again, levels of pYAP S127 remained relatively constant over the course of differentiation and after β3-AR induced signaling **(Fig. 1C).** We also measured total YAP and TAZ protein levels in an earlier pre-adipocyte progenitor cell line, C3H10T1/2 and also found that YAP protein levels stayed relatively constant over beige adipocyte differentiation **(Fig. 1D)**. However, on day 3 of differentiation total TAZ protein levels appeared to slightly increase and remained elevated until day of 11 of differentiation **(Fig. 1D).** Next, we measured the transcriptional signature of YAP and TAZ in *vivo* from the inguinal white adipose tissue of mice housed at either room temperature (23℃), cold (4℃) or at thermoneutrality (30℃). At thermoneutrality, YAP mRNA levels trended down while TAZ mRNA levels were significantly reduced **(Fig. 1D)**. Thermoneutrality blunts brown and beige adipocyte expansion and thermogenesis. Upon cold exposure, YAP and TAZ mRNA levels did not change, while CTGF and BMP4 mRNA levels decreased compared to room temperature **(Fig. 1D)**. Given that BMP4 and CTGF are target genes of YAP and TAZ, their transcript reductions at 4℃ may suggest reduced YAP and TAZ transcriptional activity. Further experiments are necessary to confirm the precise YAP and TAZ transcriptional activity during differentiation and after β3-AR induced signaling. For example, immunofluorescence microscopy of YAP and TAZ would enable us to determine YAP and TAZ spatial localization to infer transcriptional activity.

Pharmacological and genetic intervention of YAP/TAZ in beige adipocytes

Although YAP and TAZ protein levels generally did not change during differentiation we wanted to measure the impact of YAP or TAZ pharmacological interventions during beige adipocyte differentiation. In addition, we wanted to determine whether YAP and TAZ have non-redundant functions in beige adipocytes. We utilized C3H10T1/2 cells because they are an early mesenchymal derived progenitor cell line that differentiate into osteoblasts or adipocytes. C3H10T1/2 cells were differentiated toward beige adipocytes and treated with TM-25659, a small molecule enhancer of TAZ nuclear localization[148]. Treatment with TM-25659 for 8 days during differentiation significantly decreased UCP1 mRNA expression while treatment in mature adipocytes from days 6-8 of differentiation significantly increased UCP1 mRNA expression **(Fig. 2A-B)**. These data would suggest that TAZ transcriptional activity during beige adipocyte differentiation is temporally regulated; early TAZ activation inhibits while late stage TAZ activation enhances thermogenesis. C3H10T1/2 cells were also treated with verteporfin[149],

which sequesters YAP in the cytoplasm inhibiting its transcriptional activity. Verteporfin treatment for 8 days during differentiation significantly reduced UCP1 expression while treatment in mature adipocytes from days 6-8 significantly increased UCP1 expression **(Fig. 2C-D)**. During differentiation UCP1 mRNA expression levels were decreased with either TAZ activation or YAP inhibition, while in mature adipocytes UCP1 mRNA expression levels were increased with either TAZ activation or YAP inhibition. These opposing results, suggesting that YAP and TAZ have non-redundant functions during beige adipogenesis and are temporally regulated. To confirm the pharmacological effects of YAP inhibition we isolated the stromal vascular fraction (SVF) from the inguinal white adipose tissue of control mice or mice with genetic deletion of YAP. The SVF isolated from YAP knockout mice had significantly reduced UCP1 levels as well as reduced levels of additional adipogenic genes compared to control **(Fig. 2E)**. Brightfield images from the YAP knockout SVF differentiated toward beige adipocytes also suggested altered lipid droplet sizes **(Fig. 2F)**. Using the sWAT beige adipocyte cell line, verteporfin treatment in mature adipocytes increased basal and uncoupled respiration compared to control **(Fig. 2G)**, which supports our observed increase in UCP1 mRNA expression with YAP inhibition in mature C3H10T1/2 beige adipocytes.

Timed YAP gain of function during beige adipocyte differentiation

Our pharmacological and genetic interventions of YAP and TAZ suggested temporal regulation of YAP and TAZ activity during beige adipogenesis. We next generated an inducible YAP overexpressing cell line[53,149] to measure the timed YAP gain of function during differentiation. YAP overexpression increased total YAP protein levels and while slightly decreasing TAZ protein levels **(Fig. 3A).** Interestingly, YAP overexpression during 8 days of differentiation, in mature adipocytes from days 6-8 or only during the first 2 days of differentiation, decreased UCP1 protein levels **(Fig. 3A).** Gene expression in beige adipocytes after 8 days of differentiation with YAP overexpression had significantly reduced UCP1 and FABP4 mRNA levels indicating that beige adipogenesis was impaired **(Fig. 3B).** In mature adipocytes with YAP overexpression from days 6-8, UCP1 and PGC1a mRNA levels were significantly reduced indicating impairments of beige thermogenic function **(Fig. 3C).** We observed that during beige adipocyte differentiation, YAP inhibition or YAP overexpression reduced UCP1 expression. YAP activity must be tightly regulated, either too much or too little of YAP can inhibit beige adipogenesis.

Metabolic phenotype of YAP KO mice

To determine the physiological consequences of YAP activity *in vivo* we bred YAP flox mice to Adiponectin-Cre mice to generate YAP knockout (KO) mice specifically in adipose tissue. YAP protein levels were decreased in both the inguinal white adipose tissue and brown adipose tissue in the YAP KO mice compared to control **(Fig. 4A)**. UCP1 protein levels appeared

unchanged in BAT but decreased in iWAT from YAP KO mice compared to controls **(Fig. 4B)**. Total body weight remained unchanged **(Fig. 4C)**, however respiration rates were significantly decreased in the YAP KO mice compared to littermate controls **(Fig. 4D-E).** There was no apparent change in fuel utilization as the respiratory exchange ratio was unchanged **(Fig. 4F).** Given the defects in respiration were observed at room temperature, the mice would likely have impaired cold tolerance. In addition, reductions in energy expenditure suggest that if fed a high-fat diet the YAP KO mice would be more susceptible to diet induced obesity. In fact previous work found that mice lacking YAP and TAZ in white adipocytes and fed a high-fat diet developed severe lipodystrophy with adipocyte cell death[146]. This preliminary data shows that YAP is critical for maintaining energy expenditure. Studies of cold exposed YAP KO mice would likely indicate imparied brown and beige adipose tissue expansion and thermogenesis.

Discussion

Previous work in our lab along with recent work by Takahashi et al.[63], showed that actomyosin-mediated activation of YAP and TAZ induces thermogenesis in brown and beige adipocytes. On the contrary, during mesenchymal stem cell differentiation, nuclear translocation and activation of YAP and TAZ activity will favor osteogenesis over adipogenesis. We hypothesized that during the early stages of adipocyte differentiation, YAP and TAZ are inactivated but in mature brown and beige adipocytes YAP and TAZ are re-activated to mediate actomyosin-induced thermogenesis. We started by measuring mRNA and protein levels during beige differentiation to determine how YAP and TAZ may be regulated. Total protein levels of YAP and TAZ appeared relatively unchanged during differentiation and pYAP levels in the sWAT beige adipocytes did not differ. Subcellular localization dictates YAP and TAZ activity, thus immunofluorescence microscopy experiments of YAP and TAZ during differentiation would help elucidate their temporal regulation.

Given that YAP inhibition reduced UCP1 mRNA expression and thermogenesis in brown adipocytes[7], we wanted to determine whether YAP and TAZ have similar functions in beige adipocytes. To our surprise YAP and TAZ showed non-redundant and temporal activity during beige adipocyte differentiation. Activation of TAZ during differentiation decreased UCP1 mRNA expression while UCP1 mRNA expression increased with TAZ activation in mature adipocytes. When we inhibited YAP function during differentiation UCP1 mRNA expression decreased, however YAP inhibition in mature beige adipocytes increased UCP1 mRNA expression. These findings indicate that YAP and TAZ have non-redundant functions during beige adipogenesis. In addition, their activity appears to be temporally regulated given that UCP1 levels were differentially regulated during early or late-stage differentiation.

We also generated a stable pre-adipocyte cell line to induce the overexpression of YAP in beige adipocytes. To our surprise YAP overexpression during 8 days of differentiation or

during the last 2 days of differentiation resulted in reduced UCP1 mRNA and protein levels. Not only may YAP be temporally regulated but the cells may also regulate the total amount of YAP present. Either too much or too little of YAP can blunt beige adipogenesis. Given that YAP overexpression was previously shown to result in feedback downregulation of its own transcriptional activity as well as TAZ[145], additional studies are needed to confirm the exact mechanism of YAP overexpression in beige adipocytes

To help make sense of our convoluted results *in vitro*, we generated adipocyte specific YAP KO mice. YAP KO appeared to decrease UCP1 protein levels in inguinal white adipose tissue but not in brown adipose tissue. Respiration rates at room temperature of YAP KO mice were also significantly reduced compared to control mice. In the context of high-fat diet induced obesity, YAP and TAZ have been shown to be protective[146]. Thus, our YAP KO mice would likely gain more weight and become more metabolically dysfunctional if fed a high fat diet. To date nobody has shown whether YAP and TAZ alter beige adipocyte thermogenesis *in vivo*. Reductions in UCP1 protein levels in inguinal white adipose tissue suggest that the YAP KO mice would be cold intolerant compared to controls. Throughout this chapter we explored the roles of YAP and TAZ on beige adipocyte differentiation and thermogenesis. We uncovered that YAP and TAZ have non-redundant functions and may temporally regulate beige adipogenesis. Further studies are needed to completely understand the interplay of YAP and TAZ biology in beige adipocytes.

Figures

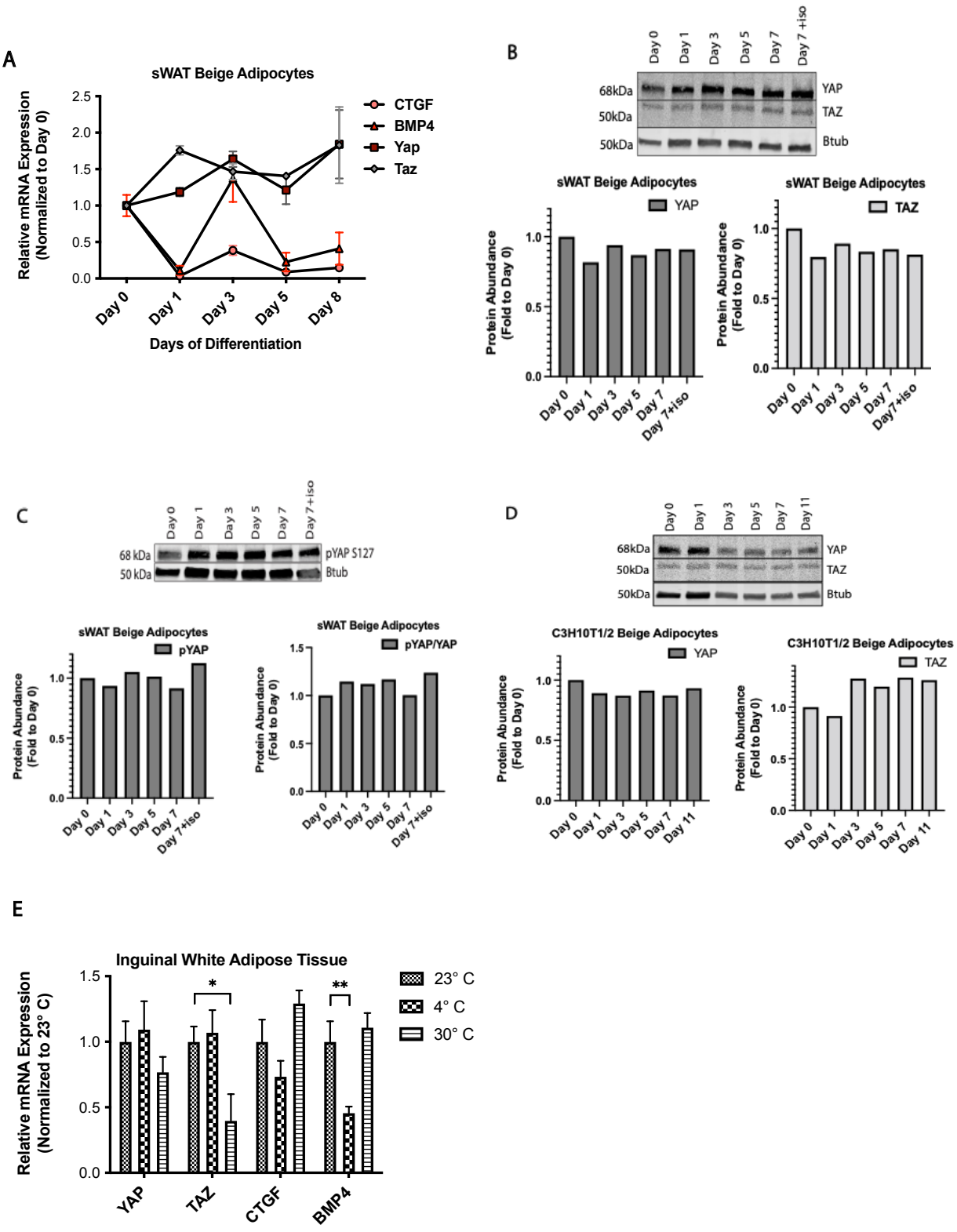
A
sWAT Beige Adipocytes
Relative mRNA Expression (Normalized to Day 0)
CTGF
BMP4
Yap
Taz
Days of Differentiation
B
Day 0
Day 1
Day 3
Day 5
Day 7
Day 7 +iso
68kDa
50kDa
50kDa
YAP
TAZ
Btub
sWAT Beige Adipocytes
YAP
Protein Abundance (Fold to Day 0)
sWAT Beige Adipocytes
TAZ
C
68 kDa
50 kDa
pYAP S127
Btub
sWAT Beige Adipocytes
pYAP
sWAT Beige Adipocytes
pYAP/YAP
D
68kDa
50kDa
50kDa
YAP
TAZ
Btub
C3H10T1/2 Beige Adipocytes
YAP
C3H10T1/2 Beige Adipocytes
TAZ
Day 11
E
Inguinal White Adipose Tissue
Relative mRNA Expression (Normalized to 23° C)
23° C
4° C
30° C
YAP
TAZ
CTGF
BMP4

Figure 1. YAP TAZ Induction. A. Relative mRNA expression from mouse beige adipocytes during differentiation, n=3 independent biological replicates. B. Western blot of YAP and TAZ from mouse beige adipocytes during differentiation and treated with 1uM of isoproterenol. Western blot of pYAPS127 from mouse beige adipocytes during differentiation and treated with 1uM of isoproterenol. D Western blot of YAP and TAZ from mouse embryonic derived cells differentiated toward beige adipocytes. E. Relative mRNA expression from inguinal white adipose tissue of mice housed at 23°C, 30°C. or 4°C, n=6 mice per group.

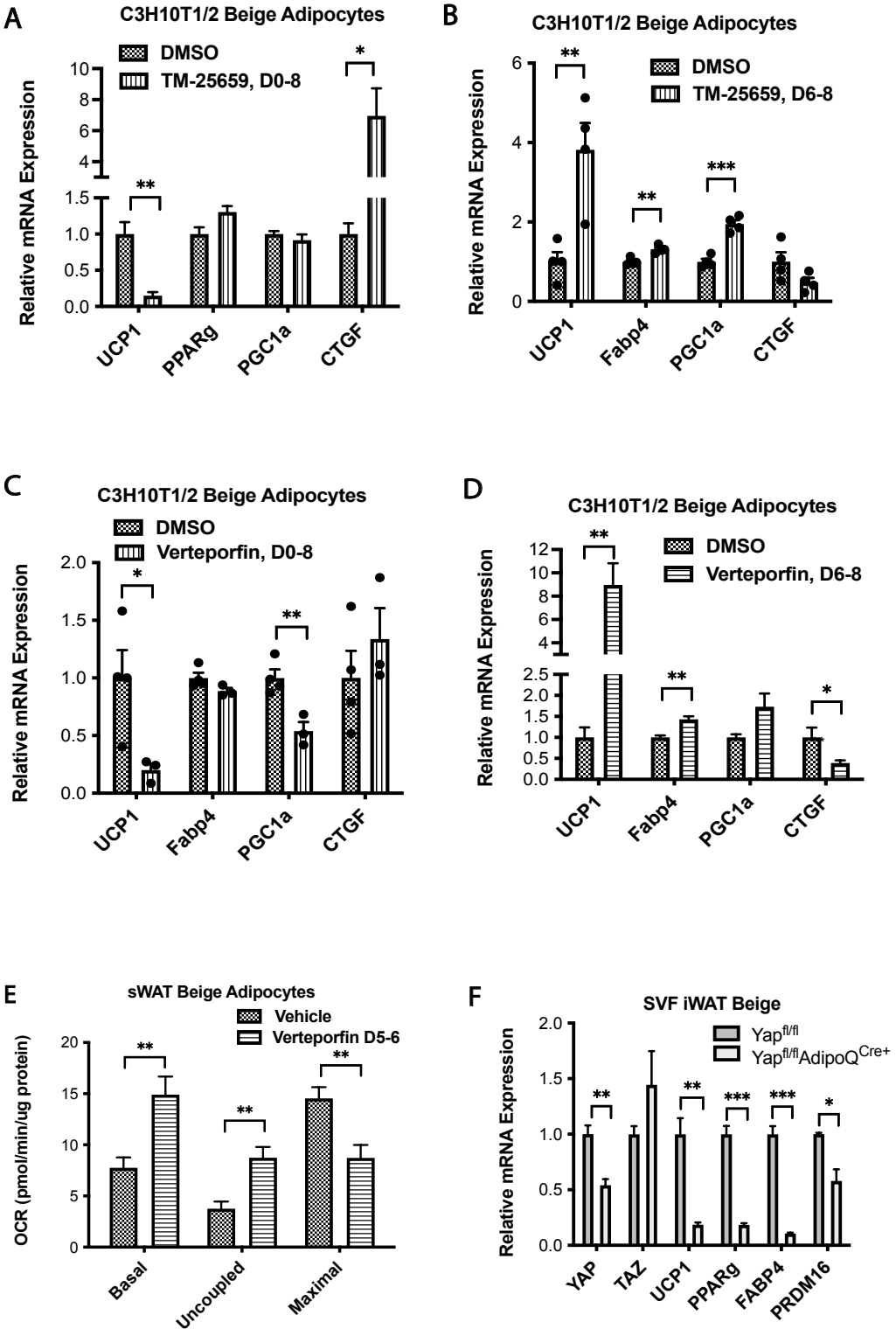
A
C3H10T1/2 Beige Adipocytes
DMSO
TM-25659, D0-8
Relative mRNA Expression
UCP1
PPARg
PGC1a
CTGF
B
C3H10T1/2 Beige Adipocytes
DMSO
TM-25659, D6-8
Relative mRNA Expression
UCP1
Fabp4
PGC1a
CTGF
C
C3H10T1/2 Beige Adipocytes
DMSO
Verteporfin, D0-8
Relative mRNA Expression
UCP1
Fabp4
PGC1a
CTGF
D
C3H10T1/2 Beige Adipocytes
DMSO
Verteporfin, D6-8
Relative mRNA Expression
UCP1
Fabp4
PGC1a
CTGF
E
sWAT Beige Adipocytes
Vehicle
Verteporfin D5-6
OCR (pmol/min/ug protein)
Basal
Uncoupled
Maximal
F
SVF iWAT Beige
Yap fl/fl
Yap fl/fl AdipoQ Cre+
Relative mRNA Expression
YAP
TAZ
UCP1
PPARg
FABP4
PRDM16

G

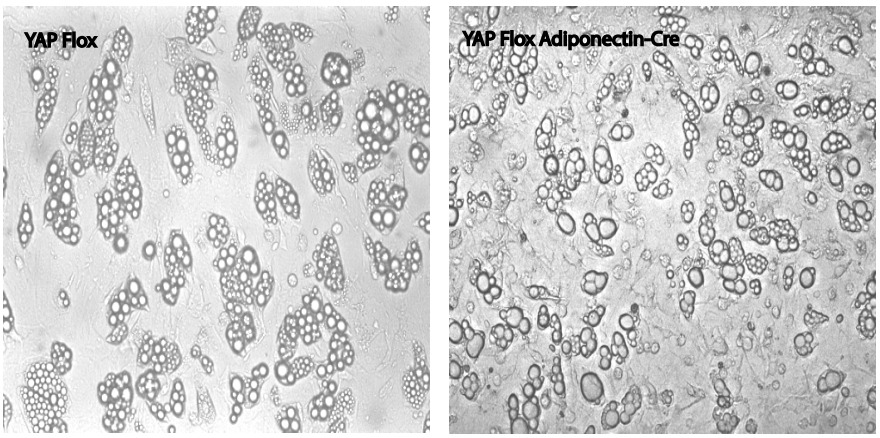

Figure 2. Pharmacological and genetic intervention of YAP/TAZ in beige adipocytes. A-D. Relative mRNA expression from mouse embryonic derived cells differentiated toward beige adipocytes. A. Treated with 10uM of TAZ activator TM25659 or control for days 0-8 of differentiation, n=3 independent biological replicates. B. Treated with 10uM of TAZ activator TM25659 or control for days 6-8 of differentiation, n=3 independent biological replicates. C. Treated with 5uM of YAP inhibitor Verteporfin or control for days 0-8 of differentiation, n=3 independent biological replicates. D. Treated with 5uM of YAP inhibitor Verteporfin or control for days 6-8 of differentiation, n=3 independent biological replicates. E. Oxygen consumption rates of mouse beige adipocytes treated with 5uM of YAP inhibitor Verteporfin or control, n=5 independent biological replicates. F. Relative mRNA expression of the stromal vascular fraction from inguinal white adipose tissue of mice with YAP knockout or control, differentiated toward beige adipocytes, n=3 independent biological replicates. G. Brightfield images of stromal vascular fraction from inguinal white adipose tissue of mice with YAP knockout or control, differentiated toward beige adipocytes.

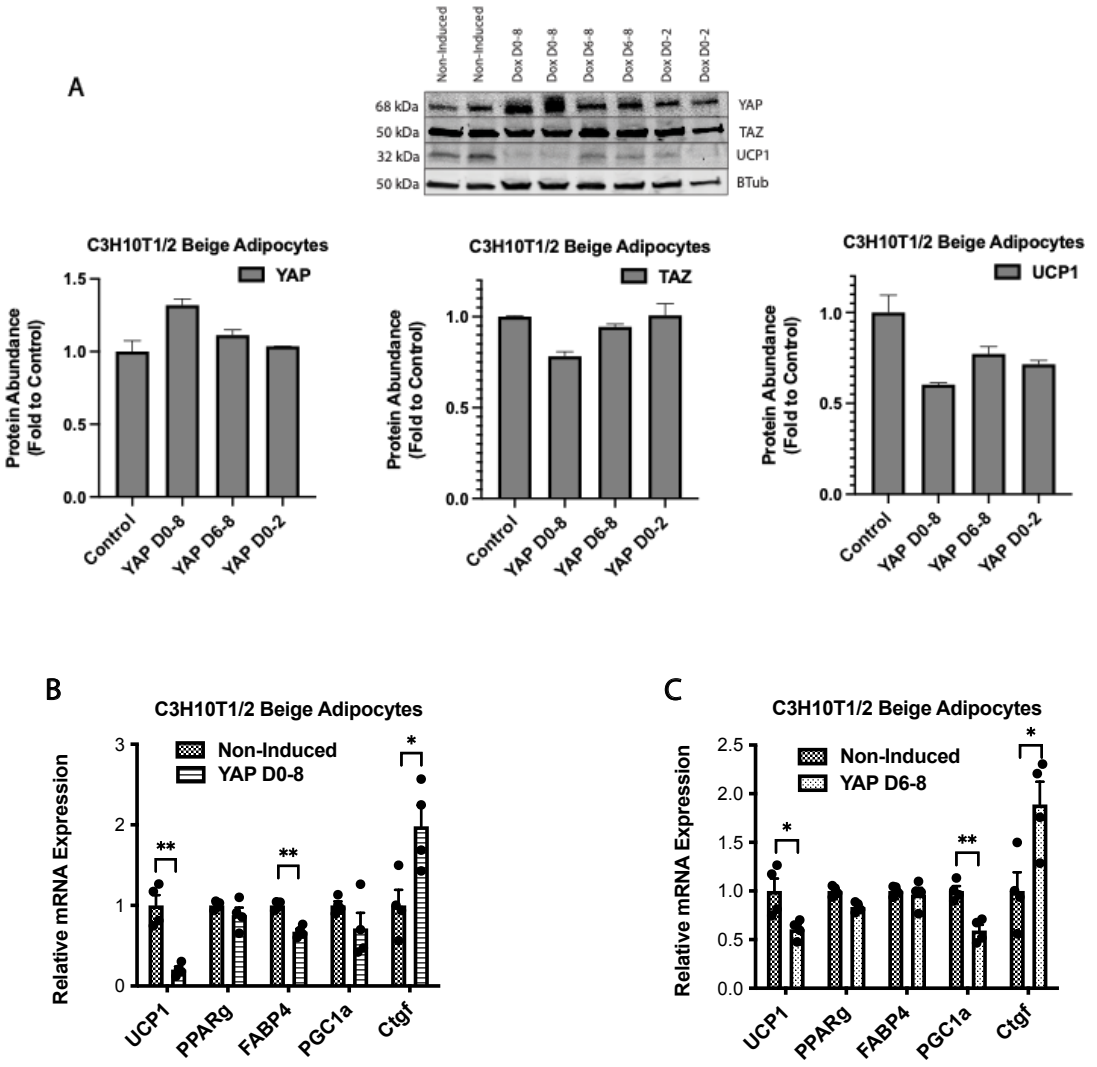

Figure 3. Timed YAP gain of function during beige adipocyte differentiation. A. Western blot of mouse embryonic derived cells differentiated toward beige adipocytes induced to overexpress YAP during differentiation from days 0-8, days 6-8, days 0-2 or control, n=2 independent biological replicates. B. Relative mRNA expression from mouse embryonic derived cells differentiated toward beige adipocytes induced to overexpress YAP during days 0-8 of differentiation, n=4 independent biological replicates. C. Relative mRNA expression from mouse embryonic derived cells differentiated toward beige adipocytes induced to overexpress YAP during days 6-8 of differentiation, n=4 independent biological replicates.

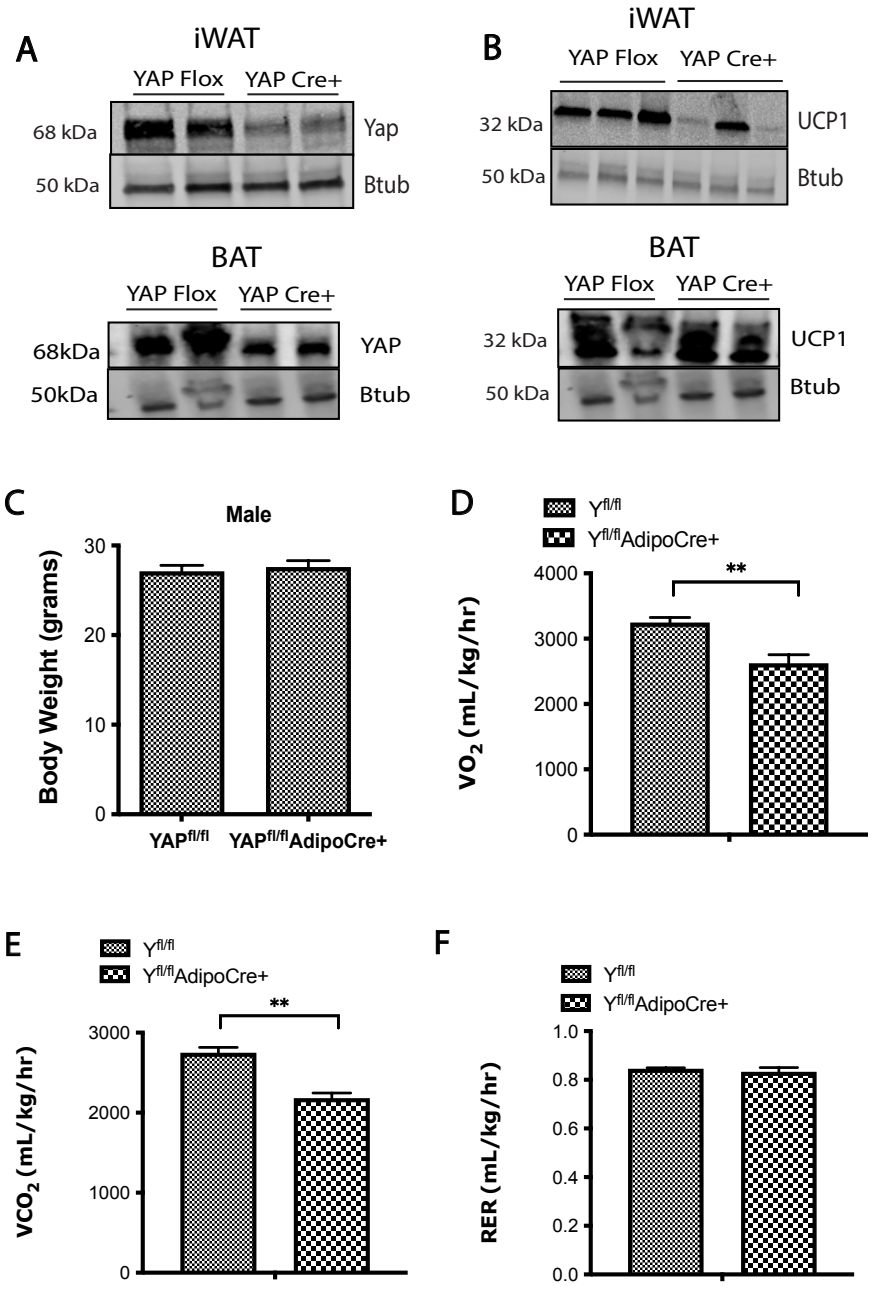

Figure 4. In vivo YAP KO. A. Western blot of YAP from inguinal white adipose tissue and brown adipose tissue of YAP KO mice or control, n=2 independent biological replicates. B. Western blot of UCP1 from inguinal white adipose tissue and brown adipose tissue of YAP KO mice or control, n=2-3 independent biological replicates. C. Body weight from YAP knockout mice (YAP fl/fl Adiponectin Cre+) or littermate controls (Yap fl/fl). D-F. Comprehensive lab animal monitoring (CLAMS) measurements from YAP knockout mice or control, n=3-6 mice per group. D. Oxygen consumption rates. E. Carbon dioxide production. F. Respiratory exchange ratio.

Materials and Methods

Animal Models

All animal experiments were performed under the guidelines established by the UC Berkeley Animal Care and Use Committee. Myh9 flox/flox mice were a gift from Dr. Robert S Adelstein (Laboratory of Molecular Cardiology, National Heart, Lung, and Blood Institute, National Institutes of Health). YAP flox/flox mice were a gift from Dr. Valerie M. Weaver (Center for Bioengineering & Tissue Regeneration, UCSF). YAP flox/flox mice were crossed with B6.FVB-Tg(Ucp1-cre)1Evdr/J from The Jackson Laboratory (strain #024670) to generate a homozygous YAP flox/flox UCP1-Cre mouse line. YAP flox/flox littermates were used as controls. All animal studies were performed using age matched male mice (6-12 weeks), cohorts of greater than or equal to six mice per genotype or treatment, and repeated at least twice.

Cell Lines

sWAT and sBAT cell lines were derived from the Kajimura lab. The preadipocytes sWAT, sBAT, and 3T3L1 along with HEK 293T cells were maintained in DMEM with 10% (v/v) serum and 1% (v/v) penicillin/streptomycin (p/s) (Gibco). sWAT and sBAT preadipocytes were differentiated to beige adipocytes and brown adipocytes respectively with maintenance media fortified with 5 µg/ml Insulin, 1 nM T3, 2 µg/ml Dexamethasone, 500 µM IBMX (Sigma), and 200 nM rosiglitazone. After 2 days of differentiation, cells were switched to maintenance media fortified with 1 nM T3 and 5 µg/ml Insulin for the remainder of differentiation. 3T3L1 preadipocytes were differentiated with maintenance media fortified with 5 µg/ml Insulin, 2 µg/ml Dexamethasone, 500 µM IBMX (Sigma). After 3 days of differentiation, the cells were switched to maintenance media fortified 5 µg/ml Insulin for the remainder of differentiation. Cells were cultured in a humidified CO2 incubator at 37 °C.

SVF Isolation and Differentiation

Brown adipose tissue or inguinal white adipose tissue was collected from 8-12 week old mice and minced with scissors. The tissue was then placed in digestion buffer (25mM NaHCO3, 12mM KH2PO4, 1.2mM MgSO4, 4.8 mM KCl, 120mM NaCl, 1.4 mM CaCl2 5mM glucose, 2.5% BSA (w/v), 1% pen-strep (v/v), 1mg/ml Collagenase (C6885 Sigma-Aldrich) pH 7.4 in PBS). Tissue was digested for 45 minutes, passed through a 100uM nylon mesh filter, and spun at 0.5 rcf for 5 minutes. Supernatant was removed and cells were resuspended DMEM/F12 (Thermo) supplemented with 10% (v/v) serum and 1% (v/v) penicillin/streptomycin (p/s) (Gibco). Cells were passed through a 70uM nylon mesh filter and spun at 0.5 rcf for 5 minutes. Cell pellet was resuspended in an erythrocyte lysis buffer (155mM NH4Cl, 6mM KH2PO4, 0.1mM EDTA, pH 7.4 in PBS) and incubated for 5 minutes. Cells were spun at 0.5 rcf for 5 minutes and resuspended in maintenance media. Cells were differentiated in maintenance media fortified with 5 µg/ml

Insulin, 5 nM T3 (Millipore 64245), 2 µg/ml Dexamethasone, 500 µM IBMX (Sigma), and 0.5 uM rosiglitazone. After 2 days the cells were switched to maintenance media fortified 5 µg/ml Insulin, 5 nM T3, and 0.5 uM rosiglitazone for the remainder of differentiation. To induce Myh9 or Myh10 knockdown during differentiation, the cells were treated with 0.5ug/ml of doxycycline on the same day of differentiation (day 0) and the differentiation was carried out as described above with media replaced every 2 days including doxycycline.

Plasmids, Lentivirus Production, Lentiviral Transduction

The pINDUCER lentiviral toolkit for inducible RNA interference was used to generate Myh9 and Myh10 knockdown cell lines. pINDUCER11 miR-RUG (#44363) was purchased from Addgene. Myh9 and Myh10 miR30-Based shRNA vectors were derived as previously described1. The shRNA top and bottom strands were annealed and then ligated into pINDUCER11 vector that had been digested with EcoRI and XhoI. The ligated plasmid was transformed into One Shot TOP10 Chemically Competent E. coli (invitrogen C404010) and plasmid DNA was isolated using QIAprep Spin Miniprep Kit per manufacturer's instructions. Lentiviruses were produced using Lipofectamine3000 (Invitrogen) according to the manufacturer's instructions. Briefly, 293T cells were transfected with pINDUCER11, psPAX2 (a gift from Didier Trono, Addgene plasmid # 12260; RRID:Addgene_12260), and pMD2.G (gift from Didier Trono, Addgene plasmid # 12259 ; RRID:Addgene_12259) in Lipofectamine3000. Supernatants were harvested at 24h and 48h later, clarified, filtered through a 0.45-µm filter and stored at -80°C. sWAT and sBAT preadipocytes were transduced with lentivirus and 10ug/ml of polybrene. After 2 days post transduction, cells positive for GFP were selected to generate inducible shRNA stable cell lines.

Myh9 shRNA oligos: (Top Strand 5'-
TCGAGAAGGTATATTGCTGTTGACAGTGAGCGCTACCCTTTGAGAATCTGATACTAGTGAAGCCACAGA
TGTAGTATCAGATTCTCAAAGGGTAGTGCCTACTGCCTCGG-3') (Bottom Strand
5'AATTCCGAGGCAGTAGGCACTACCCTTTGAGAATCTGATACTACATCTGTGGCTTCACTAGTATCAGAT
TCTCAAAGGGTAGCGCTCACTGTCAACAGCAATATACCTTC-3')
Myh10 shRNA oligos: (Top Strand 5'-
TCGAGAAGGTATATTGCTGTTGACAGTGAGCGCCCTCCACAAGACATGCGTATTTAGTGAAGCCACAGA
TGTAAATACGCATGTCTTGTGGAGGGTGCCTACTGCCTCGG-3') (Bottom Strand
5'AATTCCGAGGCAGTAGGCACCCTCCACAAGACATGCGTATTTACATCTGTGGCTTCACTAAATACGCAT
GTCTTGTGGAGGGCGCTCACTGTCAACAGCAATATACCTTC-3')

In vitro respirometry

Cellular respiration measurements were performed with a Seahorse XFe24 Analyzer. sWAT cells were plated onto V28 microplates and mitochondrial stress tests were performed on day 6-7 of differentiation. On the day of the assay, the cells were incubated with XF assay medium

supplemented with 1 mM pyruvate (Gibco), 2 mM glutamine (Gibco), and 25 mM glucose (Sigma) at pH 7.4 and sequential additions via injection ports of Oligomycin (1 µM final), FCCP (1 µM final), and Antimycin/Rotenone (1 µM final each). Stock solutions of mitochondrial stress test compounds were solubilized in 100% ethanol at 2.5 mM. Oxygen consumption rates per well were normalized to total protein concentration.

RNA isolation and Real-time quantitative PCR (qPCR)

RNA was isolated from tissues or in vitro cultures with (Zymo Research Direct-zol RNA Miniprep Plus Kits) as per the manufacturer's instructions. 1 ug of RNA was reverse transcribed using (Thermo Fisher Scientific Maxima First Strand cDNA Synthesis Kit for RT-qPCR). RT-qPCR assay was carried out using (Applied Biosystems TaqMan Fast Advanced Master Mix) and ran on the QuantStudio 5 Real-Time PCR System.. The Applied Biosystems TaqMan Fast Advanced Master Mix was used for all experiments and all primer probes used were from Integrated DNA Technologies IDT and were pre-validated. The ΔΔCT method was used to comparatively assess mRNA quantity.

Gene	**Assay ID**	**Ref Seq #**
UCP1	Mm.PT.58.7088262	NM_009463(1)
MYH9	Mm.PT.58.13928218	NM_022410(1)
MYH10	Mm.PT.58.30923223	NM_175260(1)
FABP4	Mm.PT.58.43866459	NM_024406(1)
PPARgamma	Mm.PT.58.31161924	NM_001127330(2)
PPARGC1A	Mm.PT.58.16192665	NR_027710(1)
EBF2	Mm.PT.58.29446261	NM_001276387(2)
LEP	Mm.PT.58.13515402	NM_008493(1)
ADIPOQ	Mm.PT.58.9719546	NM_009605(1)

YAP	Mm.PT.58.6477669	NM_001171147(1)
TAZ	Mm.PT.56a.32319022.g	NM_001173547(4)
CTGF	Mm.PT.58.10386125.g	NM_010217(1)
BMP4	Mm.PT.58.7116776	NM_007554(1)

Transmission electron microscopy

Cells were grown on 35mm MatTek glass-bottom dishes (#P35G-1.5-14-C MatTek Corp., Ashland, MA, USA) and fixed with 1 mL of fixative media for a minimum of 20 min. (Fixative: 2.5% glutaraldehyde and 2.5% paraformaldehyde in 0.1M sodium cacodylate buffer, pH 7.4 (EMS, Hatfield, PA, USA). Samples were rinsed (3×; 5 min, Room Temperature) in 0.1M sodium cacodylate buffer, pH 7.2, and immersed in 1% osmium tetroxide with 1.6% potassium ferricyanide in 0.1M sodium cacodylate buffer for 30 minutes. Samples were rinsed (3×; 5 min, RT) in buffer and briefly washed with distilled water (1×; 1 min, RT), then subjected to an ascending ethanol gradient followed by pure ethanol. Samples were progressively infiltrated (using ethanol as the solvent) with Epon resin (EMS, Hatfield, PA, USA) and polymerized at 60 C for 24-48 hours. Care was taken to ensure only a thin amount of resin remained within the glass bottom dishes to enable the best possible chance for separation of the glass coverslip. Following polymerization, the glass coverslips were removed using ultra-thin Personna razor blades (EMS, Hatfield, PA, USA) and liquid nitrogen exposure, as needed. Regions of interest were cut and mounted on a blank resin block with cyanoacrylate glue for sectioning. Thin sections (80 nm) were cut using a Leica UC6 ultramicrotome (Leica, Wetzlar, Germany) from the surface of the block and collected onto formvar-coated 50 mesh grids. The grids were post-stained with 2% uranyl acetate followed by Reynold's lead citrate, for 5 min each. The sections were imaged using a FEI Tecnai 12 120kV TEM (FEI, Hillsboro, OR, USA) and data recorded using a Gatan Rio 16 CMOS with Gatan Microscopy Suite software (Gatan Inc., Pleasanton, CA, USA).

Western Blotting and Protein Quantification

Protein was collected from in vitro cell culture or tissue using 1x RIPA buffer and 1X protease/phosphatase inhibitors. Protein concentration was measured using the Pierce BCA Protein Assay Kit (Thermo Fisher Scientific). Equal protein concentrations were mixed with a 6x Laemmli buffer containing 2-Mercaptoethanol and boiled at 95°C for 4 minutes. Samples were

resolved on Bio-RAD Protean-TGX gels and transferred onto nitrocellulose membrane using Bio-Rad Transblot turbo. The membranes were blocked with 5% non-fat milk dissolved in tBST for one hour and incubated with one of the following primary antibodies (dilution, company, catalogue number): anti-MyhIIA (1:1000, Cell Signaling, #3403), anti-MyhIIB (1:1000, Cell Signaling, #3404), anti-UCP1 (1:1000, Sigma, U6382), anti-βTubulin (1:1000, Cell Signaling, #2146), anti-DRP1 (1:1000, Cell Signaling, #8570), anti-pDRP1 S616 (1:1000, Cell Signaling, #3455), anti-OPA1 (1:1000, abcam, ab42364), anti-MFN2 (1:1000, Cell Signaling, #9482) Secondary antibodies (LiCor goat anti-mouse 680 LT and LiCor goat anti-rabbit 800).

Immunofluorescence confocal microscopy

For live cell mitochondrial imaging, the cells were plated onto 35mm glass bottoms dishes (Matsunami D11030H) and stained with (MitoTracker Deep Red FM #8778) per manufacturer's instructions or BODIPY 3922. Images were acquired on Zeiss LSM 980 with Airyscan at the UC Berkeley CRL Molecular Imaging Center. For fixed samples, cells were cultured on cover glass slips and fixed with 4% PFA for 10 minutes at room temperature followed by 3x washes with PBS. The cells were then permeabilized with 0.3% Triton X in Blocking Buffer (5% FBS, 2% donkey serum, 0.1% BSA in 1x PBS) for 10 minutes at room temperature. After permeabilization, the cells were washed 3x with blocking buffer and incubated in blocking buffer either for 1 hour at room temperature or overnight at 4°C. Cells were then incubated with primary antibodies diluted in blocking buffer for 1 hour at room temperature or overnight at 4°C. Following primary incubation the cells were washed 3x with blocking buffer and incubated with secondary dyes diluted in blocking buffer for 1 hour at room temperature. Following secondary incubation the cells were washed 3x with blocking buffer and mounted with either ProLong Gold antifade reagent (invitrogen P10144) or SlowFade Diamond Antifade Mountant (invitrogen S36972). Primary antibodies (dilution, company, catalog number): anti-Myh9 (1:500, BioLegend, #PRB-440P), anti-MyhIIB (1:300, Cell Signaling, #3404), anti-TOM20 (1:300, Sigma-Aldrich, WH0009804M1). Secondary antibodies were used from Jackson ImmunoResearch (1:10,000) and phalloidin conjugates from ThermoFisher were used for actin staining (1:400).

RNA-seq

Murine beige adipocytes (sWAT) were differentiated for 7 days with or without Myh9 knockdown and n=3 independent biological replicates were pooled to generate total RNA samples. Sequencing libraries were constructed from mRNA using KAPA mRNA HyperPrep Kit (KK8580) and NEXFlex barcoded adaptors (Bioo Scientific). High-throughput sequencing was performed using a HiSeq 2500 instrument (Illumina) at the UC Berkely QB3 Core. Raw reads were mapped using STAR60 against mouse (mm10) genome. DESeq261 was used to determine differential gene expression. Enriched transcription factor binding sites in gene promoters were

identified using HOMER62. RNAseq data will be available for public at the Gene Expression Omnibus (GEO) under accession GSE165940.

Isolated Mitochondria

Mitochondria was isolated as previously described[142]. Briefly, brown adipose tissue was dissected from mice and placed in STE buffer (250mM sucrose, 5mM Tris and 2mM EGTA, pH 7.4) with 1% BSA. Tissue was minced with a razor blade and placed in fresh STE buffer with 1% BSA. Minced tissue was homogenized using 3 strokes with loose fit dounce homogenizer followed by 10 strokes with tight fit dounce homogenizer. Homogenate was then filtered through 70um nylon mesh strainer and centrifuged at 8500 rcf for 10 minutes at 4°C. Pellet was resuspended in STE buffer with 1% BSA. Resuspended pellet was then centrifuged at 700 rcf for 10 minutes at 4°C. Supernatant was transferred to a new tube and centrifuged at 8500 rcf for 10 minutes at 4°C. The pellet was resuspended in STE buffer without BSA and centrifuged at 8500 rcf for 20 minutes at 4°C; this step was repeated for a total of 2 times. The mitochondrial pellet was then resuspended in 150ul of STE buffer without BSA.

In Vivo respirometry

YAP flox/flox UCP1-Cre and YAP flox/flox littermate control mice were housed under ambient temperature (23°C) and fed diet (Research Diets D12450J). At 12 weeks old the mice were cold exposed at (4°C) for 1 day followed by whole-body energy expenditure (VO2, VCO2, RER) recorded at indicated environmental temperatures using a Comprehensive Lab Animal Monitoring System (CLAMS,Columbus Instruments). Data were imported and analyzed using the web-based analysis tool for indirect calorimetry experiments (CalR)[143].

Atomic Force Microscopy

Cells were cultured on glass coverslips and differentiated toward mature adipocytes. Tension measurements were measured using the at room temperature in HEPES buffered media (10% FBS, 25mM glucose, 2mM glutamine, 1% pen/strep, and 25mM HEPES).

Quencher-based real time BODIPY-fatty acid uptake assay

The real-time fatty acid uptake assay was based on a previously published assay[144]. Cells were plated in a 96-well clear bottom plate and differentiated toward mature adipocytes. Cell media was replaced with uptake solution containing 1mM trypan blue, 3.5 g/L glucose, 2uM BODIPY-fatty acid, and 0.1% bovine serum albumin in Hank's buffered saline solution. The cells were immediately placed into a SpectraMax i3 plate reader and the fluorescence was read at an excitation of 488 nm and emission of 515 nm every minute for 90 minutes. The steady-state fluorescence over time was plotted.

Conclusion

Brown and beige adipose tissue hold the promise for combating numerous metabolic diseases. As our biological understanding of the tissues grows we will likely uncover novel mechanisms that may have therapeutic potential. The Stahl lab previously uncovered a unique mechanobiological mechanism that mediates brown adipose tissue thermogenesis, this work that laid the foundation for our work in this dissertation. At the intersection of mechanotransduction and metabolic biology we investigated whether the actomyosin network regulates beige adipose tissue development and metabolic activity.

In chapter 1 we discovered that beige adipose tissue expresses multiple type II myosin isoforms, namely non-muscle myosin Myh9 and Myh10, smooth muscle myosin Myh11, and skeletal muscle myosin Myh14. Type II myosins generate contractile force and traditionally are involved in cell protrusion and cell division. Few studies have implicated type II myosin activity in regulating metabolic processes. We uncovered that in beige adipocytes, type II myosins generate contractile force and inhibition of type II myosin activity reduces beige adipocyte thermogenesis. Further investigation into the specific functions of individual type II myosins suggested that Myh9, the most abundantly expressed isoform, is responsible for regulating beige adipocyte thermogenesis. Knockdown of Myh9 resulted in a reduction in UCP1 mRNA expression and impaired cellular respiration. Beyond UCP1 mRNA expression, loss of Myh9 impaired beige adipose tissue mitochondrial function and lipid metabolism. Our results suggest Myh9 may be acting through two parallel and possibly overlapping mechanisms. Observed reductions in cellular tension with Myh9 knockdown likely alters mechanotransduction leading to UCP1 transcriptional changes. In addition, we found Myh9 to localize with mitochondria around lipid droplets suggesting direct physical interaction with these organelles. Future studies will be needed to understand the exact mechanisms by which loss of Myh9 affects beige adipocyte thermogenesis.

In chapter 2 we sought to translate our knowledge of actomyosin mediated thermogenesis into therapeutic potential. In collaboration with Atomwise we screened 163 small molecules to increase thermogenesis in brown and beige adipocytes through type II myosin activation. After identifying compound hits through increases in UCP1 mRNA expression and cellular respiration we identified compound 0246504505 as the most potent activator of thermogenesis. We confirmed compound 0246504505 to be selective towards brown and beige adipocytes and not white adipocytes. In addition we confirmed compound 0246504505 acted independently of mitochondrial uncoupling. These results have laid the groundwork for utilizing type II myosin activators as a therapeutic approach to increase thermogenesis and energy expenditure. Compound optimization as well as confirmation of the mechanism of action will help justify the use of type II myosin activators to combat metabolic diseases.

In chapter 3 we sought to investigate the role of the mechanosensitive transcription factors YAP and TAZ in thermogenesis. YAP and TAZ activity blunts adipogenesis in mesenchymal stem cells, however inhibition of YAP and TAZ in mature brown and beige adipocytes blunts thermogenesis. We hypothesized that YAP and TAZ are inactive early during adipogenesis but are reactivated in mature brown and beige adipocytes. Our hypothesis appeared more convoluted than expected as YAP and TAZ had non-redundant functions during beige adipocyte differentiation. In addition, both YAP and TAZ appeared to be temporally regulated as UCP1 mRNA expression changed based on the the timing of YAP and TAZ activity. We showed that the quantity and timing of YAP and TAZ affects beige adipogenesis. Future studies will be needed to parse out the exact functions between YAP and TAZ in brown and beige adipose tissue.

Throughout this dissertation we investigated how classical mechanical mechanisms, namely the actomyosin network, directly influences metabolic activity in brown and beige adipose tissue. Specifically, in beige adipocytes we identified type II Myh9 as an important mechanical protein needed for beige adipocyte thermogenesis. Activating type II myosins may be a promising therapeutic approach to increase brown and beige adipose tissue activity. Small molecule type II myosin agonists targeting adipocyte myosin activity could be used to treat metabolic diseases such as type II diabetes, cardiovascular disease, and diabetes. Mechanical signals are relayed to transcriptional responses through mechanosensitive transcription factors. We further showed that YAP and TAZ are two such mechanosensitive transcription factors that can influence the outcome of beige adipocyte differentiation and thermogenic function. In conclusion, the mechanobiological activity is a critical component of metabolic regulation in brown and beige adipose tissue.

References

1. Bartelt, A. & Heeren, J. Adipose tissue browning and metabolic health. *Nature Reviews Endocrinology* vol. 10 24–36 Preprint at https://doi.org/10.1038/nrendo.2013.204 (2014).
2. Harms, M. & Seale, P. Brown and beige fat: development, function and therapeutic potential. *Nature Medicine* vol. 19 1252–1263 Preprint at https://doi.org/10.1038/nm.3361 (2013).
3. Kajimura, S., Spiegelman, B. M. & Seale, P. Brown and Beige Fat: Physiological Roles beyond Heat Generation. *Cell Metabolism* vol. 22 546–559 Preprint at

https://doi.org/10.1016/j.cmet.2015.09.007 (2015).

4. Townsend, K. L. & Tseng, Y.-H. Brown fat fuel utilization and thermogenesis. *Trends Endocrinol. Metab.* **25**, 168–177 (2014).

5. Cannon, B. & Nedergaard, J. Brown Adipose Tissue: Function and Physiological Significance. *Physiological Reviews* vol. 84 277–359 Preprint at https://doi.org/10.1152/physrev.00015.2003 (2004).

6. Surapaneni, P., Vinales, K. L., Najib, M. Q. & Chaliki, H. P. Valvular heart disease with the use of fenfluramine-phentermine. *Tex. Heart Inst. J.* **38**, 581–583 (2011).

7. Tharp, K. M. *et al.* Actomyosin-Mediated Tension Orchestrates Uncoupled Respiration in Adipose Tissues. *Cell Metab.* **27**, 602–615.e4 (2018).

8. Timmons, J. A. *et al.* Myogenic gene expression signature establishes that brown and white adipocytes originate from distinct cell lineages. *Proc. Natl. Acad. Sci. U. S. A.* **104**, 4401–4406 (2007).

9. Walden, T. B., Timmons, J. A., Keller, P., Nedergaard, J. & Cannon, B. Distinct expression of muscle-specific microRNAs (myomirs) in brown adipocytes. *J. Cell. Physiol.* **218**, 444–449 (2009).

10. Wu, J. *et al.* Beige adipocytes are a distinct type of thermogenic fat cell in mouse and human. *Cell* **150**, 366–376 (2012).

11. Murrell, M., Oakes, P. W., Lenz, M. & Gardel, M. L. Forcing cells into shape: the mechanics of actomyosin contractility. *Nat. Rev. Mol. Cell Biol.* **16**, 486–498 (2015).

12. Nobusue, H. *et al.* Regulation of MKL1 via actin cytoskeleton dynamics drives adipocyte differentiation. *Nat. Commun.* **5**, 3368 (2014).

13. McDonald, M. E. *et al.* Myocardin-related transcription factor A regulates conversion of progenitors to beige adipocytes. *Cell* **160**, 105–118 (2015).

14. Khan, A. U., Qu, R., Fan, T., Ouyang, J. & Dai, J. A glance on the role of actin in osteogenic and adipogenic differentiation of mesenchymal stem cells. *Stem Cell Res. Ther.* **11**, 283 (2020).

15. Hartman, M. A., Amanda Hartman, M. & Spudich, J. A. The myosin superfamily at a glance. *Journal of Cell Science* vol. 125 1627–1632 Preprint at https://doi.org/10.1242/jcs.094300 (2012).

16. Popa, I. & Gutzman, J. H. The extracellular matrix-myosin pathway in mechanotransduction: from molecule to tissue. *Emerg Top Life Sci* **2**, 727–737 (2018).

17. Betapudi, V. Life without double-headed non-muscle myosin II motor proteins. *Front Chem* **2**, 45 (2014).

18. Wendt, T., Taylor, D., Trybus, K. M. & Taylor, K. Three-dimensional image reconstruction of dephosphorylated smooth muscle heavy meromyosin reveals asymmetry in the interaction between myosin heads and placement of subfragment 2. *Proc. Natl. Acad. Sci. U. S. A.* **98**, 4361–4366 (2001).

19. Somlyo, A. P. & Somlyo, A. V. Ca2+ sensitivity of smooth muscle and nonmuscle myosin II: modulated by G proteins, kinases, and myosin phosphatase. *Physiol. Rev.* **83**, 1325–1358 (2003).

20. Heissler, S. M. & Sellers, J. R. Various Themes of Myosin Regulation. *J. Mol. Biol.* **428**, 1927–1946 (2016).

21. Ikebe, M. & Hartshorne, D. J. Phosphorylation of smooth muscle myosin at two distinct

sites by myosin light chain kinase. *J. Biol. Chem.* **260**, 10027–10031 (1985).

22. Ikebe, M., Hartshorne, D. J. & Elzinga, M. Identification, phosphorylation, and dephosphorylation of a second site for myosin light chain kinase on the 20,000-dalton light chain of smooth muscle myosin. *J. Biol. Chem.* **261**, 36–39 (1986).
23. Kassianidou, E., Hughes, J. H. & Kumar, S. Activation of ROCK and MLCK tunes regional stress fiber formation and mechanics via preferential myosin light chain phosphorylation. *Mol. Biol. Cell* (2017) doi:10.1091/mbc.e17-06-0401.
24. Vicente-Manzanares, M., Ma, X., Adelstein, R. S. & Horwitz, A. R. Non-muscle myosin II takes centre stage in cell adhesion and migration. *Nat. Rev. Mol. Cell Biol.* **10**, 778–790 (2009).
25. Newell-Litwa, K. A., Horwitz, R. & Lamers, M. L. Non-muscle myosin II in disease: mechanisms and therapeutic opportunities. *Dis. Model. Mech.* **8**, 1495–1515 (2015).
26. Keung, A. J., Kumar, S. & Schaffer, D. V. Presentation counts: microenvironmental regulation of stem cells by biophysical and material cues. *Annu. Rev. Cell Dev. Biol.* **26**, 533–556 (2010).
27. Engler, A. J., Sen, S., Sweeney, H. L. & Discher, D. E. Matrix elasticity directs stem cell lineage specification. *Cell* **126**, 677–689 (2006).
28. Keung, A. J., de Juan-Pardo, E. M., Schaffer, D. V. & Kumar, S. Rho GTPases mediate the mechanosensitive lineage commitment of neural stem cells. *Stem Cells* **29**, 1886–1897 (2011).
29. Tang, Y. *et al.* MT1-MMP-dependent control of skeletal stem cell commitment via a β1-integrin/YAP/TAZ signaling axis. *Dev. Cell* **25**, 402–416 (2013).

30. Fulcher, F. K., Smith, B. T., Russ, M. & Patel, Y. M. Dual role for myosin II in GLUT4-mediated glucose uptake in 3T3-L1 adipocytes. *Exp. Cell Res.* **314**, 3264–3274 (2008).
31. Cheung, S. Y., Sayeed, M., Nakuluri, K., Li, L. & Feldman, B. J. MYH9 facilitates autoregulation of adipose tissue depot development. *JCI Insight* **6**, (2021).
32. Kislev, N., Mor-Yossef Moldovan, L., Barak, R., Egozi, M. & Benayahu, D. MYH10 Governs Adipocyte Function and Adipogenesis through Its Interaction with GLUT4. *Int. J. Mol. Sci.* **23**, (2022).
33. Pfisterer, S. G. *et al.* Role for formin-like 1-dependent acto-myosin assembly in lipid droplet dynamics and lipid storage. *Nat. Commun.* **8**, 14858 (2017).
34. Zhao, P., Han, H., Wu, X., Wu, J. & Ren, Z. ARP2/3 Regulates Fatty Acid Synthesis by Modulating Lipid Droplets' Motility. *Int. J. Mol. Sci.* **23**, (2022).
35. Korobova, F., Gauvin, T. J. & Higgs, H. N. A role for myosin II in mammalian mitochondrial fission. *Curr. Biol.* **24**, 409–414 (2014).
36. Moore, A. S., Wong, Y. C., Simpson, C. L. & Holzbaur, E. L. F. Dynamic actin cycling through mitochondrial subpopulations locally regulates the fission-fusion balance within mitochondrial networks. *Nat. Commun.* **7**, 12886 (2016).
37. Yang, C. & Svitkina, T. M. Ultrastructure and dynamics of the actin−myosin II cytoskeleton during mitochondrial fission. *Nature Cell Biology* vol. 21 603–613 Preprint at https://doi.org/10.1038/s41556-019-0313-6 (2019).
38. Kage, F., Vicente-Manzanares, M., McEwan, B. C., Kettenbach, A. N. & Higgs, H. N. Myosin II proteins are required for organization of calcium-induced actin networks upstream of mitochondrial division. *Mol. Biol. Cell* **33**, ar63 (2022).

39. Donaudy, F. *et al.* Nonmuscle myosin heavy-chain gene MYH14 is expressed in cochlea and mutated in patients affected by autosomal dominant hearing impairment (DFNA4). *Am. J. Hum. Genet.* **74**, 770–776 (2004).

40. Almutawa, W. *et al.* The R941L mutation in MYH14 disrupts mitochondrial fission and associates with peripheral neuropathy. *EBioMedicine* **45**, 379–392 (2019).

41. Wade, G., McGahee, A., Ntambi, J. M. & Simcox, J. Lipid Transport in Brown Adipocyte Thermogenesis. *Front. Physiol.* **12**, 787535 (2021).

42. Lee, J. H. *et al.* The Role of Adipose Tissue Mitochondria: Regulation of Mitochondrial Function for the Treatment of Metabolic Diseases. *Int. J. Mol. Sci.* **20**, (2019).

43. Boutant, M. *et al.* Mfn2 is critical for brown adipose tissue thermogenic function. *EMBO J.* **36**, 1543–1558 (2017).

44. Pisani, D. F. *et al.* Mitochondrial fission is associated with UCP1 activity in human brite/beige adipocytes. *Mol Metab* **7**, 35–44 (2018).

45. Mooli, R. G. R., Mukhi, D., Chen, Z., Buckner, N. & Ramakrishnan, S. K. An indispensable role for dynamin-related protein 1 in beige and brown adipogenesis. *J. Cell Sci.* **133**, (2020).

46. Galmozzi, A. *et al.* ThermoMouse: an in vivo model to identify modulators of UCP1 expression in brown adipose tissue. *Cell Rep.* **9**, 1584–1593 (2014).

47. Doran, M. H. & Lehman, W. The Central Role of the F-Actin Surface in Myosin Force Generation. *Biology* **10**, (2021).

48. Kovács, M., Tóth, J., Hetényi, C., Málnási-Csizmadia, A. & Sellers, J. R. Mechanism of blebbistatin inhibition of myosin II. *J. Biol. Chem.* **279**, 35557–35563 (2004).

49. Kanzaki, M. Insulin receptor signals regulating GLUT4 translocation and actin dynamics.

Endocr. J. **53**, 267–293 (2006).

50. Choi, Y. O. *et al.* Implication of phosphorylation of the myosin II regulatory light chain in insulin-stimulated GLUT4 translocation in 3T3-F442A adipocytes. *Exp. Mol. Med.* **38**, 180–189 (2006).
51. Bedi, D., Dennis, J. C., Morrison, E. E., Braden, T. D. & Judd, R. L. Regulation of intracellular trafficking and secretion of adiponectin by myosin II. *Biochem. Biophys. Res. Commun.* **490**, 202–208 (2017).
52. Beier, N. *et al.* The novel cardiotonic agent EMD 53 998 is a potent 'calcium sensitizer'. *J. Cardiovasc. Pharmacol.* **18**, 17–27 (1991).
53. Meerbrey, K. L. *et al.* The pINDUCER lentiviral toolkit for inducible RNA interference in vitro and in vivo. *Proc. Natl. Acad. Sci. U. S. A.* **108**, 3665–3670 (2011).
54. Cui, L. & Liu, P. Two Types of Contact Between Lipid Droplets and Mitochondria. *Front Cell Dev Biol* **8**, 618322 (2020).
55. Benador, I. Y. *et al.* Mitochondria Bound to Lipid Droplets Have Unique Bioenergetics, Composition, and Dynamics that Support Lipid Droplet Expansion. *Cell Metab.* **27**, 869–885.e6 (2018).
56. Indo, H. P. *et al.* A mitochondrial superoxide theory for oxidative stress diseases and aging. *J. Clin. Biochem. Nutr.* **56**, 1–7 (2015).
57. Liu, S., Liu, S. & Jiang, H. Multifaceted roles of mitochondrial stress responses under ETC dysfunction - repair, destruction and pathogenesis. *FEBS J.* (2021) doi:10.1111/febs.16323.
58. Fan, H. *et al.* Cold-Inducible Klf9 Regulates Thermogenesis of Brown and Beige Fat. *Diabetes* **69**, 2603–2618 (2020).

59. Fang, Y., Wu, D. & Birukov, K. G. Mechanosensing and Mechanoregulation of Endothelial Cell Functions. *Compr. Physiol.* **9**, 873–904 (2019).

60. Pollak, N. M., Hoffman, M., Goldberg, I. J. & Drosatos, K. Krüppel-like factors: Crippling and un-crippling metabolic pathways. *JACC Basic Transl Sci* **3**, 132–156 (2018).

61. Houdusse, A. & Sweeney, H. L. How Myosin Generates Force on Actin Filaments. *Trends Biochem. Sci.* **41**, 989–997 (2016).

62. Wasik, A. A. *et al.* Septin 7 reduces nonmuscle myosin IIA activity in the SNAP23 complex and hinders GLUT4 storage vesicle docking and fusion. *Exp. Cell Res.* **350**, 336–348 (2017).

63. Takahashi, H. *et al.* MYPT1-PP1β phosphatase negatively regulates both chromatin landscape and co-activator recruitment for beige adipogenesis. *Nat. Commun.* **13**, 5715 (2022).

64. Barnhart, E. L. Mechanics of mitochondrial motility in neurons. *Curr. Opin. Cell Biol.* **38**, 90–99 (2016).

65. Hall, K. D. *et al.* Quantification of the effect of energy imbalance on bodyweight. *The Lancet* vol. 378 826–837 (2011).

66. Maliszewska, K. & Kretowski, A. Brown Adipose Tissue and Its Role in Insulin and Glucose Homeostasis. *International Journal of Molecular Sciences* vol. 22 1530 Preprint at https://doi.org/10.3390/ijms22041530 (2021).

67. Nedergaard, J., Bengtsson, T. & Cannon, B. Unexpected evidence for active brown adipose tissue in adult humans. *Am. J. Physiol. Endocrinol. Metab.* **293**, E444–52 (2007).

68. Lidell, M. E., Betz, M. J. & Enerbäck, S. Brown adipose tissue and its therapeutic potential. *Journal of Internal Medicine* vol. 276 364–377 Preprint at

https://doi.org/10.1111/joim.12255 (2014).

69. Trayhurn, P. Brown Adipose Tissue—A Therapeutic Target in Obesity? *Frontiers in Physiology* vol. 9 Preprint at https://doi.org/10.3389/fphys.2018.01672 (2018).
70. Yoneshiro, T. *et al.* Recruited brown adipose tissue as an antiobesity agent in humans. *J. Clin. Invest.* **123**, 3404–3408 (2013).
71. van der Lans, A. A. J. J. *et al.* Cold acclimation recruits human brown fat and increases nonshivering thermogenesis. *J. Clin. Invest.* **123**, 3395–3403 (2013).
72. Virtanen, K. A. *et al.* Functional brown adipose tissue in healthy adults. *N. Engl. J. Med.* **360**, 1518–1525 (2009).
73. Blondin, D. P. *et al.* Increased brown adipose tissue oxidative capacity in cold-acclimated humans. *J. Clin. Endocrinol. Metab.* **99**, E438–46 (2014).
74. Symonds, M. Faculty Opinions recommendation of Brown adipose tissue improves whole-body glucose homeostasis and insulin sensitivity in humans. *Faculty Opinions – Post-Publication Peer Review of the Biomedical Literature* Preprint at https://doi.org/10.3410/f.718505529.793548349 (2018).
75. Matsushita, M. *et al.* Impact of brown adipose tissue on body fatness and glucose metabolism in healthy humans. *Int. J. Obes.* **38**, 812–817 (2014).
76. Becher, T. *et al.* Brown adipose tissue is associated with cardiometabolic health. *Nat. Med.* **27**, 58–65 (2021).
77. Peres Valgas da Silva, C., Hernández-Saavedra, D., White, J. D. & Stanford, K. I. Cold and Exercise: Therapeutic Tools to Activate Brown Adipose Tissue and Combat Obesity. *Biology* **8**, (2019).

78. Colman, E. Dinitrophenol and obesity: an early twentieth-century regulatory dilemma. *Regul. Toxicol. Pharmacol.* **48**, 115–117 (2007).

79. McLaughlin, S. G. & Dilger, J. P. Transport of protons across membranes by weak acids. *Physiol. Rev.* **60**, 825–863 (1980).

80. Kotova, E. A. & Antonenko, Y. N. Fifty Years of Research on Protonophores: Mitochondrial Uncoupling As a Basis for Therapeutic Action. *Acta Naturae* **14**, 4–13 (2022).

81. Perry, R. J. *et al.* Reversal of hypertriglyceridemia, fatty liver disease, and insulin resistance by a liver-targeted mitochondrial uncoupler. *Cell Metab.* **18**, 740–748 (2013).

82. Perry, R. J., Zhang, D., Zhang, X.-M., Boyer, J. L. & Shulman, G. I. Controlled-release mitochondrial protonophore reverses diabetes and steatohepatitis in rats. *Science* **347**, 1253–1256 (2015).

83. Childress, E. S., Alexopoulos, S. J., Hoehn, K. L. & Santos, W. L. Small Molecule Mitochondrial Uncouplers and Their Therapeutic Potential. *J. Med. Chem.* **61**, 4641–4655 (2018).

84. Zhao, J., Unelius, L., Bengtsson, T., Cannon, B. & Nedergaard, J. Coexisting beta-adrenoceptor subtypes: significance for thermogenic process in brown fat cells. *Am. J. Physiol.* **267**, C969–79 (1994).

85. Chernogubova, E., Cannon, B. & Bengtsson, T. Norepinephrine increases glucose transport in brown adipocytes via beta3-adrenoceptors through a cAMP, PKA, and PI3-kinase-dependent pathway stimulating conventional and novel PKCs. *Endocrinology* **145**, 269–280 (2004).

86. Cero, C. *et al.* β3-Adrenergic receptors regulate human brown/beige adipocyte lipolysis

and thermogenesis. *JCI Insight* **6**, (2021).

87. McNeill, B. T., Suchacki, K. J. & Stimson, R. H. MECHANISMS IN ENDOCRINOLOGY: Human brown adipose tissue as a therapeutic target: warming up or cooling down? *European Journal of Endocrinology* vol. 184 R243–R259 Preprint at https://doi.org/10.1530/eje-20-1439 (2021).
88. Weyer, C., Tataranni, P. A., Snitker, S., Danforth, E., Jr & Ravussin, E. Increase in insulin action and fat oxidation after treatment with CL 316,243, a highly selective beta3-adrenoceptor agonist in humans. *Diabetes* **47**, 1555–1561 (1998).
89. Cypess, A. M. *et al.* Activation of human brown adipose tissue by a β3-adrenergic receptor agonist. *Cell Metab.* **21**, 33–38 (2015).
90. O'Mara, A. E. *et al.* Chronic mirabegron treatment increases human brown fat, HDL cholesterol, and insulin sensitivity. *J. Clin. Invest.* **130**, 2209–2219 (2020).
91. Carey, A. L. *et al.* Ephedrine activates brown adipose tissue in lean but not obese humans. *Diabetologia* vol. 56 147–155 Preprint at https://doi.org/10.1007/s00125-012-2748-1 (2013).
92. Gauthier, C., Tavernier, G., Charpentier, F., Langin, D. & Le Marec, H. Functional beta3-adrenoceptor in the human heart. *J. Clin. Invest.* **98**, 556–562 (1996).
93. Siersbæk, M. S. *et al.* Genome-wide profiling of peroxisome proliferator-activated receptor γ in primary epididymal, inguinal, and brown adipocytes reveals depot-selective binding correlated with gene expression. *Mol. Cell. Biol.* **32**, 3452–3463 (2012).
94. Evans, R. M., Barish, G. D. & Wang, Y.-X. PPARs and the complex journey to obesity. *Nat. Med.* **10**, 355–361 (2004).

95. PPARγ: a Nuclear Regulator of Metabolism, Differentiation, and Cell Growth. *J. Biol. Chem.* **276**, 37731–37734 (2001).

96. Spiegelman, B. M., Puigserver, P. & Wu, Z. Regulation of adipogenesis and energy balance by PPARgamma and PGC-1. *Int. J. Obes. Relat. Metab. Disord.* **24 Suppl 4**, S8–10 (2000).

97. Lasar, D. *et al.* Peroxisome Proliferator Activated Receptor Gamma Controls Mature Brown Adipocyte Inducibility through Glycerol Kinase. *Cell Rep.* **22**, 760–773 (2018).

98. Shen, Y. *et al.* Shared PPARα/γ Target Genes Regulate Brown Adipocyte Thermogenic Function. *Cell Rep.* **30**, 3079–3091.e5 (2020).

99. Inzucchi, S. E. *et al.* Management of hyperglycaemia in type 2 diabetes, 2015: a patient-centred approach. Update to a position statement of the American Diabetes Association and the European Association for the Study of Diabetes. *Diabetologia* **58**, 429–442 (2015).

100. Cheng, H. S. *et al.* Exploration and Development of PPAR Modulators in Health and Disease: An Update of Clinical Evidence. *Int. J. Mol. Sci.* **20**, (2019).

101. Rizos, C. V., Elisaf, M. S., Mikhailidis, D. P. & Liberopoulos, E. N. How safe is the use of thiazolidinediones in clinical practice? *Expert Opin. Drug Saf.* **8**, 15–32 (2009).

102. Wright, M. B., Bortolini, M., Tadayyon, M. & Bopst, M. Minireview: Challenges and opportunities in development of PPAR agonists. *Mol. Endocrinol.* **28**, 1756–1768 (2014).

103. Nissen, S. E. & Wolski, K. Effect of rosiglitazone on the risk of myocardial infarction and death from cardiovascular causes. *N. Engl. J. Med.* **356**, 2457–2471 (2007).

104. Gunawardana, S. C. & Piston, D. W. Reversal of type 1 diabetes in mice by brown adipose tissue transplant. *Diabetes* **61**, 674–682 (2012).

105. Gunawardana, S. C. & Piston, D. W. Insulin-independent reversal of type 1 diabetes in

nonobese diabetic mice with brown adipose tissue transplant. *Am. J. Physiol. Endocrinol. Metab.* **308**, E1043–55 (2015).

106. Liu, X. *et al.* Brown Adipose Tissue Transplantation Reverses Obesity in Ob/Ob Mice. *Endocrinology* **156**, 2461–2469 (2015).

107. Zhu, Z. *et al.* Enhanced sympathetic activity in mice with brown adipose tissue transplantation (transBATation). *Physiol. Behav.* **125**, 21–29 (2014).

108. Min, S. Y. *et al.* Human 'brite/beige' adipocytes develop from capillary networks, and their implantation improves metabolic homeostasis in mice. *Nat. Med.* **22**, 312–318 (2016).

109. Lee, C.-W., Hsiao, W.-T. & Lee, O. K.-S. Mesenchymal stromal cell-based therapies reduce obesity and metabolic syndromes induced by a high-fat diet. *Transl. Res.* **182**, 61–74.e8 (2017).

110. Tharp, K. M. *et al.* Matrix-Assisted Transplantation of Functional Beige Adipose Tissue. *Diabetes* **64**, 3713–3724 (2015).

111. Fischer, S., Windshügel, B., Horak, D., Holmes, K. C. & Smith, J. C. Structural mechanism of the recovery stroke in the myosin molecular motor. *Proc. Natl. Acad. Sci. U. S. A.* **102**, 6873–6878 (2005).

112. Lekaditi, D. & Sakellaropoulos, S. Myosin Modulators: The New Era of Medical Therapy for Systolic Heart Failure and Hypertrophic Cardiomyopathy. *Cardiol. Res. Pract.* **12**, 146–148 (2021).

113. Day, S. M., Tardiff, J. C. & Ostap, E. M. Myosin modulators: emerging approaches for the treatment of cardiomyopathies and heart failure. *J. Clin. Invest.* **132**, (2022).

114. Anderson, R. L. *et al.* Deciphering the super relaxed state of human β-cardiac myosin and

the mode of action of mavacamten from myosin molecules to muscle fibers. *Proc. Natl. Acad. Sci. U. S. A.* **115**, E8143–E8152 (2018).

115. Green, E. M. *et al.* A small-molecule inhibitor of sarcomere contractility suppresses hypertrophic cardiomyopathy in mice. *Science* **351**, 617–621 (2016).
116. Teerlink, J. R. *et al.* Cardiac Myosin Activation with Omecamtiv Mecarbil in Systolic Heart Failure. *N. Engl. J. Med.* **384**, 105–116 (2021).
117. Malik, F. I. *et al.* Cardiac myosin activation: a potential therapeutic approach for systolic heart failure. *Science* **331**, 1439–1443 (2011).
118. Liu, Y., White, H. D., Belknap, B., Winkelmann, D. A. & Forgacs, E. Omecamtiv Mecarbil modulates the kinetic and motile properties of porcine β-cardiac myosin. *Biochemistry* **54**, 1963–1975 (2015).
119. Planelles-Herrero, V. J., Hartman, J. J., Robert-Paganin, J., Malik, F. I. & Houdusse, A. Mechanistic and structural basis for activation of cardiac myosin force production by omecamtiv mecarbil. *Nat. Commun.* **8**, 190 (2017).
120. Gu, X., Ma, Y., Liu, Y. & Wan, Q. Measurement of mitochondrial respiration in adherent cells by Seahorse XF96 Cell Mito Stress Test. *STAR Protoc* **2**, 100245 (2021).
121. Webb, M. R. A continuous spectrophotometric assay for inorganic phosphate and for measuring phosphate release kinetics in biological systems. *Proc. Natl. Acad. Sci. U. S. A.* **89**, 4884–4887 (1992).
122. Radke, M. B. *et al.* Small molecule-mediated refolding and activation of myosin motor function. *Elife* **3**, e01603 (2014).
123. Kim, J. *et al.* Characterizing cellular mechanical phenotypes with mechano-node-pore

sensing. *Microsyst Nanoeng* **4**, (2018).

124. Martino, F., Perestrelo, A. R., Vinarský, V., Pagliari, S. & Forte, G. Cellular Mechanotransduction: From Tension to Function. *Front. Physiol.* **9**, 824 (2018).
125. Spiegelman, B. M. & Ginty, C. A. Fibronectin modulation of cell shape and lipogenic gene expression in 3T3-adipocytes. *Cell* **35**, 657–666 (1983).
126. Rodríguez Fernández, J. L. & Ben-Ze'ev, A. Regulation of fibronectin, integrin and cytoskeleton expression in differentiating adipocytes: inhibition by extracellular matrix and polylysine. *Differentiation* **42**, 65–74 (1989).
127. McBeath, R., Pirone, D. M., Nelson, C. M., Bhadriraju, K. & Chen, C. S. Cell shape, cytoskeletal tension, and RhoA regulate stem cell lineage commitment. *Dev. Cell* **6**, 483–495 (2004).
128. Dupont, S. *et al.* Role of YAP/TAZ in mechanotransduction. *Nature* **474**, 179–183 (2011).
129. Misra, J. R. & Irvine, K. D. The Hippo Signaling Network and Its Biological Functions. *Annu. Rev. Genet.* **52**, 65–87 (2018).
130. Pocaterra, A., Romani, P. & Dupont, S. YAP/TAZ functions and their regulation at a glance. *J. Cell Sci.* **133**, (2020).
131. Chen, Y.-A. *et al.* WW Domain-Containing Proteins YAP and TAZ in the Hippo Pathway as Key Regulators in Stemness Maintenance, Tissue Homeostasis, and Tumorigenesis. *Front. Oncol.* **9**, 60 (2019).
132. Lin, K. C. *Regulation of the Hippo Pathway Transcription Factor TEAD*. (2019).
133. Zheng, Y. & Pan, D. The Hippo Signaling Pathway in Development and Disease. *Dev. Cell* **50**, 264–282 (2019).

134. Kowalczyk, W. *et al.* Hippo signaling instructs ectopic but not normal organ growth. *Science* **378**, eabg3679 (2022).

135. Yu, F.-X. *et al.* Regulation of the Hippo-YAP pathway by G-protein-coupled receptor signaling. *Cell* **150**, 780–791 (2012).

136. Gaspar, P. & Tapon, N. Sensing the local environment: actin architecture and Hippo signalling. *Curr. Opin. Cell Biol.* **31**, 74–83 (2014).

137. Wada, K.-I., Itoga, K., Okano, T., Yonemura, S. & Sasaki, H. Hippo pathway regulation by cell morphology and stress fibers. *Development* **138**, 3907–3914 (2011).

138. Hong, J.-H. *et al.* TAZ, a transcriptional modulator of mesenchymal stem cell differentiation. *Science* **309**, 1074–1078 (2005).

139. Suh, J. S. *et al.* A cell-permeable fusion protein for the mineralization of human dental pulp stem cells. *J. Dent. Res.* **91**, 90–96 (2012).

140. Yang, J.-Y. *et al.* Osteoblast-targeted overexpression of TAZ increases bone mass in vivo. *PLoS One* **8**, e56585 (2013).

141. Zhu, Y. *et al.* Pharmacological activation of TAZ enhances osteogenic differentiation and bone formation of adipose-derived stem cells. *Stem Cell Res. Ther.* **9**, 53 (2018).

142. El Ouarrat, D. *et al.* TAZ Is a Negative Regulator of PPARγ Activity in Adipocytes and TAZ Deletion Improves Insulin Sensitivity and Glucose Tolerance. *Cell Metab.* **31**, 162–173.e5 (2020).

143. Chang, C.-C. *et al.* Hyperglycemia and advanced glycation end products (AGEs) suppress the differentiation of 3T3-L1 preadipocytes. *Oncotarget* **8**, 55039–55050 (2017).

144. Pan, J.-X. *et al.* YAP promotes osteogenesis and suppresses adipogenic differentiation by

regulating β-catenin signaling. *Bone Res* **6**, 18 (2018).

145. Kamura, K. *et al.* Obesity in Yap transgenic mice is associated with TAZ downregulation. *Biochem. Biophys. Res. Commun.* **505**, 951–957 (2018).

146. Wang, L. *et al.* YAP and TAZ protect against white adipocyte cell death during obesity. *Nat. Commun.* **11**, 5455 (2020).

147. Piccolo, S., Dupont, S. & Cordenonsi, M. The biology of YAP/TAZ: hippo signaling and beyond. *Physiol. Rev.* **94**, 1287–1312 (2014).

148. Jang, E. J. *et al.* TM-25659 enhances osteogenic differentiation and suppresses adipogenic differentiation by modulating the transcriptional co-activator TAZ. *Br. J. Pharmacol.* **165**, 1584–1594 (2012).

149. Wang, C. *et al.* Verteporfin inhibits YAP function through up-regulating 14-3-3σ sequestering YAP in the cytoplasm. *Am. J. Cancer Res.* **6**, 27–37 (2016).

150. Anderson, C. M. *et al.* Dependence of brown adipose tissue function on CD36-mediated coenzyme Q uptake. *Cell Rep.* **10**, 505–515 (2015).

151. Mina, A. I. *et al.* CalR: A Web-Based Analysis Tool for Indirect Calorimetry Experiments. *Cell Metab.* **28**, 656–666.e1 (2018).

152. Liao, J., Sportsman, R., Harris, J. & Stahl, A. Real-time quantification of fatty acid uptake using a novel fluorescence assay. *J. Lipid Res.* **46**, 597–602 (2005).

Appendix

Table 1: Myh4 targeting compounds

Matrix Tube Barcode	Molecule ID	Product URL
0246513599	MCULE-9016507145	https://mcule.com/P-17936310/
0246506947	MCULE-9095318452	https://mcule.com/P-18367492/
0247678452	MCULE-2613997288	https://mcule.com/P-449612183/
0247679531	MCULE-4257848884	https://mcule.com/P-9288580/
0246496226	DMSO	0
0246508226	MCULE-9308280251	https://mcule.com/P-8792777/
0246506615	MCULE-5970564782	https://mcule.com/P-34686779/
0246504460	MCULE-4332030827	https://mcule.com/P-11162835/
0247678501	MCULE-2463606823	https://mcule.com/P-18403226/
0247678799	MCULE-2680867110	https://mcule.com/P-9211048/
0246513628	MCULE-9480313267	https://mcule.com/P-11399633/

0247708207	MCULE-4509940526	https://mcule.com/P-9747206/
0247676774	MCULE-4175270252	https://mcule.com/P-22123187/
0246513619	MCULE-8401643179	https://mcule.com/P-21580299/
0246513623	MCULE-8098631427	https://mcule.com/P-10894643/
0247677907	MCULE-8556183948	https://mcule.com/P-4270891/
0247678683	MCULE-9353164600	https://mcule.com/P-21873097/
0246506659	MCULE-2174954861	https://mcule.com/P-26525570/
0246506730	MCULE-5889117136	https://mcule.com/P-20957080/
0247683638	MCULE-7296134364	https://mcule.com/P-13678819/
0247679512	MCULE-3627614949	https://mcule.com/P-4968896/
0246506596	MCULE-9114963293	https://mcule.com/P-34704390/

0247708187	MCULE-5602720869	https://mcule.com/P-9450968/
0247678700	MCULE-6701561201	https://mcule.com/P-7297780/
0247679508	MCULE-3050859457	https://mcule.com/P-9569068/
0246515030	MCULE-1733461815	https://mcule.com/P-21681287/
0246504466	MCULE-8038982866	https://mcule.com/P-18258691/
0247678849	MCULE-6912272211	https://mcule.com/P-8347488/
0247708253	MCULE-8721409140	https://mcule.com/P-8602048/
0246504519	MCULE-6864017875	https://mcule.com/P-11788231/
0247679491	MCULE-3771872499	https://mcule.com/P-8841997/
0247676489	MCULE-9870486332	https://mcule.com/P-13559030/
0247679132	MCULE-5023964494	https://mcule.com/P-12904314/

0246513638	MCULE-6039670137	https://mcule.com/P-18715719/
0247709109	MCULE-7875177815	https://mcule.com/P-13444544/
0246515596	MCULE-7076335344	https://mcule.com/P-21971263/
0247685414	MCULE-2457125782	https://mcule.com/P-504704333/
0246506934	MCULE-2839988207	https://mcule.com/P-17936145/
0247708220	MCULE-2301000729	https://mcule.com/P-9327189/
0246506103	MCULE-5610932164	https://mcule.com/P-14493943/
0246508262	MCULE-3612798829	https://mcule.com/P-32584606/
0247708227	MCULE-8139442946	https://mcule.com/P-8111041/
0247678800	MCULE-1998325995	https://mcule.com/P-9045783/
0246504486	MCULE-2809509385	https://mcule.com/P-34495824/

0247708204	MCULE-8897073494	https://mcule.com/P-8413462/
0247679551	MCULE-6321714376	https://mcule.com/P-7389927/
0247676122	DMSO	0
0247679136	MCULE-5430993085	https://mcule.com/P-13038998/
0246506679	MCULE-3931783299	https://mcule.com/P-858424/
0246506682	MCULE-6429429501	https://mcule.com/P-7212258/
0247679119	MCULE-1825119307	https://mcule.com/P-449666459/
0246506713	MCULE-5678910937	https://mcule.com/P-10628104/
0247708169	MCULE-6185920443	https://mcule.com/P-5177210/
0246506136	MCULE-5037735847	https://mcule.com/P-12684099/
0246504505	MCULE-7219070444	https://mcule.com/P-9019017/
0246513598	MCULE-6349086621	https://mcule.com/P-14732887/

0246508224	MCULE-8075971509	https://mcule.com/P-32002357/
0247679536	MCULE-5540238877	https://mcule.com/P-9091664/
0247679553	MCULE-1923328915	https://mcule.com/P-9365471/
0247676842	MCULE-6668938744	https://mcule.com/P-22392288/
0246506668	MCULE-1104518774	https://mcule.com/P-346528500/
0247708203	MCULE-4005962229	https://mcule.com/P-9576016/
0246504471	MCULE-7440915105	https://mcule.com/P-10787976/
0247708210	MCULE-3636249688	https://mcule.com/P-6390283/
0246506718	MCULE-7774265370	https://mcule.com/P-33117683/
0240838534	MCULE-8408250426	https://mcule.com/P-10675876/
0309677331	MCULE-8018087880	https://mcule.com/P-6951126/

0247707401	MCULE-3446831614	https://mcule.com/P-9031936/
0309677931	MCULE-4108632132	https://mcule.com/P-9292879/
0247707413	MCULE-3920573589	https://mcule.com/P-5464897/
0309645932	MCULE-4424694971	https://mcule.com/P-13974974/
0240821352	MCULE-8714404060	https://mcule.com/P-10908734/
0240837373	MCULE-2652525994	https://mcule.com/P-12049247/
0240837775	MCULE-2411089614	https://mcule.com/P-12089396/
0240836564	MCULE-3857276441	https://mcule.com/P-7297291/
0306567973	MCULE-7789965862	https://mcule.com/P-449636426/
0309649877	MCULE-2484224763	https://mcule.com/P-12648825/
0247707438	MCULE-7945627683	https://mcule.com/P-18355003/

0247707467	MCULE-5133117476	https://mcule.com/P-13820751/
0247707033	MCULE-3827895173	https://mcule.com/P-14159242/
0240821070	MCULE-9223900930	https://mcule.com/P-11919763/
0240820324	MCULE-9893631498	https://mcule.com/P-32644844/
0240821296	MCULE-9904007768	https://mcule.com/P-20934322/
0247707453	MCULE-3167716248	https://mcule.com/P-25806557/
0309622841	MCULE-6763937221	https://mcule.com/P-14586927/
0240821494	MCULE-8708300383	https://mcule.com/P-32120464/
0247707404	MCULE-4278386312	https://mcule.com/P-7532226/
0240836587	MCULE-1091463004	https://mcule.com/P-10391311/
0309652857	MCULE-2873561335	https://mcule.com/P-13232347/

0240819409	MCULE-9011931979	https://mcule.com/P-12084505/
0309677296	MCULE-1189002614	https://mcule.com/P-6503080/
0240837396	MCULE-3367779074	https://mcule.com/P-9359871/

Table 2: Myh11 Targeting Compounds

Matrix Tube Barcode	**Molecule ID**	**URL**
0247678004	MCULE-1033285295	https://mcule.com/P-9423098/
0246508203	MCULE-6017209677	https://mcule.com/P-11098150/
0246513585	MCULE-9984566597	https://mcule.com/P-11293205/
0246496200	DMSO	
0246506675	MCULE-5314623848	https://mcule.com/P-7974151/
0247708198	MCULE-7181155153	https://mcule.com/P-9455509/
0246506132	MCULE-1698349537	https://mcule.com/P-11189003/

0247708199	MCULE-5873827010	https://mcule.com/P-9543201/
0246506641	MCULE-4713432441	https://mcule.com/P-34512648/
0246508207	MCULE-8197538029	https://mcule.com/P-34496348/
0246486975	DMSO	
0247679156	MCULE-9766572582	https://mcule.com/P-13818473/
0246513630	MCULE-8638838800	https://mcule.com/P-7968654/
0247676261	MCULE-6230429312	https://mcule.com/P-13043114/
0247679503	MCULE-4647586959	https://mcule.com/P-7051703/
0247679005	MCULE-3779319225	https://mcule.com/P-13777702/
0246506553	MCULE-2777654598	https://mcule.com/P-11850716/
0247681248	MCULE-8547107706	https://mcule.com/P-15910929/
0246506123	MCULE-3783739330	https://mcule.com/P-17798550/

0247682153	MCULE-1225986948	https://mcule.com/P-449629561/
0246506579	MCULE-7155425108	https://mcule.com/P-18476878/
0246513636	MCULE-2037064518	https://mcule.com/P-34592980/
0247708184	MCULE-5537305903	https://mcule.com/P-7840223/
0247679062	MCULE-8579229017	https://mcule.com/P-11816296/
0246506651	MCULE-5378332578	https://mcule.com/P-11906401/
0247708195	MCULE-5798906217	https://mcule.com/P-20229207/
0246506945	MCULE-3686170622	https://mcule.com/P-34688221/
0247676795	MCULE-4902627909	https://mcule.com/P-13443868/
0246513870	MCULE-2080580707	https://mcule.com/P-11675061/
0247708165	MCULE-3308175211	https://mcule.com/P-7322467/

0246508258	MCULE-4385143734	https://mcule.com/P-11199357/
0246513643	MCULE-5057542128	https://mcule.com/P-14712200/
0246508184	MCULE-1365513676	https://mcule.com/P-18592915/
0247679540	MCULE-8154670380	https://mcule.com/P-9204583/
0247682861	MCULE-9900689660	https://mcule.com/P-12490000/
0246513622	MCULE-1376104069	https://mcule.com/P-14810024/
0247708185	MCULE-2522013191	https://mcule.com/P-449605523/
0246504463	MCULE-2681503791	https://mcule.com/P-18307189/
0246506683	MCULE-5503231298	https://mcule.com/P-34550990/
0247679554	MCULE-2095358695	https://mcule.com/P-9121901/
0246508214	MCULE-4561436109	https://mcule.com/P-33120155/

0247708188	MCULE-9117516272	https://mcule.com/P-5341414/
0247709095	MCULE-4679745004	https://mcule.com/P-9587074/
0247679946	MCULE-6015297118	https://mcule.com/P-5900837/
0247708201	MCULE-7230852670	https://mcule.com/P-8094206/
0246508268	MCULE-5036841658	https://mcule.com/P-14485147/
0247678443	MCULE-8398931398	https://mcule.com/P-24466050/
0247679172	MCULE-2178512266	https://mcule.com/P-13704343/
0247678662	MCULE-3594162358	https://mcule.com/P-12599058/
0246508190	MCULE-7791330896	https://mcule.com/P-4936860/
0247678841	MCULE-1525995460	https://mcule.com/P-7800648/
0246504453	MCULE-5528595894	https://mcule.com/P-32084830/

0247679486	MCULE-2064452430	https://mcule.com/P-21765802/
0246513587	MCULE-3785454275	https://mcule.com/P-34678221/
0247678409	MCULE-2934461455	https://mcule.com/P-22400002/
0247679846	MCULE-1778487609	https://mcule.com/P-10623985/
0247679082	MCULE-3049495486	https://mcule.com/P-13557966/
0247678842	MCULE-4979809789	https://mcule.com/P-32034976/
0246513627	MCULE-2782969583	https://mcule.com/P-18454455/
0247706600	MCULE-6821406472	https://mcule.com/P-32099747/
0247706732	MCULE-1566937266	https://mcule.com/P-17694425/
0247707421	MCULE-5057228580	https://mcule.com/P-10729727/
0247706623	MCULE-8722895393	https://mcule.com/P-32827286/

0247706789	MCULE-6750604026	https://mcule.com/P-8504109/
0247705914	MCULE-9444572463	https://mcule.com/P-7682823/
0247705861	MCULE-1839395242	https://mcule.com/P-18248381/
0247707489	MCULE-1101102976	https://mcule.com/P-449632075/
0247705954	MCULE-7041263011	https://mcule.com/P-7748027/
0247706982	MCULE-8261270903	https://mcule.com/P-3491203/
0247707407	MCULE-3282162420	https://mcule.com/P-18325982/
0247707399	MCULE-1701059226	https://mcule.com/P-9430893/
0247705931	MCULE-8305909486	https://mcule.com/P-9251592/
0247707434	MCULE-8261154426	https://mcule.com/P-8044797/
0247707422	MCULE-7846170611	https://mcule.com/P-449473364/